The Roles of the Respiratory Oscillators: Effects of Optogenetics and Cholinergic Perturbations on the Respiratory Functions

A thesis submitted in partial fulfillment of the requirements for the degree of

Master of Science

Department of Physiology

University of Alberta

Abstract

Previous data have revealed the important and fundamental role in respiratory control of two groups of brainstem neurons: the preBötzinger Complex (preBötC) and the retrotrapezoid / parafacial respiratory group (RTN/pFRG). The preBötC which functions as the inspiratory oscillator, essential for inspiratory bursts initiation and pattern generation and the RTN/pFRG which functions as the active expiratory oscillator and central chemoreception region. This research thesis utilized various optogenetic and pharmacological tools to further examine the behaviour of the two respiratory oscillators. Specifically we aimed to investigate how a highly controlled excitation of the preBötC neurons affects ongoing breathing and we aimed to investigate the respiratory effects of cholinergic neurotransmission on the RTN/pFRG region.

In the first chapter we investigated the effects of brief laser pulses stimulation in rats infected with an adeno associated virus that expresses a light sensitive protein (Channelrhodopsin) along with a fluorescent marker in the preBötC neurons. Previous work has revealed the importance of excitation within the preBötC network, nevertheless the effects of a highly temporally controlled excitation to the preBötC neurons was yet to be described. We tested the hypothesis that brief excitation of the preBötC neurons will drive the inspiratory activity and reset the

respiratory rhythms. Precise laser pulse stimulation to the preBötC neurons increased the respiratory frequency, induced a respiratory reset, entrained respiratory frequency and reinstated breathing in absence of ongoing activity. These results provide further evidence for an essential role of excitation in respiratory rhythmogenesis within the preBötC network and support the fundamental role of preBötC as the main inspiratory oscillator.

In the second chapter we investigated pharmacological properties of the expiratory oscillator RTN/pFRG. Previous work from our lab demonstrated the recruitment of abdominal muscles during periods of REM sleep or REM-like sleep under urethane anesthesia. Because acetylcholine is released during period of REM sleep, we hypothesized that cholinergic innervation contributes to the pFRG level of excitation and the subsequent occurrence of active expiration. We demonstrated that cholinergic innervation contributes to pFRG activation which leads to the recruitment of abdominal muscles activity and active expiration. We examined the presence of cholinergic fibers and terminals within the pFRG region, tested the pFRG response to various cholinergic modulators, and investigated the respiratory responses evoked by stimulating either medial or lateral para facial regions (RTN and pFRG). Our results demonstrate that cholinergic innervation is present within the region of the pFRG and local application of different cholinergic agonists and antagonists into the pFRG evoked various respiratory responses, which suggest that

cholinergic innervation contributes to the process of the pFRG activation and abdominal muscles recruitment.

Preface

This is an original work by: Zaki Aziz Alsahafi. The research projects presented in this thesis received research ethics approval from University of Alberta Research Ethics Board, Project name ”Neural control of breathing in adult rodents in vivo”, AUP#461 January 22, 2013.

Preface

Chapter II of this thesis has been published by Zaki Alsahafi, Clayton T. Dickson, and Silvia Pagliardini as a manuscript entitled “Optogenetic excitation of preBötzinger complex neurons potently drives inspiratory activity in vivo”, in the Journal of Physiology, Volume 593, issue 16, pages 3673-3692. I performed the experiments, analyzed the data and participated in the manuscript preparation. Clayton T. Dickson assisted with the data analysis and manuscript preparation. Silvia Pagliardini was the supervisory author responsible for the experimental design, figures and the manuscript preparation.

Preface

Chapter III of this thesis is accepted for publication in Journal of Physiology. The manuscript, entitled “Cholinergic Modulation of the paraFacial Respiratory Group” is submitted by Rozlyn C.T. Boutin, Zaki Alsahafi, and Silvia Pagliardini, I was responsible for sections 3.3.4, and 3.3.6 of this chapter, for all aspects including

performing the experiments, analyzing the data, and writing the manuscript. Rozlyn C.T. Boutin was responsible for sections 3.3.2 and 3.3.3 for all aspects including performing the experiments, analyzing the data, and writing the manuscript. Silvia Pagliardini was the supervisory author responsible for the experimental design, experimental execution and data analysis of section 3.3.1 and 3.3.5 and manuscript preparation.

Acknowledgements

To acknowledge all the participants who contributed in some way to the presented work, including Silvia Pagliradini's labs members who I have worked with throughout my master program.

To my family for all of their constant love and help during my master degree journey, and for being always supporting.

To my supervisory committee members (Dr. Greg Funk, Dr. John Greer) for their advices and comments on my research projects.

I owe my deepest gratitude to my supervisor Silvia Pagliardini, I wouldn't be able to write this thesis or even to perform the simplest experiments in the lab without her continues guidance, support, encouragement, and optimism. Throughout various complex and difficult circumstances she has been always patient and enthusiastic which helped me a lot to overcome all the obstacles that I encountered during my master program.

Table of contents

Chapter I: General introduction……1

1.1. Overview……2

1.2. The brain stem neuronal networks that control respiration……3

1.2.1. The preBötzinger Complex……7

1.2.2. Identification of the preBötzinger neurons……9

1.2.3. Anatomical and functional development of the preBötzinger……11

1.2.4 Respiratory rhythm generation……13

1.2.5 Retro-trapezoid nucleus and the para facial respiratory group……15

1.2.6 RTN/pFRG roles in respiratory control……17

1.3. Methods to manipulate neural activity……21

1.3.1 Electrical control……21

1.3.2 Pharmacological control……22

1.3.3 Optogenetics……24

1.4 Thesis aims……26

Chapter II:

Optogenetic excitation of preBötzinger complex neurons potently drives inspiratory activity in vivo……36

2.1 Introduction……...37

2.2 Methods……41

2.2.1 Ethical approval……...41

2.2.2 Viral injections into preBötC……...41

2.2.3 Photostimulation experimental approach……42

2.2.4 Histology……45

2.2.5 Data analysis and statistics……48

2.2.6 Reset analysis……49

2.3 Results……...51

2.3.1 Expression patterns of SYN-chR2-EYFP in brainstem……...51

2.3.2 Activation of preBötC neurons increases breathing……52

2.3.3 Frequency-specific activation of preBötC neurons paces breathing…...57

2.3.4 Pulses of photostimulation reset respiratory rhythm in phase-independent manner…..……59

2.3.5 Photostimulation of preBötC neurons generates rhythmic Diaphragm contractions when excitatory respiratory drive is dampened by mechanical hyperventilation……..64

2.4 Discussion……..……66

2.4.1 Technical considerations……67

2.4.2 PreBötC photostimulation increases respiratory rate and entrains Respiration……...70

2.4.3 PreBötC photostimulation produces respiratory reset……74

2.5 Conclusions……77

Chapter III:

Cholinergic Modulation of the paraFacial Respiratory Group……..……97

3.1 Introduction……..98

3.2 Methods……..…..102

3.2.1 Immunohistochemistry……..102

3.2.2 Acute experimental procedures……..103

3.2.3 Unit recordings……...105

3.2.4 Histology……....105

3.2.5 Data analysis……..106

3.3 Results……..108

3.3.1 Cholinergic innervation is present in, and localized to, the pFRG region……108

3.3.2 Inhibition of endogenous acetylcholinesterases in the pFRG increases abdominal expiratory activity……109

3.3.3 Activation of cholinergic receptors in pFRG recruits abdominal expiratory activity and active expiration……...110

3.3.4 Activation of late expiratory activity neurons within pFRG during carbachol stimulation……112
3.3.5 Activation of pFRG is antagonized by scopolamine and M3 receptor antagonists……112
3.3.6 CCh response in the medial and lateral regions surrounding the facial nucleus……116
3.4 Discussion……119
3.5 Conclusions……127

Chapter IV: General discussion……143
4.1 Overview……144
4.2 Optogenetic excitation of preBötzinger complex neurons potently drives inspiratory activity *in vivo*……145
4.3 Cholinergic Modulation of the paraFacial Respiratory Group……150
4.4 Conclusions……158
References……159

List of tables

2.1 Group average values for induced phase for different photostimulation pulse durations showing best reset for the shortest pulse durations used and increasing phase values for increasing pulse duration…….96

List of figures

Chapter I:

1.1 Schematic of the respiratory brainstem nuclei…….....28

1.2 NK1R- and μOR-expressing neurons are limited to and define the PreBötC……..…….....….30

1.3 Phox2b expression in the RTN…….…….....32

1.4 Anatomical description of RTN CO_2 – activated neurons……..……..34

Chapter II:

2.1 Distribution of EYFP labelled neurons along the rostrocaudal extension of the ventral respiratory column……...78

2.2 Effects of continuous (10 s) and high frequency (20 Hz, 20 ms pulse) photostimulation of preBötC in urethane-anaesthetized, SYN-ChR2-EYFP-treated rats…….……....80

2.3 Specificity of preBötC photostimulation……82

2.4 Reserpine pretreatment does not affect respiratory response to preBötC photostimulation……...84

2.5 Photostimulation of SYN-ChR2-EYFP-treated rats in the preBötC produces respiratory entrainment…….86

2.6 Photostimulation of SYN-ChR2-EYFP-treated rats in the

preBötC generates respiratory reset……88

2.7 A refractory period to inspiratory reset exists during early expiration……...92

2.8 Photostimulation of SYN-ChR2-EYFP-treated rats in the preBötC restores respiratory rhythms and produces respiratory entrainment in absence of ongoing respiration……..94

Chapter III:

3.1 Distribution of cholinergic terminals in both pFRG and the motoneurons in the facial nucleus……...128

3.2 Local application of physostigmine (PHYSO, 5 mM, 200 nl) in pFRG induces long lasting ABD recruitment and active expiration……..130

3.3 Local application of physostigmine (PHYSO, 5 mM, 200 nl) in pFRG does not affect spontaneous brain state alternations……132

3.4 Local application of carbachol (CCh, 10 mM, 100 nl) in pFRG induces long lasting ABD recruitment and active expiration……...134

3.5 Representative sections of adult rat brainstem indicating CCh injection sites in the pFRG of urethane anesthetized rats that promoted recruitment of ABD activity and active expiration……136

3.6 Late expiratory neurons are located at the site of CCh injection during recruitment of active expiration……...138

3.7 Scopolamine blocks CCh induced recruitment of ABD_{EMG} and active expiration…….139

3.8 Local application of carbachol (CCh, 1 mM, 50-100 nl) in the region lateral or medial to the facial nucleus induces different respiratory responses……...141

List of symbols, nomenclature abbreviations

AP	area postrema
ACh	acetycholine
ABD_{EMG}	external oblique abdominal EMG
BötC	bötzinger complex
BrdU	5-Bromo-2'deoxyuridine
Ca^{+2}	calcium ion
CCH	carbachol
ChAT	choline acetyl transferase
ChR2	channelrhodopsin
CNQX	6-cyano-7-nitroquinoxaline-2.3-dione
CO_2	carbon dioxide
cVRG	caudal ventral respiratory group
Dbx1	developing brain Homebox1
DAM	donkey anti-mouse
DAR	donkey anti-rappit
DAG	donkey anti-goat
DIA_{EMG}	diaphragmatic EMG
DRG	dorsal respiratory group
EEG	electroencephalogram
EMG	electromyography
e-pF	embryonic parafacial group
GABA	Y-aminobutyric acid
GFP	green fluorescent protein

GG_{EMG}	genioglossal EMG
LRt	lateral reticular nucleus
HF	high frequency
I_{CAN}	ca^{2+} activated inward cationic current
INaP	persistent Na^{+} current
IO	inferior olivary complex
KF	Kölliker fuse
M3	type 3 muscarinic receptors
Na^{+}	sodium ion
NA	nucleus ambiguus
NeuN	neuronal nuclear marker
NK1R	neurokinin-1 receptor
nREM sleep	non rapid eye movement sleep
NTS	nucleus of the solitary tract
PB	parabrachial nucleus
Phox2b	paired-like homebox 2b
Pre I	pre-Inspiratory neurons
Pn	ventral pontine nucleus
PreBötC	prebötzinger complex
PRG	pontine respiratory group
Physo	physostgmine
REM sleep	rapid eye movement sleep
RTN/pFRG	retrotrapezoid nucleus / para-facial respiratory group
rVRG	rostral ventral respiratory group
SD	standard deviation

SO	superior pontine complex
SP5	spinal trigeminal nucleus
SP-SAP	saporin conjugated with substance P
SST	somatostatin peptide
T_E	expiratory time
TH	tyrosine hydroxylase enzyme
T_I	inspiratory time
V	motor nucleus of the trigeminal nerve
V4	fourth ventricle
VACHT	vesicular acetylcholine transporter
V_E	minute ventilation
VGLUT	vesicular glutamate transporter 2
VRC	ventral respiratory column
VSC	ventral spinocerebellar tract
V_T	tidal volume
XII	hypoglossal motor nucleus

CHAPTER I

General Introduction

1.1 Overview

Respiration is a complex and essential behaviour for living organisms. It involves a series of sensory, motor, metabolic tasks that interact and coordinate various inputs with each other within milliseconds in order to supply mammalian body oxygen and energy demands and to get rid of the harmful carbon dioxide. In this thesis I examined how the respiratory oscillators behave toward various forms of stimulation. The first chapter of this thesis review the brainstem respiratory control centers and focused mainly on the preBötC complex and the RTN/pFRG functions in addition to a brief review of methods available to manipulate neuronal activity, with a focus on the optogenetic techniques.

1.2 The brainstem neuronal network that controls respiration

Understanding how the respiratory rhythm is generated by the brainstem presents a fundamental challenge within the field of respiratory neurophysiology. Respiratory network within the brainstem has been identified in the pons and the medulla oblongata. The pontine respiratory group (PRG) in the pons, the dorsal respiratory group (DRG), and ventral respiratory group (VRG) in the medulla are composed of heterogeneous respiratory neuronal populations with various respiratory related functions. (Fig. 1.1, A-B). The PRG is situated in the dorsolateral pons and contains neuronal populations of the Kolliker Fuse (KF) nucleus and the parabrachial (PB) complex. These areas interact with multiple medullary respiratory networks and contribute to respiratory phase transition (Cohen, 1979; Okazaki *et al*., 2002; Ezure and Tanaka, 2006). The dorsal respiratory group (DRG) consists of neurons located within the nucleus of the solitary tract (NTS). The NTS is a relay nucleus for different chemoreflexes and mechanoreflexes inputs. Descending afferents also synapse onto DRG neurons. The DRG transmits these inputs to respiratory motoneurons and other ventral respiratory column (VRC) compartments in order to modulate respiration to fit various physiological demands (Alheid *et al*., 2011; Smith *et al*., 2013).

The VRC is situated ventrolaterally on each side of the medulla (Smith *et al*., 2013) (Fig. 1.1 A-B) and includes the Bötzinger (BötC), preBötC, the rostral, and the caudal ventral respiratory group (VRG). The BötC is located rostral to the preBötC and caudal to the facial motor nucleus. The BötC includes mainly inhibitory expiratory neurons (Smith *et al*., 2007), including glycinergic and GABAergic neurons (Ezure *et al*., 2003) that provide inhibitory inputs to various VRC compartments (Jiang and Lipski,1990) and to spinal phrenic motoneurons (Tian *et al*., 1998). The BötC neurons have been proposed to provide inhibition to the preBötC inspiratory neurons in order to facilitate the switch between inspiration and expiration (Smith *et al*., 2007). Janczewski and colleagues (2013) reported that blocking inhibitory inputs from BötC and preBötC neurons did not alter the respiratory frequency suggesting that inhibition is not necessary for respiratory rhythmogenesis, however other results demonstrate that blocking inhibition between the BötC and preBötC perturbs the respiratory rhythm (Marchenko *et al*., 2016).

The preBötC, an essential element in respiratory rhythmogenesis, is situated caudal to the BötC and will be fully described later in this introduction. Caudal to the preBötC lays the rostral ventral respiratory group (rVRG) which consists of mainly excitatory bulbospinal inspiratory premotor neurons that project to both main inspiratory pump the diaphragm through the phrenic motoneurons (Dobbins and Feldman, 1994), and the accessory inspiratory muscles the external intercostal

muscles through the thoracic motoneurons (Stornetta *et al*., 2003). On the other hand, caudal ventral respiratory group (cVRG) contains excitatory expiratory bulbospinal premotor neurons that project to spinal thoracic and lumbar motoneurons (Shen and Duffin, 2002; Janczewski *et al*., 2002).

The RTN/pFRG, a cluster of neurons located between the facial motor nucleus and the ventral medullary surface, is situated in the most rostral region of the VRC. The RTN/pFRG plays a role in the generation of respiratory rhythm in early life (Onimaru *et al*., 1988, 2006; Onimaru and Homma, 2003; Thoby-Brisson *et al*., 2009), central chemoreception (Mulkey *et al*., 2004; Guyenet *et al*., 2005), and it has been proposed to function as an oscillator for active expiration in adulthood (Pagliardini *et al*., 2011, Huckstepp *et al*., 2015).

Studies utilising *in vitro* and *in vivo* rodent models have provided evidence that the preBötC is the site for inspiratory rhythmogenesis (Smith *et al*, 1991; Rekling and Feldman, 1998; Feldman and Del negro, 2006). Moreover, other evidences suggest the presence of a second neuronal group located in the RTN/pFRG area that may play a role in respiratory rhythm generation in the neonatal rodent (Onimaru 1988, 2006; Onimaru and Homma, 2003; Ballanyi *et al.,* 1999) and in adulthood (Pagliardini *et al*., 2011; Huckstepp *et al*., 2015). Regardless of the developmental changes the contribution of the RTN/pFRG in the respiratory control

process continues during postnatal development and throughout life (Guyenet *et al*., 2005, 2009; Abbott *et al*., 2009, 2011; Stornetta *et al*, 2006; Thoby-Brisson *et al*., 2009, Pagliardini *et al*., 2011, Huckstepp *et al*., 2015)

1.2.1 The preBötzinger complex

The preBötC has been proposed to contain the neurons necessary for inspiratory rhythm generation (Smith *et al*., 1991). The preBötC role in respiratory control has been investigated by using various experimental approaches, including isolated rodent brainstem spinal cord (*en bloc*) preparations and the medullary slice preparations. A respiratory rhythmic motor output is still generated and can be monitored by recording the activity of the hypoglossal and phrenic nerve rootlets in the brainstem-spinal cord preparations. The hypoglossal nerve innervates the genioglossus (a muscle in the tongue that is inspiratory modulated) and the phrenic nerve innervates the diaphragm (the main inspiratory pump muscle in mammals). Therefore, recording the activity of these nerves is a measure of inspiratory output. In brainstem-spinal cord preparations, serial transverse sections extending from rostral to caudal direction revealed the location of the respiratory rhythm generating center, as the respiratory rhythm persists until a transection was made through the mid medulla, where the preBötC is located (Smith *et al*., 1991). In medullary slice preparations, reduction of excitatory synaptic transmission by local microinjection of 6-cyano-7-nitroquinoxaline-2,3-dione (CNQX), a non-N-methyl-D-aspartate glutamate receptor antagonist into the preBötC suppresses and then abolishes the respiratory oscillations (Smith *et al*., 1991), suggesting that glutamatergic

transmission within the preBötC is necessary for respiratory rhythm generation (Funk *et al*., 1993). Bilateral microinjection of tetrodotoxin, a sodium channel blocker, into the preBötC in anaesthetised cats eliminated the respiratory rhythmic activity which causing persistent central apnea (Ramirez *et al*., 1998). In addition, bilateral destruction of preBötC neurokinin-1 receptor (NK1R)-expressing neurons by locally injecting the toxin saporin conjugated with Substance P (SP-SAP) in adult rats can produce serious abnormalities in breathing pattern. SP-SAP$^{(preBötC)}$ lesioned rats display an ataxic breathing pattern and severely depressed ventilatory responses (Gray *et al*. 2001). These experiments identified the preBötC as being necessary for respiratory rhythm generation *in vivo*.

1.2.2 Identification of preBötzinger neurons

Identifying the precise location and the phenotype of the preBötC neurons has been one of the main goals in the field of respiratory neurobiology. Gray and colleagues (1999) applied various peptidergic drugs to the preBötC and reported the evoked respiratory responses. In neonatal medullary slice preparation, local application of the neuropeptide substance P (SP) directly into the preBötC increased the frequency of the respiratory burst activity. It has been proposed that the powerful respiratory excitation is mediated through the membrane neurokinin-1 receptor (NK1R) given that SP is the endogenous ligand for this receptor. Immunohistochemical analyses of the rat VRC revealed that a subpopulation of neurons within the preBötC expresses high levels of NK1R (Fig. 1.2) (Gray *et al*., 1999; Guyenet and Wang, 2001; Guyenet *et al*., 2002; Pagliardini *et al*., 2003). Moreover, Wang and colleagues (2001) examined the NK1R expression in the VRG and found that the highest concentration of NK1+ neurons was in a region overlaps with the identified preBötC region (Wang *et al*., 2001), thus the NK1R has been proposed as an anatomical marker for preBötC neurons.

Moreover, in medullary slice preparation local application of the μ opioid receptor agonist [D-Ala2,N-Me-Phe4,Gly5-ol] enkephalin acetate (DAMGO) into the preBötC dramatically reduced the respiratory frequency (Gray *et al*., 1999). Gray and colleagues (1999) distinguished the preBötC NK1 neurons based on the expression of μ opioid receptors. Histological analyses of the NK1R expressing preBötC neurons demonstrate that a subpopulation of these neurons co-express the μ opioid receptor (Fig. 1.2) (Gray *et al*., 1999) which provides some explanations to the preBötC opioids sensitivity (Montandon *et al*., 2002). A subgroup of preBötC neurons express the neuropeptide somatostatin (SST) with high co-expression of NK1R (Stornetta *et al*., 2003). Later on, Tan and colleagues (2012) identified then proposed the glycoprotein reelin as a marker for the preBötC neurons. Moreover, neurons within the preBötC are predominantly propriobulbar with few being bulbospinal (Ellenberger and Feldman, 1990; Dobbins and Feldman, 1994). Therefore, the preBötC consists of a heterogeneous neuronal populations with glutamatergic connections that influence their function. PreBötC neurons have extensive projections throughout the brainstem respiratory network (Tan *et al*., 2010). The preBötC neurons project mainly to: contralateral preBötC, the ipsi- and contralateral BötC, ventral respiratory column caudal to the preBötC, and the RTN/pFRG. The preBötC neurons project to respiratory control centers in the pons as well (Tan *et al*., 2010). The widespread connectivity of the preBötC with other

brainstem respiratory neural populations further supports the proposed role of preBötC as the main respiratory oscillator. Moreover, it has been demonstrated that the preBötC neurons are derived from the Dbx1-expressing progenitors (Bouvier *et al*., 2010; Gray *et al*., 2010). The discovery of the preBötC genetic and anatomical markers facilitates later studies in which specific neuronal populations are either eliminated or perturbed within the preBötC in order to examine their function in respiratory control.

1.2.3 Anatomical and functional development of the preBötC

Rodent models have been used to study anatomical and functional development of the preBötC. Given the importance of NK1 as an anatomical marker for the preBötC, the spatiotemporal pattern of the preBötC NK1R neurons has been examined by double labelling for the 5-Bromo-2'deoxyuridine (BrdU) and NK1 in order to reveal the ontogenesis of the preBötC neurons. In the preBötC region strong NK1R labelling was observed at E15 in mice and E17 in rats (Pagliardini *et al*., 2003; Thoby-Brisson *et al*., 2005). Another method to study the anatomical development of preBötC neurons is to record the rhythmic activity of the preBötC neurons in order to detect the generation of first inspiratory bursts. The emergence of the preBötC spontaneous rhythmic activity at E17 in rats and E15 in mice corresponds with the first ultrasound detection of the rhythmic fetal breathing

movements (Kobayashi *et al*., 2001; Pagliardini *et al*., 2003; Onimaru *et al*., 1988; Thoby-Brisson *et al*., 2005). Studies using transgenic mice revealed that the preBötC NK1 and SST immunoreactive neurons are derived from the transcription factor Dbx1 (Bouvier *et al*., 2010; Gray *et al*., 2010). They showed that mice lacking the transcription factor Dbx1 displayed a failure of inspiratory bursts generation *in vitro* and lack of spontaneous breathing movements *in vivo* (Bouvier *et al*., 2010; Gray *et al*., 2010). Thus, it was proposed that the preBötC Dbx1 neurons are essential for normal respiratory rhythm generation. Selective photonic destruction of preBötC Dbx1 neurons in neonatal mouse slices impairs the respiratory frequency and attenuates the motor output magnitude (Wang *et al*., 2014). More recent work has further investigated the role of the preBötC Dbx1-expressing neurons in the respiratory functions. The preBötC Dbx1 neurons have either pre inspiratory or inspiratory pattern of discharge, stimulating these neurons influence the respiratory rhythm or pattern, respectively (Cui *et al*., 2016).

1.2.4 Respiratory rhythm generation

Understanding the mechanism and location of the respiratory rhythm generation site is one of the ultimate goals in the field of respiratory neurophysiology. The preBötC has been postulated to contain the neurons necessary for inspiratory rhythm generation (Smith *et al*., 1991). Based on previous studies that showed the importance of excitatory transmission in the preBötC for rhythm generation (Funk *et al*., 1993; Mackenzie *et al*., 2006) currently there are two major hypotheses that explain the process of rhythm generation in the preBötC complex. The first hypothesis suggests that a small population of neurons with pacemaker properties situated in the preBötC complex initiate and drive inspiration. The presumed PreBötC pacemaker neurons are characterized by their intrinsic bursting proprieties (Del Negro *et al*., 2002; Del Negro *et al*., 2005; Feldman *et al*., 2013).

The preBötC neurons with pacemaker properties represent only 5-25% of preBötC inspiratory neurons (Del Negro *et al*., 2005). It has been proposed that pacemaker preBötC neurons are excitatory/glutamatergic although some inhibitory/glycinergic neurons in the preBötC display intrinsic pacemaker properties (Winter *et al*., 2009; Morgado-Valle *et al*., 2010). The bursting of preBötC pacemaker neurons depends on a persistent Na+ current (I_{NAP}) and Ca-sensitive, non-sensitive cation current (I_{CAN}, Feldman and Del Negro, 2006). However, the observation that some preBötC neurons display an intrinsic bursting proprieties

doesn't explain whether they are essential for respiratory rhythm generation or not. Selective destruction of the preBötC pacemaker neurons will be necessary in order to examine their influence on the rhythmogenesis process, so far all the available *In vitro* or *In vivo* data didn't provide conclusive evidence whether the preBötC pacemaker neurons are essential for the inspiratory rhythm generation process or not.

The second hypothesis for respiratory rhythmogenesis is the group pacemaker hypothesis (Feldman and Del Negro, 2006). In the group pacemaker hypothesis the inspiratory burst is generated through both recurrent excitation and pacemaker neurons. According to this proposed mechanism, recurrent excitation builds up via positive feedback process during the pre-inspiratory period to recruit intrinsic currents (I_{CAN} and I_{NAP}) that in turn generate an inspiratory burst. The inspiratory burst termination is still unresolved issue, but it could be due to synaptic inhibition (Feldman and Del Negro, 2006).

1.2.5 Retro-trapezoid nucleus and the para facial respiratory group

The RTN/pFRG is composed of heterogeneous neuronal populations that show different patterns of respiratory modulated activity and project to the respiratory ponto medullary centers (Smith *et al*., 2013, Mulkey *et al*., 2004, Guyenet *et al*., 2005). The RTN was initially described in cats as a group of neurons caudal to the trapezoid body that projects to the rostral and ventral respiratory groups (Smith *et al*., 1989). RTN neurons are sensitive to changes in CO_2/pH levels therefore it has been proposed to function as a central chemoreception area (Mullkey *et al*., 2004; Takakur *et al*., 2008; Abbott *et al*., 2009,2011; Guyenet *et al*., 2009). RTN provides excitatory inputs to the respiratory centers in the ventrolateral medulla which modulates respiration in order to meet various metabolic demands (Mulkey *et al*., 2004, Guyenet *et al*., 2005). Connelly and colleagues (1990) recorded different respiratory modulated neuronal activities within the region of the RTN which suggests that the RTN region may encompass multi-functional respiratory modulated neurons. Later on, studies showed that the RTN neurons express the transcription factor Phox2b (Stornetta *et al*., 2006). In addition, it has been demonstrated that the chemo sensitive RTN neurons are glutamatergic (Mulkey *et al*., 2004) and NK1R positive (Nattie and Li, 2002) (Fig. 1.3, 1.4). Moreover, selective photo-activation of Phox2b expressing RTN neurons transfected with

channelrhodopsin-2 *in vivo* increased ventilation, which is consistent with their proposed role as chemo sensitive neurons (Abbott *et al*., 2009, 2011).

The embryonic pFRG contains neurons within the same region of the RTN around the facial motor nucleus. These neurons show the first recorded inspiratory rhythmic neuronal activity at E14.5 in mice (Thoby-Brisson *et al*., 2009), and they are Phox2b-positive glutamatergic neurons derived from Egr2-expressing progenitors (Thoby-Brisson *et al*., 2009). It is still unknown whether the RTN/pFRG neurons are identical, overlap, or have distinct functions throughout different developmental stages. The identity and anatomical delineation of the para facial groups is a complex issue in the field of respiratory neurophysiology. Multi-functional neuronal populations expressing various anatomical and genetic markers are located within a restricted zone around the facial nucleus, thus it is challenging to distinguish between the para facial neuronal populations.

1.2.6 RTN/pFRG roles in respiratory control

Onimaru and colleagues (1988, 1997, 2003, and 2006) demonstrated the presence of pre inspiratory rhythmic activity in the pFRG in brainstem-spinal cord preparation of newborn rats. In this preparation, pFRG neurons were firing just before the inspiratory motor output, hence classified as pre inspiratory (pre I) neurons (Onimaru and Homma, 2003). It was proposed that the preI neurons provide a rhythmic excitatory drive that entrains the preBötC inspiratory oscillator (Onimaru and Homma, 2003). By applying optical imaging techniques Oku and colleagues (2007) found that the pFRG rhythmic activity is reduced then shifted into inspiratory pattern during early neonatal development. Moreover, *In vivo* results further support the pFRG contribution in the respiratory control process. In juvenile rats, complete transection of the brainstem at the level of the caudal tip of the facial nucleus abolished active expiration, however rhythmic inspiration remained unaffected (Feldman and Janczewski, 2006). The RTN/pFRG rhythmic activity is absent in adult anesthetized rats at rest (Pagliardini *et al*., 2011).

The RTN neurons sensitivity to CO_2/pH levels is state-dependent, more powerful during wakefulness and non-rapid eye movement (non-REM) sleep and reduced during rapid eye movement (REM) sleep (Burke *et al*., 2015). Selective photoactivation of the RTN neurons increases the respiratory frequency during wakefulness and non-REM sleep, but does not alter the respiratory frequency during

REM sleep (Burke *et al*., 2015). Respiration during REM sleep becomes irregular and sleep disordered breathing occurs most frequently during REM sleep (Orem and Kubin, 2006). Skeletal muscles atonia is another characteristic of REM sleep, which affects skeletal and respiratory muscles. Interestingly, the diaphragm, the main inspiratory muscle, remains relatively unaffected (Orem and Kubin, 2006). However, evidence from our laboratory showed that, at least in adult rats, expiratory modulated abdominal muscle activity is frequently recruited during REM sleep (Pagliardini *et al*., 2012; Andrews and Pagliardini, 2015). Moreover, the abdominal muscle recruitment during REM sleep is preceded by increased respiratory irregularities, which tend to be more regular once the abdominal muscles are recruited (Andrews and Pagliardini, 2015). Thus, the abdominal muscles recruitment could contribute to maintain ventilation during REM epochs. Moreover, the proposed conditional expiratory oscillator pFRG might be state-dependant modulated (Andrew and Pagliardini, 2015).

The observation that inspiration and/or expiration could be independently controlled lead to the hypothesis that respiratory movements are controlled by dual respiratory oscillators. It has been proposed that a subpopulation of pFRG/RTN neurons represents an expiratory oscillator that is coupled to the inspiratory oscillator, the preBötC, to generate coordinated respiratory rhythms (Feldman & Del Negro 2006; Janczewski & Feldman 2006). The differential effects evoked by local

application of μ-opiates agonists on the preBötC inspiratory neurons and the pre inspiratory RTN/pFRG neurons provided additional evidence that the respiratory rhythm might be generated by dual oscillators. In slice preparations local application of the μ-opiates agonists into the preBötC slowed the respiratory frequency, while in *en bloc* preparations which contains both the preBötC and the pFRG/RTN μ-opiates agonists induced a quantal slowing (Gray *et al*., 1999; Mellen *et al*., 2003, Takeda *et al*., 2001). Quantal slowing reflects the incomplete process of inspiratory rhythm generation, preI bursts generated by the opioid insensitive oscillator failed to generate inspiratory bursts due to the opioid induced depression, therefore an overall elongation of the respiratory period is observed (Mellen *et al*., 2003). Additionally, other selective opiate agonist experiments (Janczewski and Feldman, 2006) suggest that active expiration is driven by another opiate insensitive oscillator. This oscillator is characterized by being silent under resting conditions, however upon certain stimulations, such as: increase metabolic demands, or exercise, generates expiratory rhythmic oscillations (Pagliardini *et al*., 2011). Selective stimulation of RTN/pFRG by either disinhibition or optogenetic excitation generates active expiration which further supports the role of RTN/pFRG as a conditional expiratory oscillator (Pagliardini *et al*., 2011). Thus, the absence of significant rhythmic neuronal activity in the RTN/pFRG under resting conditions (Fortuna *et al*., 2008) reflects the absence of active expiration (Feldman & Del Negro 2006).

Currently it is still under investigation whether the two functions of the RTN/pFRG (conditional expiratory oscillator and central chemoreception area) are controlled by the same neuronal population or there are two or more distinct neuronal groups within the RTN/pFRG region. Pagliardini and colleagues (2011) demonstrated that stimulating the lateral pFRG area by either direct excitation or local disinhibition elicited active expiration. Moreover, brief optogenetic stimulation of pFRG neurons generated active expiration and reset the respiratory rhythm. Light pulses immediately terminated the ongoing inspiration by inducing an active expiration (Pagliardini *et al*., 2011). Photoactivation of the more medial RTN Phox2b neurons induced a respiratory reset as well, however in this case respiratory reset was caused by elongation of the inspiratory time (Abbott *et al*, 2011). The different results achieved by stimulating either RTN or pFRG suggest that these two adjacent regions may play different roles in respiratory control. Huckstepp and colleagues (2015) recently investigated the roles of the two adjacent para facial regions in controlling respiratory activity. By manipulating the parafacial areas with different forms of hyperpolarization or disinhibition they provided further evidence for the role of the lateral parafacial region,(corresponding to the pFRG) as a conditional expiratory oscillator, silent at rest and generating active expiration when activated. Moreover, they found that the ventral para facial group (corresponding to the classic chemosensitive area of RTN) is responsive to changes in pH/CO_2 and

integrates other sensory afferents affecting respiratory drive (Huckstepp *et al*., 2015).

1.3 Methods to manipulate neural activity

Controlling neural activity in order to test a hypothesis is one of the ultimate experimental techniques in neuroscience research. Physical, electrical, genetic and pharmacological methods were developed to provide different forms of neural control in order to fit different experimental needs and procedures. Each method has different advantages and disadvantages, choosing the best tool for each experimental model is an important aspect in order to get as accurate results as possible. Additionally, combining one or more of neural control methods would facilitate more precise perturbation in order to adjust stimulus parameters or to limit stimulation into a predefined area of interest. In the next sections I will provide examples of various respiratory studies that utilized one or more of neural control methods.

1.3.1 Electrical control

Electrical stimulation has been used to study respiratory responses by providing either direct or indirect stimuli to different nerves or brain regions. In 1954 Baxter and Olszewski used electrical stimulation to study the role of pontine

tegmentum in inspiratory responses, demonstrating that electrical stimulation of different points within the pontine tegmentum evoked several inspiratory responses. Later on, in 1969 Howard and colleagues stimulated the carotid sinus nerve in adult cats then recorded the phrenic nerve activity in order to study phase resetting of the respiratory rhythm.

Electrical stimulation lacks spatial control because the current injection stimulates every neuron within the region of interest regardless of cell phenotype, as well as axons in passage. However, electrical stimulation has a good temporal control and can be used when the stimulation is not targeting a specific neuronal population, thus the stimulation site is only anatomically controlled.

1.3.2 Pharmacological control

Neural activity can be also manipulated pharmacologically, for example by using selective agonists or/and antagonists that bind to specific receptors and affect neuronal functions. Pharmacological techniques have high spatial precision as neuromodulation is specific to the neurons expressing certain markers (receptor, enzyme, etc). Pharmacological tools have been used widely in the field of respiratory research, for example different opiate agonists have been used to test respiratory oscillator theories (Takeda *et al*., 2001; Mellen *et al*., 2003; Gray *et al*., 1999; Janczewski & Feldman 2006). In other studies, the use of toxin conjugated to

peptides eliminated specific subpopulation in preBötC area therefore demonstrated the fundamental role of these neurons in respiratory rhythmogenesis (Gray *et al*., 1991; Mckay *et al*., 2005). Pharmacological agents have a good spatial control but their temporal control is limited as their effect depends on drug diffusion, intracellular responses, and drug metabolism. Nevertheless, pharmacological agents facilitate the identification of the respiratory oscillators (Gray *et al*., 1999; Mellen *et al*., 2003).

1.3.3 Optogenetics

Neuroscience research is based on a variety of excitation, inhibition, ablation, and lesioning methods to induce either gain of or loss of function in order to control different neuronal populations of interest. Recently, optogenetic techniques have been developed to minimize the limitations of other experimental approaches and to precisely perturb, control, excite, or inhibit any neuronal population.

Optogenetics technique is an approach to control the neural activity of any neuronal population by integrating both optic and genetics tools (Stuber *et al*., 2013). This experimental approach allows a better control of both the stimulation parameters and the targeted neurons. Light pulse stimulation allows activity within specific neuronal populations to be selectively controlled with high temporal and spatial precision. Optogenetics tools can be used either to stimulate or to inhibit the activity of neural populations by using different light activated proteins (Fenno *et al*., 2011) along with specific light wavelengths (Butler, 2012).

Moreover, the ability of optogenetic techniques to modulate the transduced tissue activity depends mainly on light delivery method. Optic fibers have been used in *in vivo* studies in both behaving and anesthetized animal models to deliver light pulses in order to initiate the desired effects (Zhang *et al*., 2010).

Channelrhodopsin (ChR2) based optogenetics is a method used to activates neurons. ChR2 is a light-sensitive ion channel that opens and depolarizes neurons

when excited by 473nm blue light (Nagel *et al*., 2003). ChR2 based optogenetics provide extremely high temporal control. Viral vectors and other genetic tools have been used to introduce the opsins into the host tissue of interest (Zhang *et al*., 2006). Lentiviruses and adeno-associated viruses incorporate their DNA into the host cell which facilitates the photosensitive channels expression in the tissue of interest (Buchschacher, 2003). In optogenetics, viral vectors specificity is determined by controlling opsin expression by means of insertion of a specific promoter into the viral vector, limiting the spatial expression of the injected viral vector, and/or targeting light stimulation to a specific region (Fenno *et al*., 2011). Therefore, a combination of an adeno-associated virus with specific cell-type promoter allows specifically targeting neuronal populations of interest.

The photosensitivity of the opsin genes is not reduced by inserting the sequence of a fluorescent protein into the viral vector which is an advantage for post-mortem histological opsins identification (Zhang *et al*., 2006). Therefore, viral vectors composed of cell-type specific promoters, opsins, fluorescent tag genes is a current approach for delivering opsin genes into a specific neuronal population (Zhang *et al*., 2006).

1.4 Thesis aims

Understanding the mechanisms underlying respiratory rhythmogenesis is one of the ultimate research goals in the field of respiratory neurophysiology. Projects presented in this thesis were aimed to investigate the effects of different stimuli on the respiratory oscillators.

In the first project, by using optogenetics techniques, which provide a high temporal resolution, I determined the ventilatory responses elicited by a fine temporal activation of the preBötC neuronal network. While previous pharmacological studies have demonstrated that respiratory rhythm and pattern can be influenced by multiple pharamchological agents both *in vivo* and *in vitro*, no previous studies were conducted to test the respiratory responses evoked by brief depolarization of the preBötC network. We hypothesized that if an excitatory drive is necessary for rhythm generation process, brief depolarization of the preBötC neurons by laser pulses will activate the respiratory network and increase the respiratory rate, in addition to finely control onset and reset of breathing during ongoing breathing and in absence of ongoing respiratory events. We therefore aimed to examine the respiratory responses elicited by a generalized non-selective optogenetic excitation to the preBötC network.

In the second project, we investigated the stimulatory effects of cholinergic transmission on the pFRG activity recruitment and active expiration. Recent results

from our lab demonstrate that active expiration occurs during REM epochs, however mechanisms involved in abdominal muscles recruitment both during anesthesia and in natural sleep are still unknown.

By considering the proposed role of the pFRG as a conditional expiratory oscillator we proposed that the pFRG may become active during REM epochs and this activation may be responsible for active expiration. We hypothesized that cholinergic inputs may contribute to the RTN/pFRG level of excitation, therefore we aimed to examine the respiratory responses evoked by cholinergic perturbations on the RTN/pFRG under urethane anesthesia.

By locally applying acetylcholinesterase inhibitor and cholinomimetics along with pFRG neurons recording and histological examinations, we demonstrated that cholinergic transmission contributes to the pFRG neurons excitation and promotes both active recruitment of abdominal muscles and active expiratory flow, demonstrating pFRG sensitivity to cholinergic neurotransmission under urethane anesthesia. Moreover, distinct results were achieved by stimulating with cholinomimetics either the medial (RTN) or lateral (pFRG) parafacial regions. These results improve our insights into the role of cholinergic transmission in expiratory muscles recruitment and active expiration, add additional evidence for the pFRG as a conditional expiratory oscillator, and suggest that RTN and pFRG regions may provide different contributions to respiratory control.

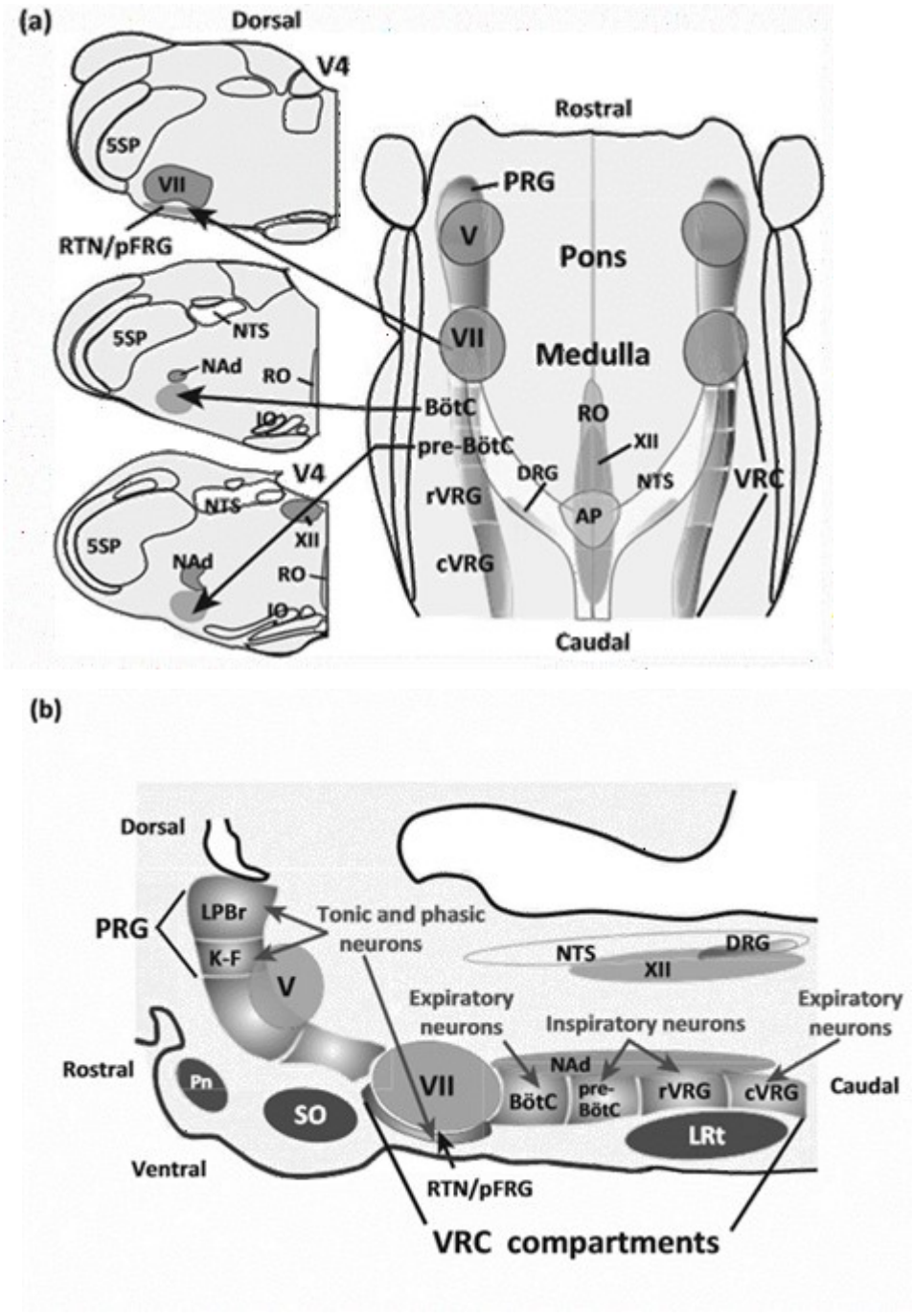

Figure 1.1 Schematic of the respiratory brainstem nuclei

A) Horizontal (right) and serial coronal (left) representational sections of the brainstem respiratory compartments. **B)** a parasagittal view of one side of the brainstem illustrating various respiratory compartments involved in distinct

respiratory functions. Inspiratory, expiratory, tonic, and phasic neurons are indicated. Abbreviations: AP, area postrema; LRt, lateral reticular nucleus; NAd, nucleus ambiguus, dorsal division; Pn, ventral pontine nucleus; SO, IO, superior and inferior olivary complexes; SP5,spinal trigeminal nucleus; V, motor nucleus of the trigeminal nerve; V4, fourth ventricle; XII, hypoglossal motor nucleus. **[** Used with permission, Modified from Smith *et al*., 2013]

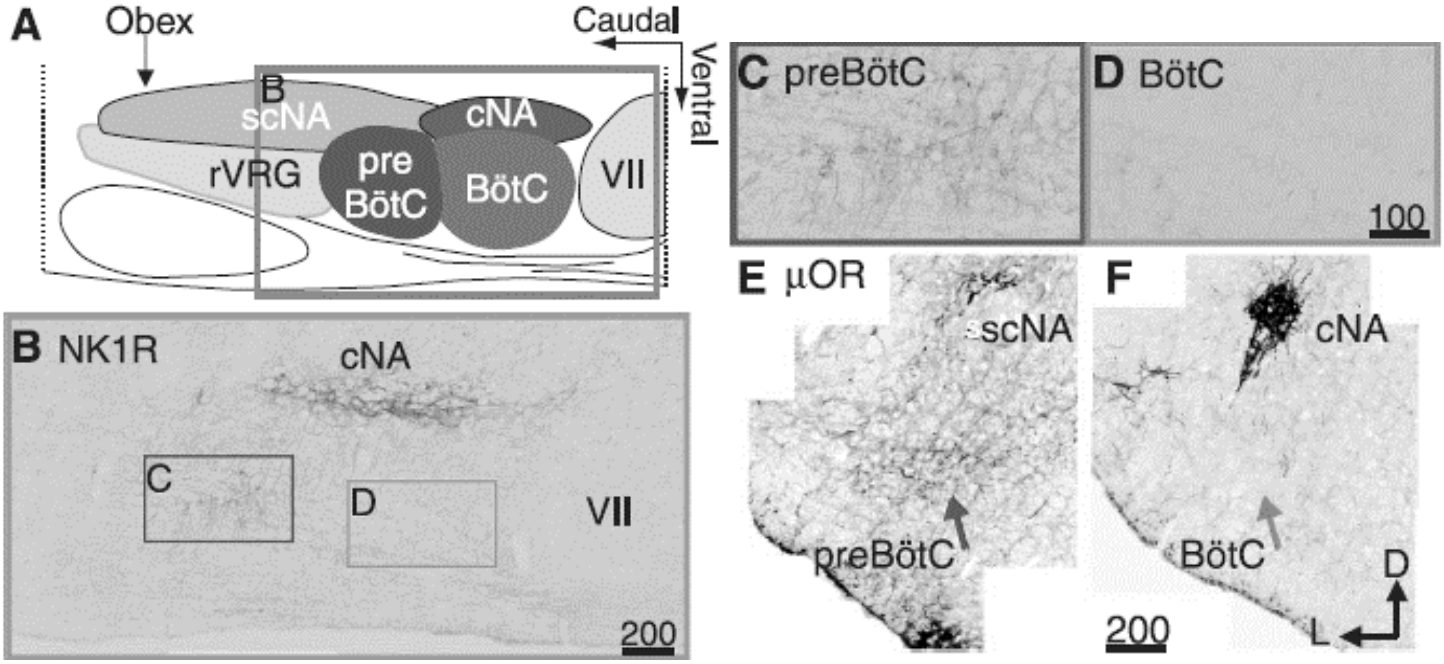

Figure 1.2 NK1R- and μOR-expressing neurons are limited to and define the preBötC.

(**A**) Illustration of the location and boundaries of ventral respiratory column regions and adjacent nucleus ambiguus motoneuron pools in sagittal section. (**B**) NK1R expression in a single sagittal section through the respiratory column corresponding to box in (A). Higher magnification images showing cell soma staining from preBötC (**C**) and relative lack of staining in BötC (**D**). Confocal, negative composite images of μOR immunohistochemical staining indicating different expression levels

in the preBötC (**E**) (blue arrow) and BötC (**F**) (red arrow) in transverse section. **[** Used with permission, From Gray *et al*., 1999].

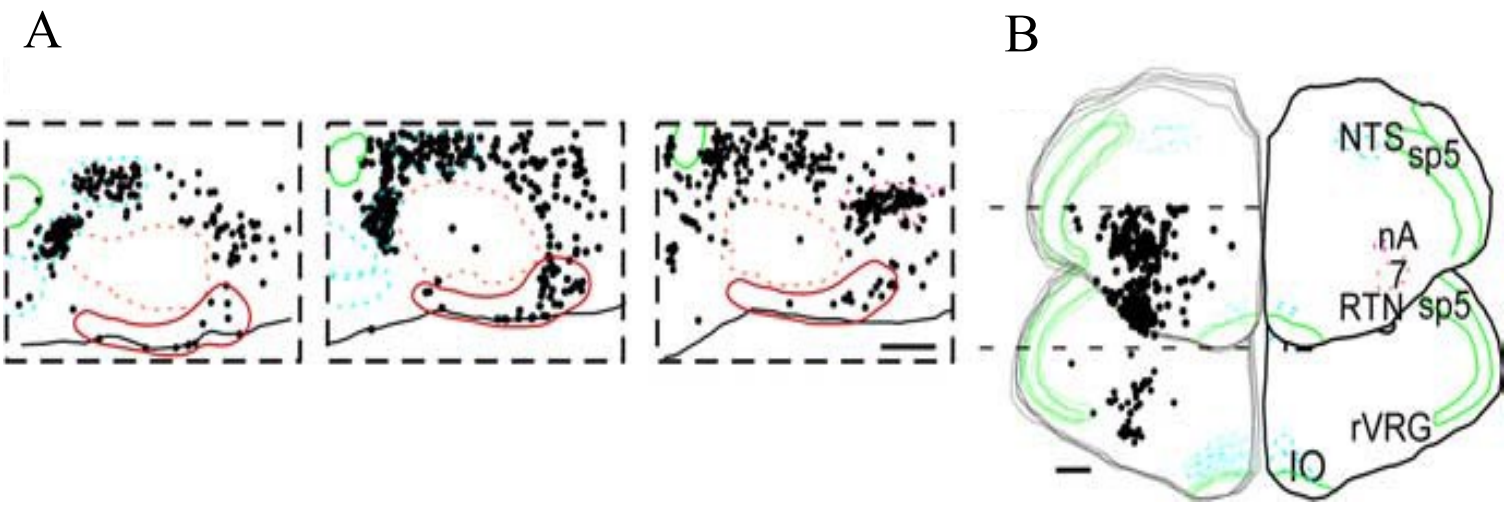

Figure 1.3 Phox2b expression in the RTN

A. Location of Phox2b-ir neurons in parasagittal sections (from left to right: 2.4, 2.2, and 1.9 mm lateral to the midline). The dense clusters of Phox2b-ir neurons located dorsal and rostral to the facial motor nucleus are the parasympathetic neurons of the inferior and superior salivatory nuclei. The motor neurons of nucleus ambiguus are also labeled. ***B***, Top left side is a stack of five coronal sections (90 µm apart) straddling the region from bregma_11.4 to_11.9 mm according to Paxinos and Watson (1998) and is therefore centered on the caudal most end of the facial motor nucleus. The bottom left stack of five sections spans the region from bregma_12.6 to_13.1 mm and encompasses the preBötC and rVRG regions. Each dot in ***A*** and ***B*** represents a single Phox2b-ir neuron placed on the section by computer-assisted

plotting. The right-hand side of each section in ***B*** is traced as an overlay of the left-hand stack to illustrate the specific brain areas. Scale bars: 500 µm. [Used with permission, Modified from stornetta *et al*., 2006]

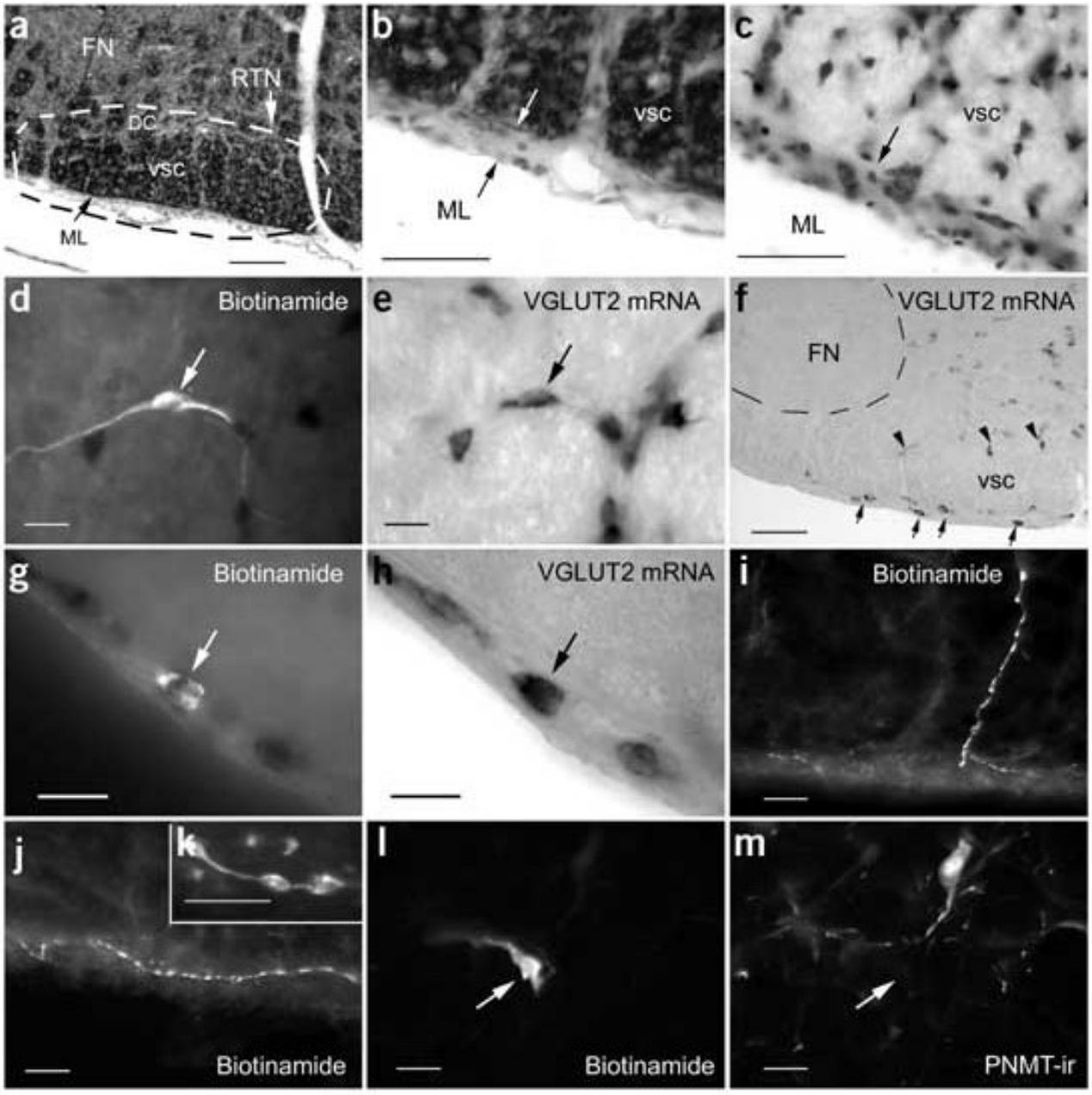

Figure 1.4 Anatomical description of RTN CO_2 – activated neurons

A) Approximate boundary of RTN (30 µm-thick coronal section processed with Woelcke's iron-hematoxylin myelin stain; bregma level -11.5 mm). RTN is bisected

by the ventral spinocerebellar tract (vsc; darkly stained) into a dorsal-cap region (DC) and a ventral or marginal layer (ML). **B)** The ML at higher magnification. **C**) ML in a Nissl-stained coronal section. **D.E)** CO_2 - activated neuron of RTN dorsal cap labeled with biotinamide (d, Alexa 488 fluorescence) contains intense VGLUT2 mRNA reaction product (e, bright-field). **F)** Darkly labeled VGLUT2 mRNA−positive neurons are present both within the ML (arrows) and the dorsal cap of RTN (arrowheads) but are absent from the facial motor nucleus (FN). **G.H)** Glutamatergic CO_2 - activated neuron located in ML. (g) Biotinamide; Alexa Fluor 488 fluorescence. (h) VGLUT2 mRNA; bright-field illumination of the same field. (i) Characteristic vertical dendrite of biotinamide-labeled CO_2 - activated neuron (dorsal-cap neuron). Dendrite extends to and bifurcates at right angles within the ML. **J)** Superficial dendrite located within the ML of RTN (continuation of the dendrite shown in i). **K)** Typical varicose dendrite of CO_2-activated neuron within the ML. (l,m) Biotinamide-labeled CO2-activated neuron of RTN (l, arrow, Alexa 488 fluorescence) lacks PNMT immunoreactivity (m, Cy3 fluorescence), and hence it is not a C1 cell. Calibration bars, 100 µm (a,f); 50 µm (b,c); 20 µm (d, e, g-j ,l ,m); 10 µm (k) [Used with permission, From Mulkey *et al*., 2004].

CHAPTER II*

Optogenetic Excitation of PreBötzinger Complex Neurons Potently Drives Inspiratory Activity in Vivo

---

*Previously published paper.

Zaki Alsahafi, Clayton T. Dickson, and Silvia Pagliardini

J Physiology 593.16 (2015) pp 3673–3692

My contribution to this study includes performing the experiments, analying the data and participating in the manuscript preparation. Clayton T. Dickson assisted with the data analysis and manuscript preparation. Silvia Pagliardini was the supervisory author responsible for the experimental design and the manuscript preparation.

2.1 Introduction

The neural control of respiratory rhythms occurs in the brainstem and is produced by a rhythmogenic neural network within the region of the preBötzinger complex (preBötC). This area has been identified in rodents, large mammals and humans (Smith *et al*., 1991; Gray *et al*., 1999; Pagliardini *et al*., 2003; Wenninger *et al*., 2004; Thoby-Brisson *et al*., 2005; Schwarzacher *et al*., 2011). Although the precise cellular mechanisms of respiratory rhythm generation are unresolved (Feldman *et al*., 2013), the necessity and sufficiency of the preBötC for respiratory rhythm generation has been demonstrated in vivo and in vitro in experiments where preBötC neurons have been destroyed, temporally inactivated, or genetically deleted (Gray *et al*., 2001; Tan *et al.,* 2008; Bouvier *et al.,* 2010; Gray *et al.,* 2010).

Breathing has to be coordinated with a host of other motor behaviours, and to do so it requires coordination of these behaviours and their sensory feedback with the moment-to-moment regulation of breathing. The ability to integrate this information, and consequently adapt respiratory rhythms, is therefore an essential property of the respiratory rhythm generator in order to pace respiration, integrate volitional breathing, maintain adequate levels of blood gases, and coordinate orofacial behaviours like vocalization, whisking, sniffing and swallowing (Dick *et al.,* 1993; Gariepy *et al.,* 2012; Moore *et al.,* 2013, 2014). Prior studies have investigated how different feedback mechanisms or structures that provide direct or

indirect inputs to the preBötC region affect ongoing respiratory rhythms, in an attempt to demonstrate how afferent information such as peripheral and central chemoreceptors (Eldridge, 1972a,b; Eldridge *et al*., 1989; Paydarfar *et al.,* 1998; Abbott *et al.,* 2011), somatosensory inputs (Potts *et al*., 2005), superior laryngeal nerve activity (Oku & Dick, 1992), or the parafacial respiratory group (pFRG) (Pagliardini *et al.,* 2011) influence the inspiratory oscillator and, consequently, ventilation.

Brief electrical stimulation of different structures can generate a phase-dependent (Type 1) or a phase-independent (Type 0) reset of the respiratory rhythms depending on the strength of the stimulus (Winfree, 2001). For example, carotid sinus nerve stimulation (Eldridge, 1972b; Paydarfar *et al.,* 1998) generates Type 1 respiratory reset, with changes in inspiratory and expiratory time according to the phase of the respiratory cycle at which stimulus is delivered (Eldridge, 1972b). Electrical stimulation of either superior laryngeal nerve via a facilitatory mechanism, (Paydarfar *et al*., 1986; Oku & Dick, 1992), or midbrain reticular formation via an inhibitory mechanism, on the contrary, generates a phase-independent (Type 0) respiratory reset (Paydarfar & Eldridge, 1987).

More recently, optogenetic stimulation has been used in place of electrical stimulation to demonstrate reset properties of the respiratory rhythms. Optogenetic stimulation of Phox2b cells in the retrotrapezoid nucleus (RTN) generates a Type 1

reset behaviour (Abbott *et al.,* 2011), whereas Type 0 expiratory-driven respiratory reset was generated by optogenetic stimulation of the pFRG (Pagliardini *et al.,* 2011). Direct stimulation of the inspiratory oscillator has been obtained in the past via electrical or pharmacological manipulations of the preBötC region in vivo (Speck & Feldman, 1982; McCrimmon *et al.* 1986; Solomon *et al.,* 1999; Wang *et al.,* 2002), but these techniques lack precise spatial and /or temporal specificity and in these cases, a fine description of respiratory reset or entrainment properties is not available. Respiratory rhythms can also be entrained through paced RTN stimulation (Abbott *et al.,* 2011) or somatic afferent electrical stimulation (Funk *et al.,* 1992; Potts *et al.,* 2005; Giraudin *et al.,* 2012) up to 2 times the baseline frequency.

Here, using optogenetic techniques, we directly excited neurons of the preBötC in a temporally and spatially specific manner in order to deliver an excitatory stimulus directly to the core unit of inspiratory rhythmogenesis.

We hypothesized that if an excitatory drive is necessary for rhythmogenesis, optogenetic stimulation of preBötC will strongly activate the network and consequently increase respiratory rate. In addition, we hypothesized that if excitatory connections between neurons of the respiratory oscillators are key for driving respiratory activity, a brief but synchronous excitation of the circuit elements would reset the rhythm and entrain it at very high rates with short delay while having little effect on ongoing respiratory rhythm if stimulus was delivered during inspiration.

Our results indicate that photostimulation of the preBötC in vivo induced an instantaneous increase in breathing rate and was also able to entrain rhythm at very high frequencies (4-fold the ongoing frequency) as well as reset inspiratory rhythms with Type 0 characteristics. Furthermore, we identified the presence of a refractory period during and following inspiration when excitatory inputs are not capable of generating an additional inspiratory event.

2.2 Methods

2.2.1 Ethical approval

Animal care and experimental protocols were approved by the Health Science Animal Policy and Welfare Committees of the University of Alberta according to the guidelines established by the Canadian Council on Animal Care and it is in compliance with the guidelines of The Journal of Physiology (Drummond, 2009).

2.2.2 Viral injection into preBötC

An adeno-associated virus (AAV, serotype 2/5) that expresses channelrhodopsin (ChR2) and the fluorescent protein EYFP driven by the synapsin promoter (SYN-ChR2-EYFP) was produced, characterized and titrated at the University of North Carolina Virus Vector Core Facility, Chapel Hill, NC, USA (4×1012 molecules ml–1). The same serotype virus that expresses EYFP driven by the synapsin promoter but lacks expression of the light-sensitive protein (SYN-EYFP, University of North Carolina Vector Core) was also used at the same concentration for control experiments.

Unilateral viral injection into the preBötC was performed in 270–320 g Sprague–Dawley rats under anaesthesia (ketamine (90 mg kg–1), and xylazine (10 mg kg−1), administered I.P.) using standard aseptic procedures. Rats were

positioned on a stereotaxic frame with bregma 5 mm below lambda. The occipital bone was exposed and a small window was opened to perform viral injections. A glass pipette with external tip diameter of ~30 µm was inserted into the preBötC and the adeno virus (500 nl) was delivered by controlled back-pressure injection (20 p.s.i., 15 – 35 ms pulses; PicoSpritzer III Parker, Milton, ON, Canada). Coordinates were as follows (in mm): + 0.9 rostral, + 2.0 lateral and − 2.8 ventral to the obex. The electrode was left in place for 5 min after injection to minimize backflow of virus up the electrode track. Neck muscles and skin were sutured back at the end of the surgery and rats were allowed to recover with pain medication, food and water *ad libitum* for at least 2 weeks. The surgical procedures and viral injection produced no observable long term behavioural or respiratory effects.

2.2.3 Photostimulation experimental protocol

Two to three weeks after viral injection, rats were anaesthetized with isofluorane (2 % in air) while the femoral vein was cannulated, and then urethane (1.5–1.7 g (kg body weight)$^{-1}$) was gradually delivered I.V. to induce permanent and irreversible anaesthesia. Body temperature was kept constant at 37 ± 1°C with a servo-controlled heating pad (Harvard Apparatus, Holliston, MA, USA). Respiratory flow was measured via a tracheal cannula connected to a pressure transducer (F10L, GM Instruments, Kilwinning ,UK) and signal was measured in millivolts (Valydine, Northridge, CA, USA). Tidal volume was obtained by

integration of airflow amplitude and millivolt values were converted to millilitres of air by comparison with a 5 - point calibration curve constructed by the experimenter at the time of the experiments (0.5 – 5 ml range). Coupled EMG wire electrodes (CoonerWire, Chatsworth, CA, USA) were implanted into diaphragm (DIA), genioglossus (GG) and abdominal (ABD) muscles. EMG wires were connected to differential amplifiers (AM Systems, Sequim, WA, USA) and activity was sampled at 2 kHz (Powerlab 16/35; AD Instruments, Colorado Springs, CO, USA). Rats were vagotomized at mid-cervical level and then positioned supine in a stereotaxic frame. The larynx was displaced, and the ventral surface of the occipital bone was exposed. The occipital bone was drilled to expose the ventral surface of the brainstem while the meninges overlying the brain tissue were left intact. The end of a 200 µm-diameter optical fibre connected to a 473 nm laser (IkeCool, Anaheim, CA, USA) was positioned ipsilaterally, touching the ventral surface of the brainstem. Distance from the preBötC region was therefore 300 – 500 µm, according to the histology and the Paxinos atlas. Laser power was set to deliver light at 10 – 12 mW. Timed photostimulations were delivered under the command of the LabChart7 acquisition software connected to the laser power supply. To find the position with the strongest response to laser stimulation in rats infected with SYN-ChR2-EYFP, the ventral surface was probed at 2 mm from the midline with trains of high frequency photostimulation (20 ms pulses at 20 Hz, ×300) at 1 min intervals (three times in

each location) along the rostrocaudal axis with 500 μm step intervals. Only one or two rostrocaudal positions resulted in an increased respiratory frequency response according to the experimental procedure. Once the most responsive site was identified, either a single pulse of light stimulation (10 s) or a train of high frequency laser pulses (20 ms pulses at 20 Hz, ×300) were delivered several times to test for the respiratory response to photostimulation. Stimulation parameters were similar to what used in previous optogenetics studies on breathing control (Abbott *et al.,* 2009; Pagliardini *et al.,* 2011) and were identical for both SYN-ChR2-EYFP virus and SYN-EYFP experiments.

Entrainment responses were tested by delivering 15 brief photostimulations (150 – 250 ms in length) at increasing frequencies (0.7 – 3 Hz). Respiratory reset in rats infected with SYN-ChR2-EYFP was tested by delivering light pulses at random phase of the respiratory cycle (150 single light pulses, 100 ms to 1 s pulse length). The ability to generate respiratory activity uniquely by photostimulation was tested in mechanically hyperventilated rats once they reached their apnoeic threshold. During this experimental procedure, rats were connected to the mechanical ventilator with the ventilation rate set at about 10 – 15 breaths min^{-1} above the rats respiratory rate baseline. Within a short time from the beginning of the hyperventilation protocol, rhythmic diaphragmatic EMG (DIA_{EMG}) contractions were reduced and eventually lost. Once spontaneous breathing ceased,

photostimulation (150 – 250 ms pulse length) was delivered to the preBötC at frequencies that varied between 0.7 and 3Hz. Alternatively, a single 10 s light pulse or a train of photostimulation at high frequency (20 ms pulse length at 20 Hz) were delivered.

Four SYN-ChR2-EYFP preBötC rats, were treated with reserpine (10 mg kg−1), 12–18 h prior to the beginning of the optogenetic experiment, in order to reduce catecholaminergic influences on respiratory rhythmic activity. The behaviour of rats was monitored just prior to anaesthesia to ensure that catecholaminergic depletion took place (Clement et al. 2008).

2.2.4 Histology

At the end of each experiment, rats were transcardially perfused with 4% paraformaldehyde in phosphate buffer (PB). The brains were collected, post-fixed, and 50 µm brainstem transverse sections were cut with a VT1000 Vibratome (Leica, Wetzlar, Germany). Serial sections were either directly mounted on slides and coverslipped or immunoreacted for detection of specific neuronal markers (one section every 200 µm). Immunohistochemistry was performed according to the following protocol. Free-floating sections were rinsed in phosphate-buffered saline (PBS) and incubated with 10 % normal donkey antiserum (NDS) and 0.3 % Triton X-100 for 60 min to reduce non-specific staining and increase antibody penetration.

Sections were incubated overnight with primary antibodies diluted in PBS containing 1 % NDS and 0.2 % Triton X-100. The following day, sections were washed in PBS, incubated with the specific secondary antibodies conjugated to the fluorescent probes (Cy3 / Cy5-conjugated donkey anti-rabbit; Cy2-conjugatedanti-chicken;Cy3-conjugated anti-mouse; Jackson ImmunoResearch, West Grove, PA, USA) diluted in PBS and 1% NDS for 2 h. Sections were further washed in PBS, mounted, and cover slipped with Fluorsave mounting medium (Millipore, Billerica, MA, USA).

The primary antibodies used for this study detected the following proteins: green fluorescent protein (GFP; raised in chicken; Aves Labs, Tigard, OR, USA dilution 1:1000), neuronal nuclear marker (NeuN; raised in mouse; Millipore, 1:500), the receptor for substance P (NK1R; raised in rabbit; Millipore, 1:1000), the tyrosine hydroxylase enzyme (TH; raisedinrabbit; Millipore, 1:5000) the somatostatin peptide, (SST; raised in rabbit, Santa Cruz Biotechnology, Dallas, TX, USA1:600) and the immediate early gene cFos (raised in rabbit, Millipore, 1:1000).

Slides were then observed under a LSM512 Zeiss confocal microscope with a × 20 magnification objective or a Leica DM5500B fluorescent microscope. Rostrocaudal acquisitions of serial sections were performed along the respiratory column, from the end of the lateral reticular nucleus to the caudal tip of the facial nucleus. Acquisition of images within a 630×630 µm region were taken below the

nucleus ambiguus in between the lateral edge of the inferior olive and the medioventral extension of the spinal trigeminal tract. Within this region, SST and NK1R-expressing neurons identify the area and the rhythmogenic neurons within the preBötC complex (Gray *et al.,* 1999; Pagliardini *et al.,* 2003; Stornetta *et al.,* 2003). Within this defined area, NeuN-, NK1R- and SST-expressing neurons were identified and counted in order to determine the serial distribution of infected (EYFP-expressing) neurons. Since TH-expressing neurons are distributed more widely than preBötC, colocalization between EYFP and TH was studied in a wider area within the ventral medulla to incorporate the entire C1 neuron group in the histological analysis. For cFos immunopositive nuclei, serial rostrocaudal images of the ventral respiratory column were taken with a Leica DM5500B microscope with a × 20 magnification. Images were acquired with Metamorph (Molecular Devices, Sunnyvale, CA, USA) program and cFos positive nuclei were counted in a 1344 × 1024 µm window just below the nucleus ambiguus in both the stimulated and unstimulated side and a difference between the two sides was calculated along the rostrocaudal extension of the ventral respiratory column for both SYN-ChR2-EYFP and SYN- EYFP viruses.

2.2.5 Data analysis and statistics

Airflow, laser onset/offset, and EMG traces were acquired on a PowerLab 16/35 acquisition system and analysed using LabChart7 Pro (AD Instruments), Excel 2013, Matlab, and Origin8 (Origin-Lab, Northampton, MA, USA) software. The absolute value of EMG signals was digitally rectified and integrated with a time constant of 0.08 s to calculate peak amplitude. The respiratory airflow signal (ml s^{-1}) was used to calculate respiratory rate, period, tidal volume (V_T) and minute ventilation (V_E). Changes in period, respiratory rate and EMG peak amplitude were calculated and averaged for 15 respiratory cycles before photostimulation, and during the photostimulation period along the rostrocaudal respiratory column, and in the location where maximal respiratory response occurred. Statistical significance of respiratory changes before and during photostimulation was tested with a Student's paired t test ($P < 0.05$). The ability to entrain respiration with photostimulation was tested on a series of trials where coupling between laser pulses and inspiratory onset was detected on a breath by breath basis. Inspiratory activity was considered successful if ∫DIA peak amplitude reached at least 40 % of its value compared to baseline conditions. When coupling of photostimulation and inspiratory efforts occurred in 15 breaths over 15 photostimulation pulses (the length of the trial test), entrainment was considered to be 100%. Entrainment response was also

determined with a regression analysis between stimulus frequency and respiratory frequency output. Data are presented as averages ± standard error.

2.2.6 Reset analysis

We analysed perturbations (i.e. reset) in the otherwise stable respiratory rhythms that were evoked by delivering short duration (100 – 1000 ms) pulses of photostimulation at random phases of the ongoing oscillation. By triggering on a threshold (inward) value of the respiratory flow we were able to define the beginning of each inspiratory cycle and to calculate the baseline respiratory period in every trial. These values were used to convert latency values from the onset of inspiration into degrees (0–360 deg. where 0 deg. indicates the beginning of inspiration) by normalizing the ratio of latency values to the average cycle period across 360 deg. (for a graphical representation see Fig. 2.6). In this way, we could characterize the phase at which stimulation was delivered in addition to the phase of subsequent inspiratory events similarly to previously established methods (Pagliardini et al. 2011). Phase measurements for each experimental condition were binned in increments of 18 deg across the full 360 deg cycle and were analysed using circular statistics to test for non-uniformity (i.e. the systematic clustering of angular values) using the Raleigh z distribution (Zar, 1996). The average phase angle was calculated using the method of Batschelet (as described by Zar, 1996, pp. 608–610) and was characterized by a vector with an angle equal to the average phase and with a length

between 0 and 1 that reflected the angular dispersion of the individual phase values (where 0 reflects random and non-significant dispersion of angular values and 1 reflects a perfect alignment of angular values). A second-order circular analysis using the method of Hoteling (as described by Zar, 1996, pp. 638–639) was also applied across experiments on these individual experimental vectors to compute a grand average vector (again having both an angle and length) and also to test for non-uniformity, again using the Raleighz distribution. Phase measurements were obtained using custom software written in Matlab7.4 (The MathWorks).Results were plotted using Origin8 software.

When stimulation was delivered during inspiration (i.e. during active airflow) we determined if stimulation had any effect on ongoing inspiratory time (Ti).This was done by binning the average changes in Ti (compared to control values) as a function of stimulus phase across 10 deg. intervals through inspiration.

To determine the extent of the refractory period during 150 – 250 ms photostimulation experiments, we identified the rate of success (i.e. the ratio of short-latency generation of inspiratory events divided by the total number of stimulations) within intervals of 10 deg. from the offset of inspiration until the value of success rate reached 1 for every experiment (n = 5; 80 deg).

2.3 Results

2.3.1 Expression patterns of SYN-ChR2-EYFP in brainstem

Histological examination of transverse sections obtained from SYN-ChR2-EYFP-treated rats confirmed that injections were in the preBötC region (Fig. 2.1). Although some sparse scattered large EYFP-expressing neurons were located medial to the location of preBötC, the majority of EYFP-expressing neurons were located within the region of the preBötC, just below the nucleus ambiguus at a distance between 400 and 1200 µm from the caudal pole of the facial nucleus (Fig. 2.1). No viral infection of nucleus ambiguus motoneurons was evident. In infected neurons, the virus was weakly expressed in the somal region and more intensely localized in cellular processes.

We performed cell counting of EYFP-expressing neurons in a 630 μm^2 region centred just below the nucleus ambiguus, between the spinal trigeminal tract and the lateral edge of the inferior olive, where respiratory neurons of the ventral respiratory group are located (Gray et al. 2001). In this region, an average of 107.8 ± 5.9 neurons per section (43.3 ± 1.9 % of the NeuN-positive neurons; n = 5) expressed EYFP (Fig.2.1). EYFP expression was also identified in specific neuronal subpopulations of the ventrolateral medulla. These included neurons expressing the receptor for substance P (NK1R) and the peptide somatostatin (SST), two classic anatomical

markers used for the identification of preBötC respiratory neurons (Gray *et al.,* 1999; Stornetta *et al.,* 2003), as well as neurons expressing tyrosine hydroxylase (TH), an enzyme present in C1 noradrenergic neurons (Abbott *et al.,* 2013a). Although not exclusively present in the preBötC area, high concentration of NK1R and SST demarcate the area where rhythmogenic neurons have been identified in both the perinatal and adult rodent brain (Gray *et al.,* 1999, 2001; Pagliardini *et al.,* 2003; Stornetta *et al.,* 2003; Tan *et al.,* 2010). Within the preBötC region, 56.0 ± 3.1 % of NK1R-expressing neurons and 39.6 ± 2.3 % of SST-expressing neurons also co-expressed EYFP (n = 6). A much smaller proportion of TH-expressing neurons (8.6 ± 0.6%, n = 6), which were usually localized medial and ventral to NK1R and SST-expressing neurons, co-expressed EYFP at the rostrocaudal level of the preBötC region.

2.3.2 Activation of preBötC neurons increases breathing frequency

We initially tested the response to a train of high frequency (HF) photostimulation (20 ms pulses at 20 Hz, 15 s), 2 mm lateral to the midline starting at 1 – 2 mm caudal to the hypoglossal nerve root exit and then moving along the rostrocaudal axis in 500 µm step intervals, with the optic fiber in contact with (but not penetrating) the ventral surface of the medulla (Fig.2.2). Photostimulation was most effective at the rostrocaudal level of the hypoglossal nerve root exit, at a distance of 0.5 – 1 mm from the caudal pole of the facial nucleus, a location that

corresponds to the site of preBötC in adult rats (Janczewski *et al.,* 2013). High frequency photostimulation increased breathing rate by 23.69 ± 3.77% (from 41.41 ± 2.74 to 50.51 ± 2.37 breaths min^{-1} (bpm); n = 9; P = 4.95 × 10−6; Fig. 2.2C). Continuous photostimulation (10s) delivered in the same location, produced an even more profound increase in breathing rate as the breathing frequency increased by 38.5 ± 8.1% (from 41.2 ± 3.2 to 55.2 ± 2.6 bpm; n = 9; P = 2.92 × 10^{-5}). The increase in breathing frequency reached its maximum value almost instantly and remained at the same level through the 10s stimulation period. No statistical difference was observed when respiratory frequency was compared between the first and the last 5s of the stimulation period (51.2 ± 2.4 and 50.0 ± 2.7 bpm; respectively; n = 9; P = 0.13). In addition, the specific frequency response to photostimulation was reproducible over the entire course of the experiment (3–5 h; data not shown).

Within each respiratory cycle, inspiratory time (T_I) increased by 26.6 ± 0.1 % (from 0.37 ± 0.04 to 0.48 ± 0.07 s; n = 7; P = 2.1 × 10^{-2}) with HF photostimulation and by 12.2 ± 0.1 % (from 0.35 ± 0.04 to 0.41 ± 0.07 s; n = 6; P = 9.1 × 10^{-2}) with continuous photostimulation. Expiratory time (T_E) decreased by 38.2 ± 0.1 % (from 1.11 ± 0.13 to 0.69 ± 0.11s; n = 7; P = 3.2 × 10^{-3}) with HF photostimulation and by 34.4 ± 0.1 % (from 0.98 ± 0.08 to 0.66 ± 0.11 s; n = 6; P=4.9 × 10^{-3}) with continuous photostimulation.

Tidal volume (V_T) decreased by 11.7 ± 6.7 % during HF photostimulation (from 3.15 ± 0.49 to 2.74 ± 0.46 ml; n = 7; P = 2.4×10^{-2}) and by 23.4 ± 6.3 % during continuous photostimulation (from 2.73 ± 0.44 to 2.14 ± 0.43 ml; n = 6; P = 4.6×10^{-3}). No significant change was observed in minute ventilation (V_E) with either HF stimulation (from 130.4 ± 17.5 to 137.7 ± 19.6 ml min^{-1}; n = 7; P = 0.18) or with continuous photostimulation (from 119.7 ± 18.5 to 123.2 ± 23.7 ml min^{-1}; n = 6; P = 0.35; Fig. 2.2C).

During both HF and continuous photostimulation, DIA_{EMG} (n = 9), genioglossal $_{EMG}$ (GG_{EMG}, n = 4) and abdominal $_{EMG}$ (ABD_{EMG}, n = 6) activity was measured on a breath by breath basis. Integrated DIA_{EMG} peak amplitude was decreased by 13.1 ± 3.6% (n = 9; P = 3.2×10^{-3}) with HF photostimulation and by 24.4 ± 4.8% (n = 9; P = 3.5×10^{-4}) with continuous photostimulation (Fig. 2.2C). Genioglossus EMG activity was successfully recorded in four experiments, while in three additional experiments GG_{EMG} activity was eventually lost because of the XII root damage during the exposure of the ventral surface of the brainstem. When GG_{EMG} activity was successfully recorded, EMG amplitude increased (P = 0.046; n = 4) with both HF (+ 19.5 ± 8.2 %) and continuous photostimulation (+13.1 ± 5.3). In one experiment, $\int GG_{EMG}$ peak amplitude was instead reduced by 8.02 % with continuous photostimulation (Fig. 2.2C). PreBötC photostimulation had no effect on tonic ABD_{EMG} activity (n = 6; P = 0.14) and did not recruit active expiration (Fig.

2.2A). In order to confirm that photostimulation preferentially activated neurons within the preBötC, serial sections of perfused brains from stimulated rats were immunoreacted for cFos expression, a marker for neuronal activity. Although a basal level of cFos-activated cells was present on both sides of the ventral respiratory column (58.4 ± 5.2 cells per section on the treated side and 58.8 ± 5.6 cells per section on the untreated side caudal to the preBötC; P = 0.5; n = 3) the photostimulated side contained a higher number of cFos-positive cells in the rostrocaudal region of the respiratory column corresponding to the preBötC (+36.2 ± 8.7 cells per section, P = 1.6 × 10−3; n = 3; Fig.2.3A). In addition, in control experiments where a virus lacking the light-sensitive protein (SYN-EYFP) was used, no difference was observed between stimulated and unstimulated sides (P = 0.16; n = 3; Fig. 2.3A).

This suite of responses evoked by photostimulation was site specific. If the viral injection site was more rostral, e.g. in the Bötzinger complex (n = 4), photostimulation depressed respiratory frequency and tidal volume (from 42.8 ± 3.5 to 36.1 ± 5.2 bpm, n = 4; P = 2.5 × 10^{-2}) as displayed in Fig. 2.3B and C.

Photostimulation experiments performed using the control adeno-associated virus lacking the light-sensitive protein (SYN-EYFP) injected into the preBötC did not produce any significant changes in respiratory activity (from 40.5 ± 2. 6 to 40.8

± 2.5 bpm; n = 4; P = 0.15) and did not respond to different patterns of stimulation (Fig. 2.3D).

Catecholaminergic systems are not necessary for respiratory rhythmogenesis although they are known to provide an important drive to respiratory networks (Doi & Ramirez, 2008; Gargaglioni *et al.,* 2008; Hodges & Richerson, 2008; Lalley, 2008). In order to test if our photo-elicited effects were dependent upon catecholamine release we pretreated four SYN-ChR2-EYFP-treated rats with reserpine (10 mg kg–1, I.P.) 12 – 18 h prior to optostimulation. Reserpine depletes catecholamine stores and reduces the influence of neurons containing serotonin, adrenaline, noradrenaline and dopamine (Henry *et al.,* 1994; Schuldiner, 1994). Baseline respiratory rate in reserpine-treated rats was reduced compared to untreated rats (32.5 ± 5.3 compared to 41.4 ± 2.7 bpm in untreated SYN-ChR2-EYFP rats), indicating that reserpine effectively reduced excitatory cathecolaminergic drive. Despite this, reserpine had no effect on the ability of HF photostimulation in the preBötC to modulate respiratory frequency (P = 0.17); respiratory rate increased by 47.2 ± 10.5 % (from 32.5 ± 5.3 to 46.6 ± 5.2 bpm; n = 4; $P = 4.4 \times 10^{-3}$) in reserpine-treated rats (Fig. 2.4A).

2.3.3 Frequency-specific activation of preBötC neurons paces breathing

We then tested whether short duration and phasic activation of preBötC neurons was able to entrain the ongoing inspiratory rhythm in adult-anaesthetized SYN-ChR2-EYFP-treated rats (Figs. 2.4B and 2.5; n = 11). We delivered short trains of 15 brief (150 ms) pulses of photostimulation at increasing frequencies (0.7–3 Hz) to the preBötC region in SYN-ChR2-EYFP-treated rats. Photostimulation reliably entrained ongoing inspiration (measured by either the respiratory flow or the DIA_{EMG} activity) at frequencies much higher than baseline respiratory rate (Fig. 2.5). Scatter plots of the relationship between stimulus frequency and respiratory frequency across experiments are shown in Fig.2.5C. Photostimulation reliably entrained respiratory frequency with a success rate of 99.5 ± 0.2 % using stimulus frequencies below 2 Hz and a success rate of 93.02 ± 4.77 % using a 3 Hz stimulus (n=3). Inability of the diaphragm to follow stimulation frequency led either to small amplitude DIA_{EMG} contractions that did not reach threshold or to skipped events which reduced the success rate for entrainment. Overall, linear regression analysis between stimulus frequency and induced inspiratory events indicated a high correlation between the two variables (R^2 = 0.998). The ability of entraining respiratory activity persisted throughout the duration of these stimulation experiments (3 – 5 h; n = 7; P = 0.28). Similar results were obtained after reserpine pretreatment (n = 4; Fig. 2.4B).

Photostimulation-driven entrainment caused a reduction in peak $\int DIA_{EMG}$ amplitude by 33.0 ± 8.7% (n = 4; P = 1.6 × 10^{-2}) and 50.2 ± 7.4% (n = 3; P = 1.0 × 10^{-2}) with 2 and 3 Hz photostimulation frequencies, respectively. Entrainment caused a gradual reduction in tidal volume (V_T) upon 2 Hz (from 3.5 ± 0.2 to 1.8 ± 0.1 ml; n = 4; P = 1.7 × 10^{-3}) and 3 Hz (from 3.4 ± 0.2 to 1.5 ± 0.1 ml; n = 3; P = 9.9 × 10^{-3}) photostimulation. As a consequence of increased breathing rate, minute ventilation (V_E) was increased during 2 Hz (from 155.0 ± 5.9 to 215.4 ± 1.9 ml min^{-1}; n = 4; P = 3.5 × 10^{-4}), and 3 Hz photostimulation (from 156.5 ± 7.7 to 246.5 ± 11.1 ml min^{-1}; n = 4;P =7.2 × 10^{-3}). Respiratory events during entrainment at higher frequency were also characterized by a 3-fold increase in variability in $\int DIA_{EMG}$ peak amplitude and a 10-fold increase in variability in V_T compared to pre-photostimulation values.

During entrainment induced by preBötC photostimulation, neither active expiration nor ABD_{EMG} contraction was observed. All respiratory parameters returned immediately to baseline levels following the end of the photostimulation period.

2.3.4 Pulses of photostimulation reset respiratory rhythm in a phase-independent manner

Given that photostimulation of the preBötC entrained breathing, we examined the ability of short-duration (125 ms to 1 s) single light pulse stimulation to reset breathing in SYN-ChR2-EYFP-treated rats (Fig. 2.6). We repetitively applied stimulation at very low rates (0.1 Hz) during ongoing spontaneous breathing. We ensured that stimulation was delivered at random phases of ongoing respiration by confirming that the distribution of stimulation phases demonstrated homogeneity (see Fig. 2.6). Despite being delivered at random phases, post-stimulus inspiratory episodes tended to show stimulus locking as shown by post-stimulus locking in both overlays and on average, suggesting phase reset (Fig. 2.6A). Indeed, in every case, 100 – 150 ms photostimulus pulses induced a prompt recruitment of inspiration with an average delay of 97 ± 17 ms when delivered during the inter-inspiratory period (n = 6). However, and as shown in the stacked traces in Fig. 2.6B, when photostimulation occurred during inspiration (i.e. during active air inflow), the ongoing respiratory activity appeared only minimally affected (see green trace) although the subsequent inspiratory cycle did tend to show phase locking to the stimulation in the overlays and average traces (Fig. 2.6A and B).

To systemically analyse the effect of reset induced by photostimulation of preBötC neurons, we determined the phase values relating the onset of stimulation

to both the ongoing respiratory cycle (stimulus phase) and to the onset of the subsequent inspiration (induced phase) (Fig.2.6C). Phase resetting is observed in Fig.2.6D which plots stimulus phase against induced phase for all stimulation trials in this experiment. For reference, the averaged airflow trace is aligned according to the same inspiratory trigger used for the stimulus phase values. During the inter-inspiratory interval when there was no airflow, the phase reset to stimulation was immediate and well-locked to the onset of laser pulses (averaging approximately 30 deg or 112.5 ms in this example as shown by the bottom horizontal line). However, during inspiratory airflow phase, the induced phase was not immediate but rather appeared to stabilize the subsequent inspiration at a relatively consistent phase that was just less than 360 deg. (330 deg. or 1.2 s in this example). Regardless, stimulation was very successful at perturbing the subsequent phase of the ongoing stimulation as shown by comparing the data for actual stimulation trials to those from the non-stimulated case (inset).

By plotting the cyclic distribution of these angular values and using circular statistics (see Methods section) we determined whether phase values were randomly distributed across the cycle or were clustered at a preferred phase (Fig. 2.6 E and F). Consistent with the random delivery of stimuli across all phases of the respiratory cycle, the stimulus phase distribution (Fig. 2.6 E: open bars in histogram and black fill in the inset polar plot) appeared randomly distributed, although in this case the

test for non-uniformity was significant (Raleigh z: 3.4, P = 0.03). In contrast, the distribution of induced phase values (red fill in both histogram and inset polar plot) showed a marked clustering suggestive of stimulus-induced phase reset. Indeed, for the experiment depicted the distribution was highly non-uniform (Raleigh z: 86.5, P = 1.6255×10^{-49}), and the average phase was represented by a vector having a phase angle of 21 deg. and normalized length (radius) of 0.85 (Fig. 2.6 E, red arrow in histogram and red circle in polar plot). Vector lengths close to 1 are indicative of low dispersion (i.e. variance) of the distribution of individual angular values as well as indicative of significant phase preferences (i.e. non-uniformity) in polar distributions (Zar, 1996). Indeed, the marked clustering of induced phase is suggestive of robust (i.e. Type 0) resetting (Paydarfar *et al.*, 1986; Paydarfar & Eldridge, 1987; Winfree, 2001). In contrast, and as observed in the inset in Fig. 2.6 E, the distribution of stimulus phases showed much less clustering (radial value of average angle=0.17).

Across all experiments, and for different stimulus durations, the distributions of the average induced phase were clustered at short phases (13–44 deg) from the onset of stimulation and each showed significant non-uniformity. As shown in Fig. 2.6 F for the shortest stimulus duration (125 ms), the average angle as computed across all experiments (whose individual average vector ends are indicated by red dots) was 13 deg. and had a normalized radius of 0.9 (red line). The low dispersion

(variance) of average angular values across experiments is obvious in terms of the prominent clustering of individual experimental vectors. In contrast, individual experimental values for stimulation phase (black dots and line in Fig.2.6 F) showed highly variable angles and shorter vector lengths. As a result, the overall average vector across experiments (blackline) had a low radial value and did not demonstrate significant non-uniformity.

Altogether, the best reset (according to least dispersion/greatest group average vector lengths) was driven by the shortest pulse durations used (125 ms) as shown in Table 2.1. Although there was a significant positive linear relationship between stimulus duration and the average (group) angular values for induced phase (correlation coefficient = 0.97), this relationship was probably not related to the increased temporal/phase offset of stimuli since each duration step involved a temporal doubling which was not observed in the translation of increased phase values.

Given the apparent variable reliability of phase reset during airflow itself (see panels B and D of Fig. 2.6), we systematically assessed evidence of reset during this period. First, we determined if the delivery of laser stimulation had an effect on the length of the ongoing inspiratory event. If stimulation was ineffective during this period then we would expect that stimulation would have little effect on the average duration of this phase. We identified 10 deg phase intervals within the inflow period

(see Fig. 2.7A) and calculated inspiratory time (Ti) as a function of stimuli delivered across these phases. The average value of Ti during control conditions was 83.7 ± 4.3 deg (309 ± 4 ms; n = 6). Figure 2.7B shows the control normalized values of Ti as a function of stimulus phase. While there was a tendency for Ti values to be slightly reduced when stimulation was delivered in early phases with a tendency for increased Ti values when stimulation was delivered in late phases of inspiration, a within subjects ANOVA revealed no significant differences (P = 0.3) between control and stimulation Ti values. Thus, timing of stimulation during inspiratory flow did not alter the Ti of the ongoing inspiration.

We also observed that in early expiration (i.e. outflow period, Fig. 2.6 B, red trace) photostimulation could fail to generate an immediate (within 200 ms) inspiratory event. Thus, we calculated the rate of success (see Methods section) as a function of the phase of stimulation (in 10 deg intervals) following the end of the inspiratory (inflow) cycle. These data are shown in Fig. 2.7 C. With the exception of only one experiment, an inspiratory event could be generated with 100% success only after a period of 60 ± 4.5 deg. (215.2 ± 0.1ms; n = 5) delay from the end of inspiratory (inward) airflow. The remaining experiment displayed a longer refractory period of 100 deg (408 ms). These results indicate that if an excitatory stimulus is delivered to the inspiratory oscillator within 215 ms from the end of an inspiratory event, inspiration cannot be reliably regenerated.

2.3.5 Photostimulation of preBötC neurons generates rhythmic diaphragm contractions when excitatory respiratory drive is dampened by mechanical hyperventilation

We used mechanical hyperventilation to reduce arterial blood PCO_2 and thus excitatory drive to preBötC provided by central chemoreceptors (Guyenet *et al*., 2008). Once rats reached the apneic threshold (i.e. no rhythmic contractions were observed in DIA_{EMG}), we examined whether photostimulation would be sufficient to reactivate rhythmicity in preBötC neurons and thus, inspiratory musculature. Photostimulation applied to the preBötC was sufficient to both generate and entrain rhythmic respiratory activity as demonstrated by the reappearance of rhythmic DIA_{EMG} contractions (Fig.2.8). Continuous photostimulation (10s) and brief trains of HF photostimulation into the preBötC generated rhythmic DIA_{EMG} activity with a frequency of 39.4 ± 5.37 and 35.8 ± 2.1 bursts min^{-1}, respectively (n = 7). Respiratory rate obtained during photostimulation was not significantly different from the baseline respiratory frequency before hyperventilation (n = 7; P = 0.52 and 0.10 for continuous and HF photostimulation, respectively). Short trains of photostimulation at various frequencies (1–3 Hz, 0.25–0.15 s pulse length) drove DIA_{EMG} contractions up to 159.2 ± 16.4 bursts min^{-1} (n = 3) with a success rate of 100 % (15 breaths per 15 light pulses) upon 3 Hz photostimulation.

Overall, linear regression analysis between stimulus frequency and respiratory period calculated from the induced DIA_{EMG} contractions indicated a high correlation between the two variables (R^2 = 0.99). Interestingly, DIA_{EMG} contractions immediately stopped at the end of each set of photostimulation and rats quickly regained their ability to produce independent respiratory rhythmic activity at pre-ventilation levels when disconnected from the ventilator. Again, we found no instances of ABD_{EMG} recruitment or active expiration during photostimulation in these instances.

2.4 Discussion

Our results demonstrate that unilateral photostimulation of ChR2-expressing preBötC neurons potently drives rhythmic inspiration. Photostimulation increased respiratory frequency, generated rhythmic inspiratory muscle recruitment, entrained and reset respiratory rhythms, and generated inspiratory activity in the temporary absence of central respiratory drive. This is the first demonstration in vivo that direct optogenetic activation of preBötC neural circuits drive and control respiratory rhythm over a wide range of frequencies with a very fast response.

The necessity and sufficiency of preBötC in respiratory rhythmogenesis has been demonstrated by mean of selective sectioning (Smith *et al.,* 1991), toxic lesions (Gray *et al.,* 2001; McKay *et al.,* 2005), genetic ablation (Bouvier *et al.,* 2010; Gray *et al.,* 2010), laser ablation (Hayes *et al.,* 2012; Wang *et al.,* 2014), and acute inactivation (Tan *et al.,* 2008). Analysis of how respiratory rhythms are entrained and reset by selective stimulation of other regions in the brain have also elucidated how structures in the pons and medulla affect rhythmicity of the respiratory oscillator (Speck & Feldman, 1982; Paydarfar & Eldridge, 1987; Abbott *et al*., 2011; Pagliardini *et al*., 2011; Bonis *et al.,* 2013). None of these studies demonstrated such high respiratory frequency response and entrainment fidelity as in the current study. While entrainment was achieved by either RTN photostimulation (Abbott *et al.,* 2011) or limb somatic afferent stimulation (Potts *et al.,* 2005) to reach at most 2

times the intrinsic operating range of breathing frequency, here we showed that upon preBötC photostimulation breathing rate increased up to 4-fold with inspiratory muscle recruitment following stimulus onset with a very brief delay (<100 ms); indicating a very fast response to stimulation. Further, we demonstrated that in response to brief photostimulation across the respiratory cycle, a strong (Type0) inspiratory-driven respiratory reset was generated and we identified the presence of a critical refractory period of ~200 ms where inspiratory events could not be recruited.

Altogether, these data further demonstrate the fundamental dependence on excitatory mechanisms for burst initiation and the consequent rhythmogenic inspiratory-driving properties of the preBötC network.

2.4.1 Technical considerations

One potential limitation of this study is that optogenetic activation of preBötC neurons was non-specific. It is likely that all neurons in the preBötC region, including excitatory, inhibitory and modulatory, were activated. We do not consider this lack of specificity to be of major significance in the context of our experimental question, which was to examine the efficacy of a finely tuned excitatory drive to the entire preBötC network and its effect on rhythmogenesis. Within the region of the

preBötC there are several different phenotypes of neurons: those expressing NK1R (Gray et al. 1999), SST (Pagliardini *et al*., 2003; Stornetta *et al.,* 2003), the transcription factor Dbx1 (Bouvier *et al.,* 2010; Gray *et al.,* 2010) and inhibitory GABAergic (Kuwana *et al.,* 2006) and glycinergic neurons (Winter *et al.,* 2009; Morgado-Valle *et al.,* 2010; Sherman *et al.,* 2015). In addition, not all preBötC neurons are respiratory related. Our histological results indicate that our infections targeted 40% of the total number of preBötC SST+ neurons and 56% of the total number of preBötC NK1R+ neurons. Both sets of neurons have been proposed to be rhythmogenic elements (Gray *et al.,* 2001; Tan *et al.,* 2008). Even though the expression of the virus encompassed a wider area of the preBötC, it was the positioning of the probe combined with the location of viral expression that contributed to the high specificity and high reliability of the response to photostimulation (especially when comparing to responses obtained during BötC stimulation).

Given the limited (< 10 %) infection rate of TH-expressing neurons in the ventral medulla and the persistence of photostimulatory effects following reserpine pretreatment (Granata *et al*., 1986; Lambas-Senas *et al.,* 1986; Fritschy *et al.,* 1991), it is unlikely that the observed excitatory effects were generated by the stimulation of the adjacent C1 noradrenergic population (Abbott *et al*., 2012, 2013b).

We cannot exclude that a portion of the infected neurons are inhibitory respiratory neurons (Morgado-Valle *et al*., 2010; Winter *et al*., 2010) whose role in respiratory rhythmogenesis has been recently investigated (Janczewski *et al*., 2013; Sherman *et al*., 2015). While selective photo-stimulation of preBötC glycinergic neurons generated early inspiratory termination, apnoeas, or inspiratory onset delay (depending on the timing of stimulation, Sherman *et al*., 2015), activation of an heterogeneous population of preBötC neurons (present results) increased respiratory frequency, powerfully entrained the breathing rhythm, and, following a refractory period, reset inspiratory rhythm with a consistent delay. Moreover, in our experiments, stimulation during inspiration had very limited effect. These observations are all consistent with an excitatory-driven burst initiation process. Perhaps in contrast, selective excitation of preBötC inhibitory neurons may have a greater effect outside the rhythmogenic circuitry of the preBötC, given their projection patterns to other brainstem structures affecting the activation phase and timing of specific respiratory musculature.

Stimulation of only a few preBötC inspiratory neurons (4 – 9 of unknown phenotype) is sufficient to trigger an ectopic inspiratory burst in vitro (Kam *et al.* 2013b). Although not tested, similarities between responses evoked by holographic stimulation of just a few neurons and our data suggest that activation of small subsets may also be sufficient to entrain rhythm and that inspiratory burst initiation is

conceivably not determined by a limited specialized subpopulation of preBötC neurons, but probably by excitatory processes distributed within the preBötC respiratory network. Thus, regardless of whether we are stimulating excitatory or inhibitory preBötC neurons, the excitatory effects clearly pre-dominate, meaning that, if anything, our results under-estimate the ability of preBötC photostimulation to reset and entrain rhythm.

Our results support the hypothesis that there is a core of distributed neurons responsible for respiratory rhythmogenesis within the preBötC. It will be critical to determine if and how the different preBötC neuronal subpopulations differentially drive respiratory rhythms *in vivo*.

2.4.2 **PreBötC photostimulation increases respiratory rate and entrains respiration**

Trains of HF photostimulation and continuous photostimulation both generated an immediate increase in breathing rate whereas neither abdominal muscle activity nor active expiratory rhythm was recruited. Given our previous results with optostimulation of the expiratory rhythm generator (pFRG, Pagliardini *et al.*, 2011), which showed prominent recruitment of expiratory muscles and active expiration, this further supports the hypothesis that inspiration and active expiration are

generated by distinct rhythmogenic neuronal networks (Janczewski & Feldman, 2006; Feldman *et al*., 2013). Interestingly, while DIA_{EMG} activity decreased with increasing respiratory rate, the activity of the GG muscle was more variable and overall increased with photostimulation.

The effect of photostimulation on the peak of DIA_{EMG} contraction is probably the consequence of the reduced inspiratory time and faster alternation between inspiratory and expiratory phases. Two potential mechanisms may be responsible for the increase in peak amplitude of GG_{EMG} activity: (i) activation of hypoglossal (XII) premotoneurons that exist in the heterogeneous region of the preBötC or in the overlying (dorsal) region; or (ii) direct activation of XII nerve activity via ventral positioning of the laser. Histological analysis of EYFP-expressing neurons showed no labelling dorsal to the nucleus ambiguus or in the premotor area (Li *et al.,* 1993; Dobbins & Feldman, 1995; Woch *et al.,* 2000; Koizumi *et al.,* 2013; Koshiya *et al.,* 2014). Thus, the likelihood of stimulating premotoneurons dorsal to the preBötC is extremely low. Furthermore, total transmitted light power falls rapidly as it travels through tissue (50 % reduction in 100 μm and 90% in 1mm of brain tissue, Aravanis *et al.,* 2007) such that neurons dorsal to the preBötC are unlikely to be excited when the laser is applied from the ventral surface of the medulla. In addition, when viral injections were off-target, photostimulation had no effect on respiratory rate or on $\int GG_{EMG}$ activity, suggesting that non-specific stimulation of other nuclei or the XII

nerve root are probably not responsible for the $\int GG_{EMG}$ increase. It is therefore intriguing to conclude that preBötC also contains neurons that shape respiratory motor pattern in the upper airways in vivo. This hypothesis has been previously supported by in vitro experiments (Kam *et al.,* 2013a), and recently corroborated by selective laser ablation experiments in vitro (Wang *et al.,* 2014). Tracing experiments also support the presence of preBötC neurons that directly project to the XII nucleus (Koizumi *et al.,* 2013; Koshiya *et al.,* 2014).

We also tested the possibility that entrainment could be induced by rhythmic preBötC photostimulation both during spontaneous breathing and in the absence of ongoing respiration. In vagotomized, spontaneously breathing, urethane-anaesthetized rats, respiratory rate is usually low, around 30 – 40 bpm (0.5 – 0.7 Hz) (Pagliardini *et al.,* 2011). Following trains of photostimulation at progressively increasing rates, entrainment was consistently achieved up to 180 bpm (3 Hz), indicating the ability of the respiratory network to promptly and faithfully reach high rates upon preBötC activation. Of note, these rates are 4 times higher than resting values under these experimental conditions, and ~2 times higher than those observed in awake rats during quiet breathing. Under this stimulation protocol recruitment of DIA_{EMG} activity was elicited with a short delay (~100 ms) and laser stimulus settled during early inspiration. These results are far more dramatic than the ones observed during photostimulation of the RTN, a major provider of excitatory drive to the

preBötC (Abbott *et al.,* 2011) or during sensory stimulation (Potts *et al.,* 2005). RTN photostimulation increased respiratory rate, phrenic nerve discharge amplitude, and produced a slow decay in respiratory response upon stimulus cessation. In addition, entrainment was achieved only at low frequencies in anaesthetized rats (~60 bpm) with recruitment of active expiration in vivo and significant delay between laser stimulation and phrenic nerve discharge (~230 deg; (Abbott *et al.,* 2011)). A limited range in entrainment frequency (1.2–2.2 times the ongoing respiratory rate) following somatic sensory stimulation was also observed in rat in situ preparations (Potts *et al.,* 2005). In our experiments, preBötC photostimulation induced an immediate frequency response and an instantaneous return to baseline frequencies upon stimulus cessation in similar (but not identical) experimental conditions to Abbott and colleagues (2011). In addition, entrainment was achieved over a wider range of respiratory frequencies, with progressive decrease in $\int DIA_{EMG}$ amplitude. These results indicate the potency of the respiratory response to preBötC photostimulation, compared to other brainstem structures that may influence respiratory rhythmicity.

When rats were maintained just below their apnoeic threshold, tonic photostimulation recruited rhythmic DIA_{EMG} activity with a frequency that was not different from the animals' baseline breathing rate. These results imply that an increase in excitability of preBötC neurons was sufficient to reinstate respiratory

rhythmicity. In addition, when photostimulation was delivered to induce entrainment, respiratory activity was again driven to 180 bpm and DIA_{EMG} contractions followed photostimulation pulses faithfully with short delays. In both cases, at the end of photostimulation we did not observe any additional DIA_{EMG} contractions, indicating that the effect is strictly dependent on the imposed excitation provided by photoactivation. Again, these results are even more dramatic than what observed following RTN photostimulation (Abbott *et al.,* 2009, 2011).

2.4.3 PreBötC photostimulation produces respiratory reset

Together with previous indications of the importance of the preBötC in inspiratory rhythm generation (Feldman *et al.,* 2013), our demonstration of an excitatory stimulus-induced reset of ongoing respiratory activity constitutes very strong evidence of a direct perturbation to the inspiratory oscillator. PreBötC photostimulation generated a Type 0 resetting. Consistent with this nomenclature (Winfree, 2001), this reset was robust, occurred quickly, and was associated with short-latency recruitment of inspiratory diaphragmatic activity. In addition, suggestive of an excitatory perturbation that has an effect primarily on burst initiation, respiratory rhythm was minimally perturbed when photostimulation occurred during inspiration. Indeed, we would only expect interruption of the

ongoing inspiratory event and subsequent reset during inspiration via inhibitory mechanisms, as demonstrated recently with selective stimulation of glycinergic neurons in the preBötC (Sherman *et al.,* 2015). Interestingly, we have previously observed such inhibitory reset during optogenetic stimulation of the expiratory rhythm generator (pFRG) which probably has reciprocal connections with the preBötC (Pagliardini *et al.,* 2011) and could also provide a strong, phase-independent, Type 0 reset. In contrast to pFRG stimulation, however, reset in the present work was achieved at shorter latencies and did not involve activation of expiratory musculature.

It is of note that previous studies have also investigated respiratory rhythm reset by means of direct stimulation of brainstem regions associated with breathing or their afferent systems (Eldridge,1972b; Speck & Feldman,1982; Paydarfar & Eldridge, 1987; Oku & Dick, 1992; Abbott *et al.,* 2011; Bonis *et al.,* 2013). While those using electrical stimulation are perhaps difficult to resolve because of the ill-defined locus of excitation it is thought that stimuli that do perturb respiration in this manner would ultimately exert their effects on the rhythm generator. Here, by directly targeting preBötC directly, we were able to consistently obtain inspiratory recruitment and reset upon stimulation.

Similar to in vitro holographic stimulation of a few preBötC inspiratory neurons (Kam *et al.,* 2013b), we identified the presence of a refractory period of

~200 ms following an inspiratory event during which another burst could not be triggered by optogenetic stimulation, suggesting that this is an intrinsic property of the preBötC inspiratory network both in in vitro and in vivo conditions. A speculative mechanism to be tested is strong post-excitatory inhibition that shunts even strong excitatory inputs.

2.5 Conclusions

In summary, our results further support the key role of preBötC network in respiratory rhythmogenesis. As we have shown, excitation of this network potently drives, entrains and resets inspiratory activity. Our data demonstrate that excitatory mechanisms in the interconnected preBötC network are sufficient for pacing rhythmic inspiration. Given the importance of respiratory rhythmogenesis for survival, it will be of substantial interest to understand the precise cellular and circuit mechanisms of how this oscillation is generated.

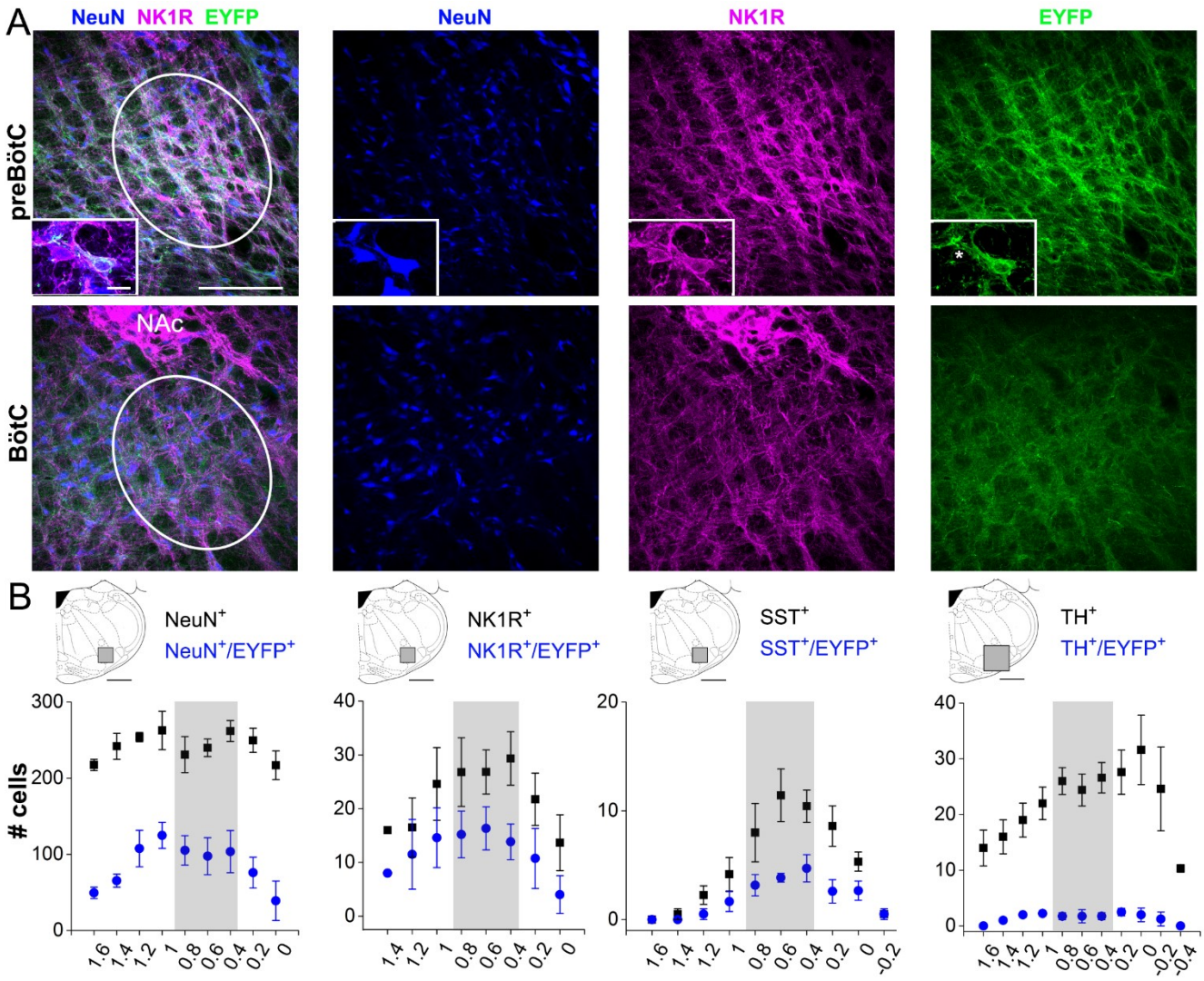

Figure 2.1 Distribution of EYFP labelled neurons along the rostrocaudal extension of the ventral respiratory column

A, three-colour confocal mosaics (left) and single-colour images (right) showing co-localization of NeuN (blue), NK1R (magenta) and EYFP (green) in transverse sections taken at the level of the preBötC (top) and BötC (bottom).

Inset displays two NK1R positive neurons, one expressing EYFP and one lacking EYFP expression (asterisk). *B*, rostrocaudal (right–left) distribution of total NeuN+ and NeuN+/EYFP+ neurons, NK1R+ and NK1R+/EYFP+ neurons, SST+ and SST+/EYFP+ and TH+ and TH+/EYFP+ neurons after unilateral injection of SYN-ChR2-EYFP virus into the preBötC. Diagrams above plots illustrate the area (grey zone) where cell counts were performed. On the *x*-axis of plots the distance (in mm) from the caudal tip of the facial nucleus is indicated. Grey zone in plots indicate the area of high density of SST+ and NK1+ neurons corresponding to preBötC. Calibration bars in *A*: main panels, 200 μm; insets, 20 μm.

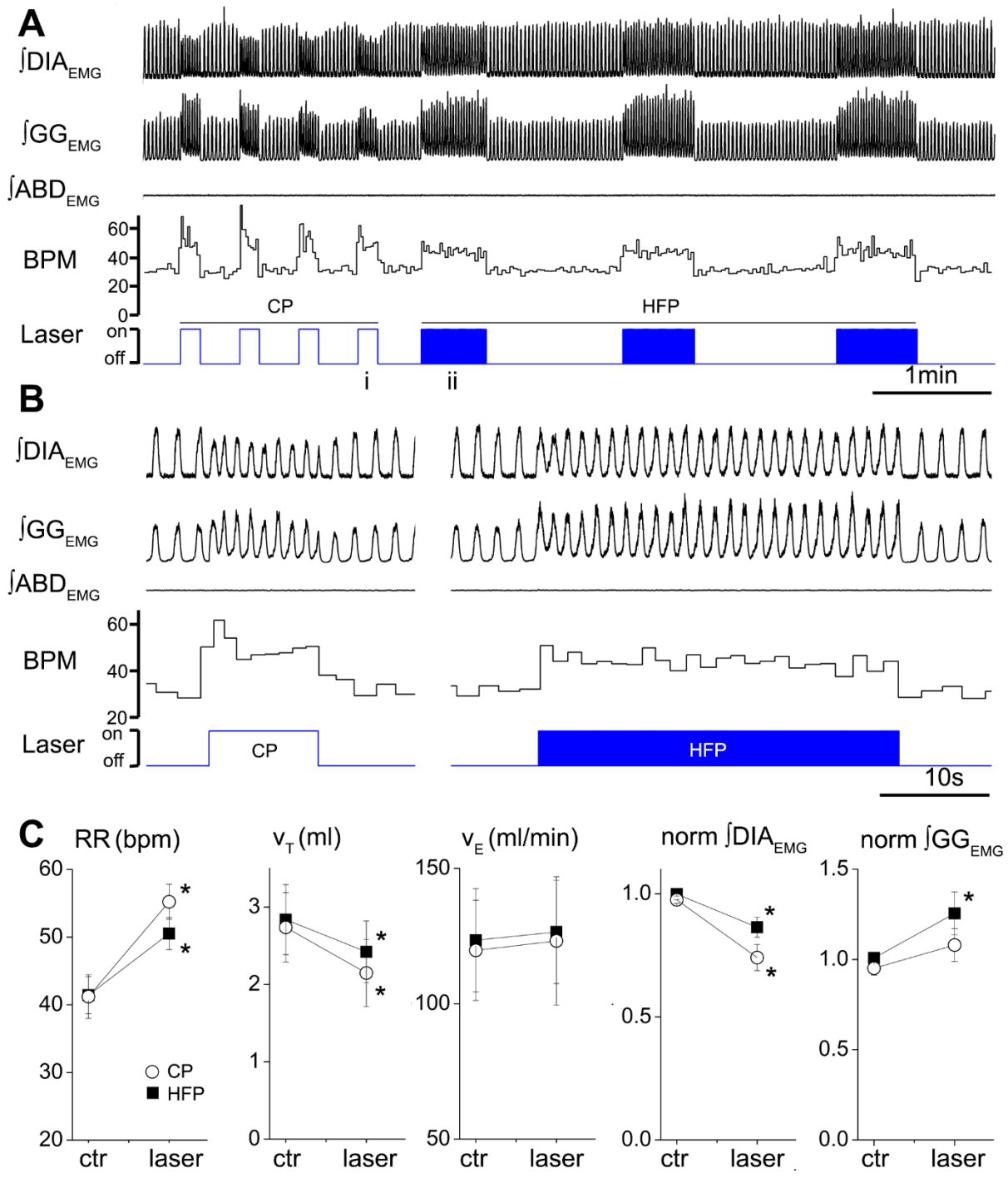

Figure 2.2 Effects of continuous (10 s) and high frequency (20 Hz, 20 ms pulse) photostimulation of preBötC in urethane-anaesthetized SYN-ChR2-EYFP-treated rats

A, long trace recording of $\int DIA_{EMG}$, $\int GG_{EMG}$, $\int ABD_{EMG}$, respiratory rate (breaths min–1, BPM) and laser activation shows that repeated photostimulation of preBötC induce reproducible and consistent increases in respiratory frequency in the presence of a continuous photostimulation (left, CP) and in presence of brief light pulses delivered at high frequency (HFP, 20 ms pulse at 20 Hz, right). Photostimulation events expanded in B are indicated with 'i' and 'ii' below the photostimulation protocol diagram. B, details of photostimulation protocols delivered in A. C, population data indicating changes in respiratory rate (RR), tidal volume (V_T), minute ventilation (V_E) and normalized changes in DIA_{EMG} and GG_{EMG} activity upon CP (circles) and HF photostimulation (squares).

∗Statistically significant changes ($P < 0.05$) compared to pre-stimulation values.

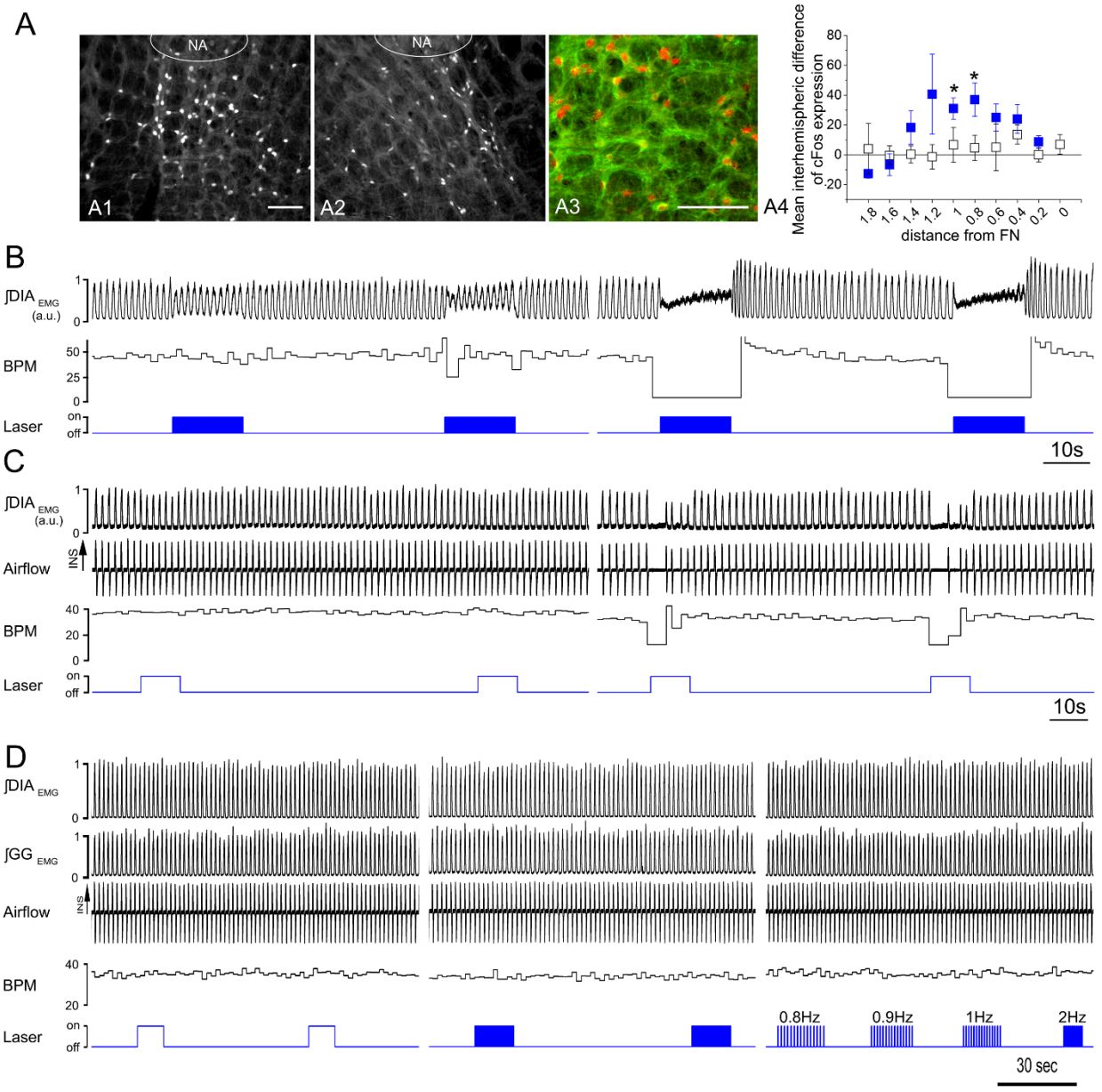

Figure 2.3 Specificity of preBötC photostimulation

A, expression of cFos in SYN-ChR2-EYFP and SYN-EYFP-treated rats indicates local activation of neurons in the preBötC upon photostimulation. *A*1 and *A*2, cFos expression in the ventrolateral medulla of unilaterally SYN-ChR2-EYFP injected rat

after photostimulation experiment indicates the presence of an increased number of cFos positive neurons in the photostimulated side (*A*1) compared to the non-stimulated side (*A*2). Several EYFP-expressing neurons display cfos positive nuclei (*A*3). Plot in *A*4 indicates difference in number of cFos positive cells between stimulated and unstimulated side for both SYN-ChR2-EYFP (blue squares) and SYN-EYFP (white squares) treated rats along the respiratory column. The *x*-axis shows (in mm) the distance from the facial nucleus.

∗Significant difference in cell number between stimulated and unstimulated side. *B* and *C*, two examples of the effect of photostimulation in preBötC and BötC when viral injection was misplaced and infected preferentially BötC neurons. Changes in $\int DIA_{EMG}$ and respiratory frequency (BPM) upon either HFP (*B*) or CP (*C*) laser stimulation in preBötC (left) and BötC (right). Note lack of significant response when preBötC is photostimulated and strong respiratory depression when BötC is photostimulated. *D*, lack of response to photostimulation of preBötC when control SYN-EYFP virus is expressed in the preBötC. HFP, CP and 100 ms brief pulses at different frequencies (0.8, 0.9, 1.2 Hz) were delivered in control rats to test for ChR2-independent responses. Calibration bars in *A*1 and *A*3, 200 μm (*A*2 same as *A*1).

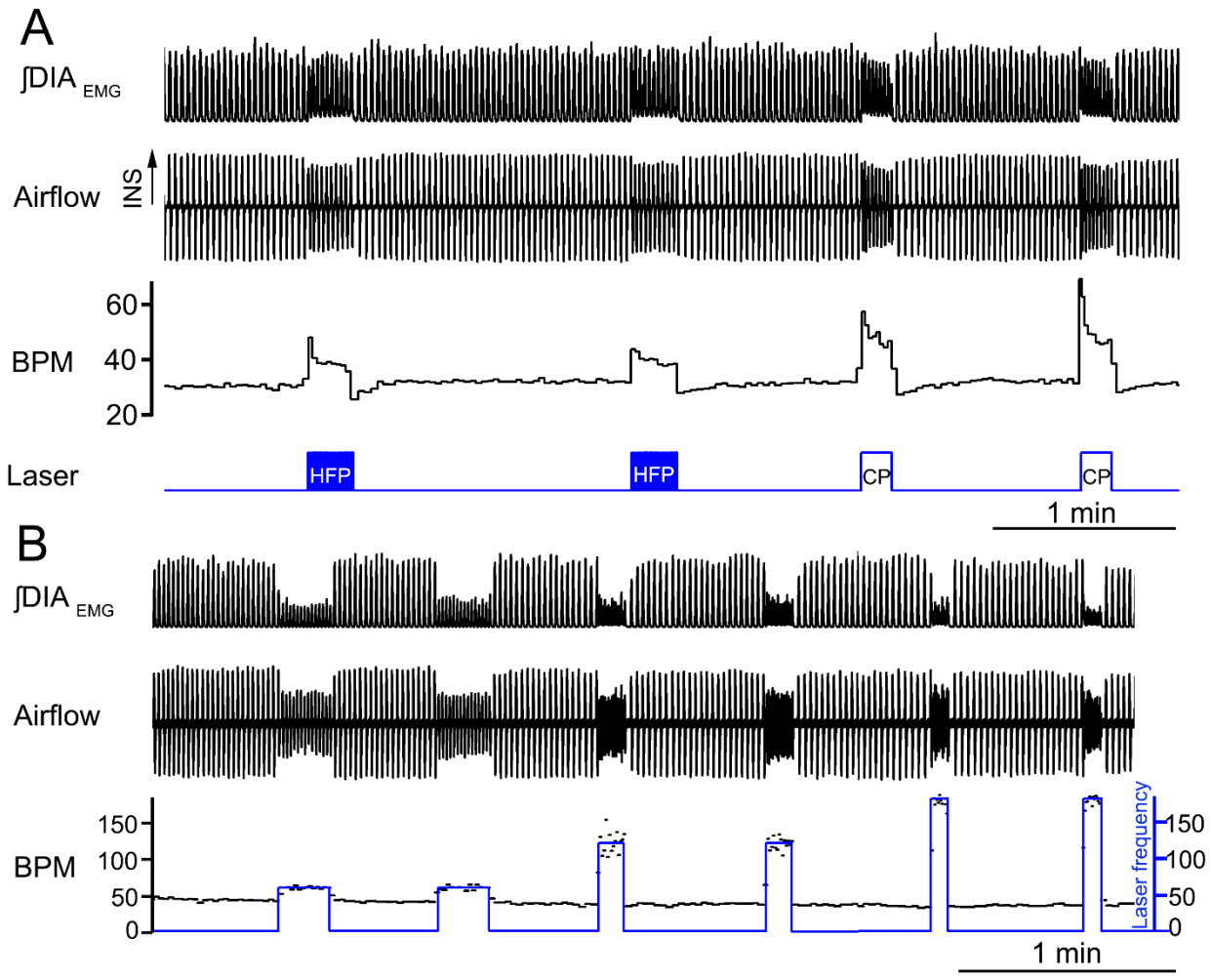

Figure 2.4 Reserpine pretreatment does not affect respiratory response to preBötC photostimulation

Photostimulation of preBötC in SYN-ChR2-EYFP-treated rats pretreated with reserpine display similar responses to high frequency (HFP) and continuous photostimulation (CP) (*A*) compared to SYN-ChR2-EYFP-treated rats. *B*, reserpine pretreatment does not affect the ability to entrain respiratory rhythm with brief pulses

of photostimulation at progressively increasing stimulation frequencies (1 Hz, 2 Hz, 3 Hz).

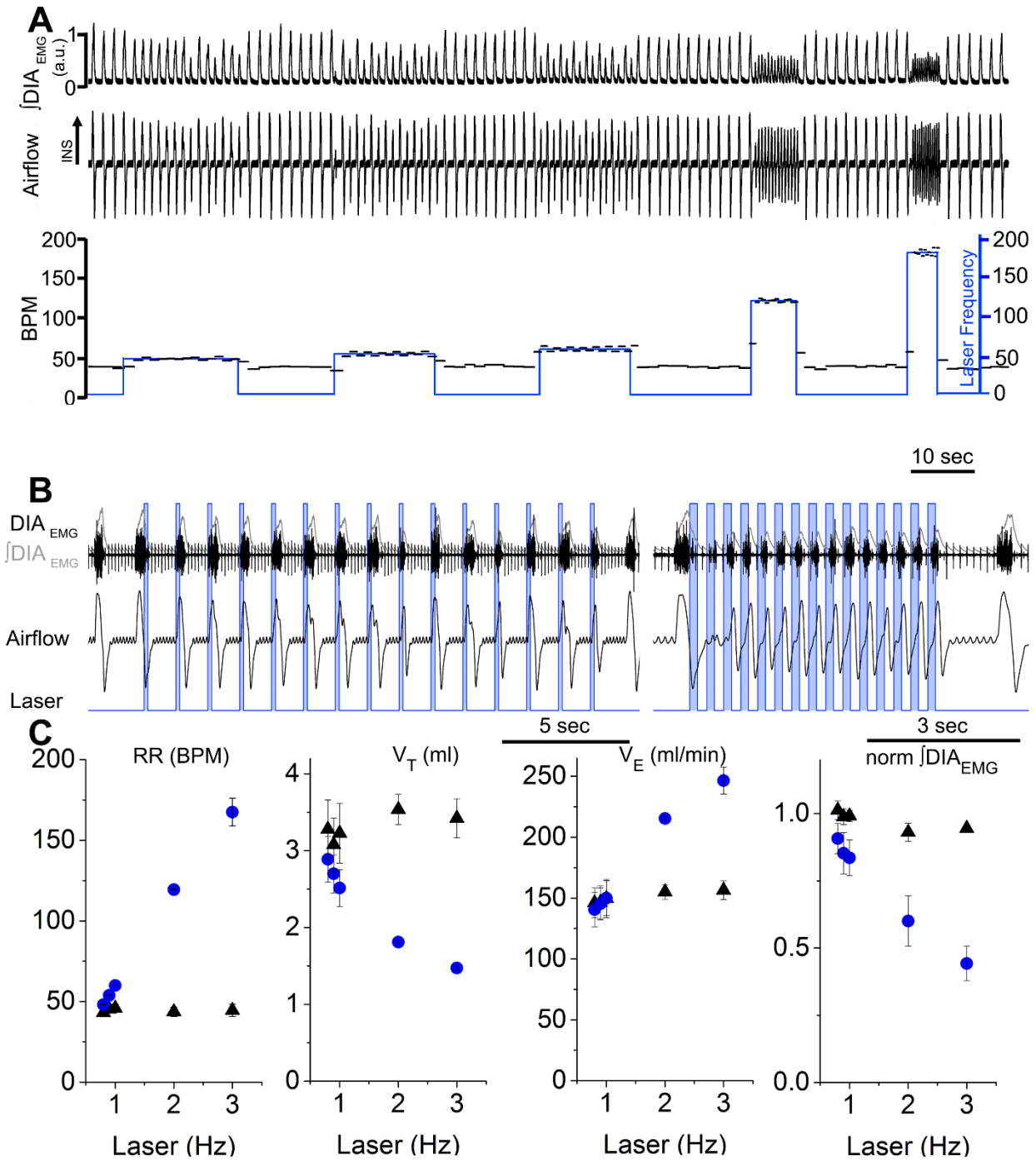

Figure 2.5 Photostimulation of SYN-ChR2-EYFP-treated rats in the preBötC produces respiratory entrainment

A, long trace recordings of $\int DIA_{EMG}$, respiratory airflow, and derived instantaneous respiratory frequency (BPM scale is on left) and laser frequency (blue; stimulation frequency scale is on right, events min^{-1}) during photostimulation at progressively higher rate (0.8, 0.9, 1, 2, 3 Hz, respectively). *B*, details of respiratory traces during photostimulation entrainment at 1 Hz (left) and 3 Hz (right). Boxes in *B* indicate the time in which laser is turned on. Note the fast recruitment of DIA_{EMG} activity and consequent movement of respiratory flow in response to laser stimulation.

C, relationship between photostimulation frequency and respiratory rate, tidal volume, minute ventilation and $\int DIA_{EMG}$ in SYN-ChR2-EYFP-treated rats (circles) compared to baseline activity (triangles). Each point represents the average value (± SEM) obtained from four SYN-ChR2-EYFP-treated rat experiments. Note the limited variability of respiratory rate at multiple entrainment frequencies, reflecting successful entrainment.

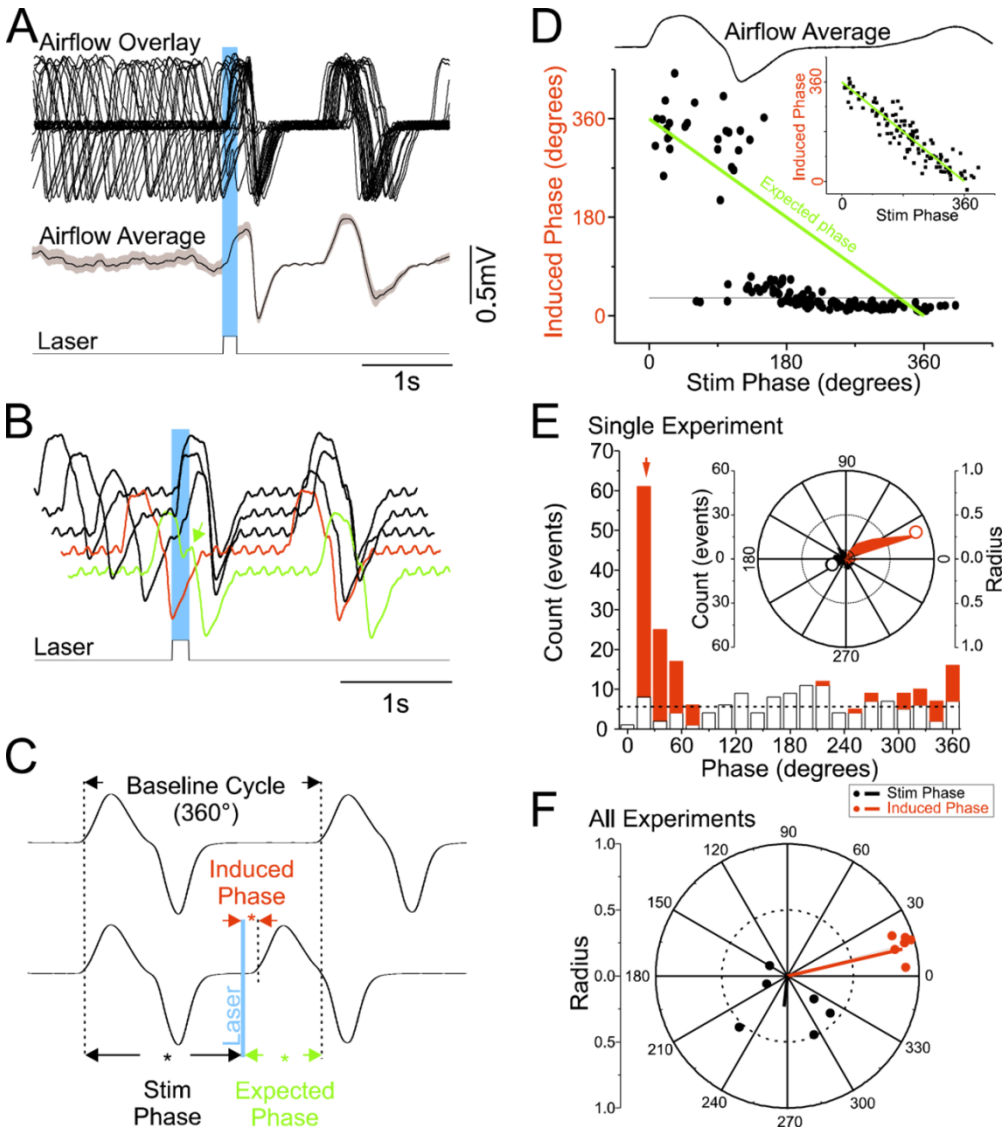

Figure 2.6 Photostimulation of SYN-ChR2-EYFP-treated rats in the preBötC generates respiratory reset

A, superposition of respiratory airflow traces (top, $n = 27$) and average airflow trace (centre) during 150 ms pulse photostimulation (bottom), which resets and aligns the subsequent inspiratory event. The greyed area behind the dotted line on average airflow trace indicates the standard error of the mean. *B*, overlay of five respiratory

airflow traces from the same experiment in *A* arranged by the phase of stimulus delivered during ongoing respiration. The red trace indicates a lack of immediate response to photostimulation when it occurs during the post-inspiratory phase (refractory period). The green trace shows a slight prolongation of inspiration (green arrow) when the stimulus is delivered during the inspiratory phase. *C*, calculation of phase perturbations by laser photostimulation. Top trace: baseline respiratory flow cycle (from 0 to 360 deg, measured from the onset of one inspiration to the next, see arrows). Bottom trace: respiratory flow cycle during stimulation. Stimulus phase: onset of photostimulation with respect to the phase of respiration (black asterisk and arrows); induced phase: onset of inspiration subsequent to delivery of photostimulation (red asterisk and arrows); expected phase: expected onset of the next inspiratory cycle with respect to stimulus onset if photostimulation had no effect (360 deg minus stimulus phase; green asterisk and arrows). *D*, average respiratory flow (top) and distribution of induced phases as a function of stimulus phase (bottom). The expected phase is shown as a green line which assumes that the subsequent phase in the absence of stimulation will occur at 360 deg from the onset of respiration (see inset for non-stimulated case). Horizontal line indicates the average induced phase for the major short latency cluster (at 30 deg) occurring for stimulus phases beyond _90 deg. Note, however, another prominent cluster at longer induced latencies at _330 deg that occurred for stimulus phases shorter than _90 deg.

E, distribution of events for stimulus and induced phases during multiple trials of 125 ms photostimulation delivered during the same experiment as shown in *A*. While stimuli were distributed in a near-uniform fashion randomly across all phases of respiration (open bars), the stimulus-induced phase values (red bars) demonstrated clustering at a tight range of preferred phase angles. The red arrow indicates the average angle for the distribution of induced phases (21 deg).

The horizontal dotted line indicates the expected value of both distributions across phases based on an average random assignment. These data are also plotted in polar form in the inset with stimulus phase as a black fill and induced phase as a red fill. Left scale bar indicates radial distance for number of events (0 – 60) for both stimulus and induced phase with divisions indicated by concentric circles on the plot itself. Innermost concentric circle represents the average expected value of the distribution similarly to the histogram representation. The average preferred angle and radius for both the stimulus and the induced phase is overlaid as an open dot (black and red, respectively). Right scale bar indicates normalized radial length for this average vector (0–1 with divisions again indicated by concentric circles on plot). Radial values close to 1 (represented by external circle) are indicative of low dispersion of angles and significant phase preferences in polar distributions. Note the marked difference of average radii between stimulus and induced phases. *F*, distribution of preferred phases of stimulus-induced respiration for six separate

experiments at the same stimulus duration (vector end-points plotted as dots) and the calculated grand average vectors (plotted as lines) across all experiments (stimulus phase in black, induced phase in red). Note the tight similarity of clustering in induced (but not stimulus) phase angles across experiments.

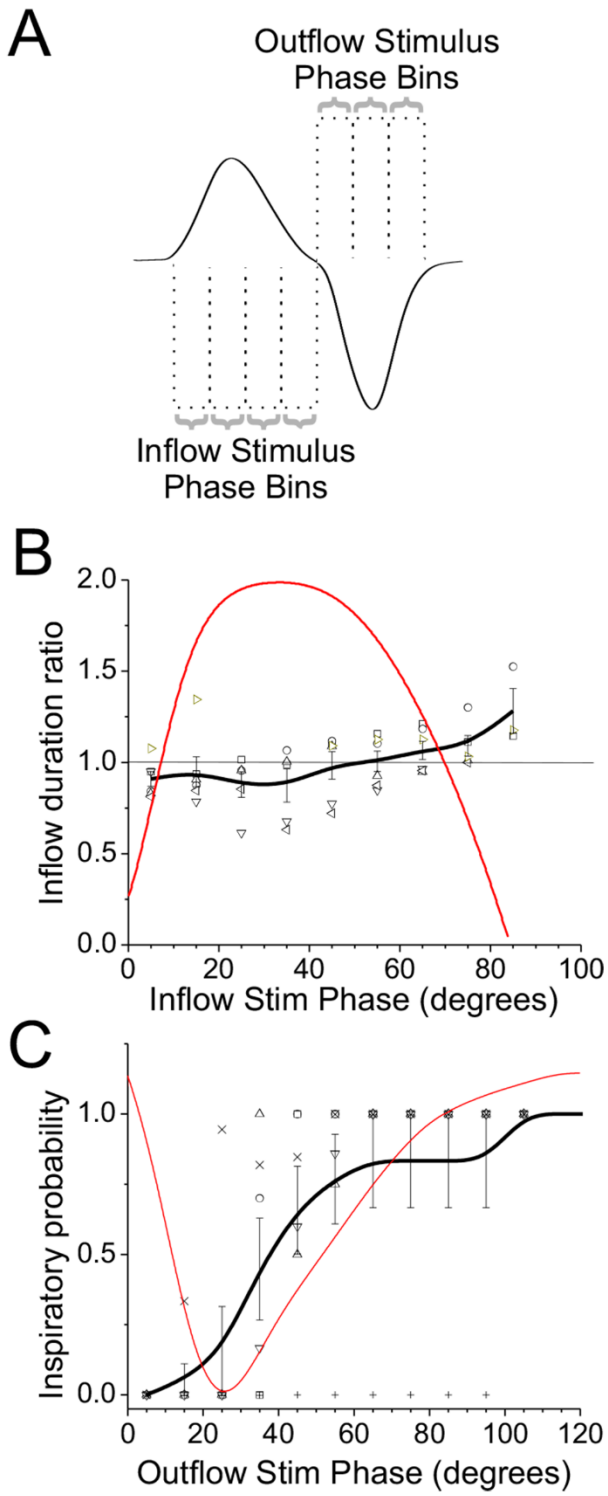

Figure 2.7 A refractory period to inspiratory reset exists during early expiration

A, effect of laser photostimulation during active airflow. Inflow and outflow measures were collected for stimuli occurring in specific phase bins as illustrated. *B*, inspiratory duration is unaffected by stimulation during inspiratory flow. Across individual experiments, the duration of inflow during stimulation was calculated and expressed as a ratio of the baseline inflow duration based on the phase of stimulus delivery. Red line shows the actual average airflow trace occurring as a function of phase. Grey-scale symbols indicate results for individual experiments and black line is an average of values calculated in binned increments of 10 deg from onset of inspiration across the 6 experiments. Note a tendency for inflow duration to increase as stimuli were delivered at later phases of inspiratory inflow. *C*, refractory period for photostimulation-induced inspiration occurring during early expiration. Across experiments, the probability of successfully eliciting inspiration (i.e. the number of successful trials over the total number of trials) as a function of stimulus phase was calculated and plotted. Red trace shows the actual average airflow trace occurring as a function of phase. Grey-scale symbols indicate results for individual experiments and black line is an average of values calculated in binned increments of 10 deg from onset of inspiration across the 6 experiments. At the initial phase of expiratory flow, there is a marked limited success of photostimulation to evoke inspiration which gradually improves at later phases.

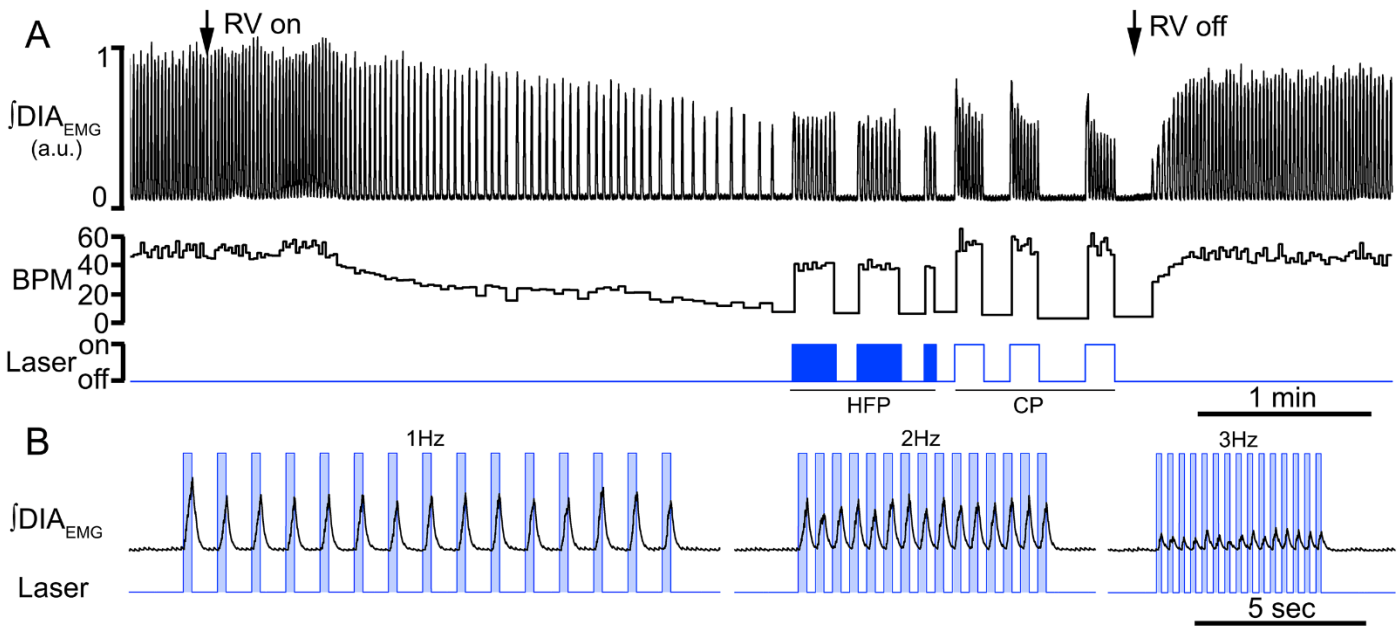

Figure 2.8 Photostimulation of SYN-ChR2-EYFP-treated rats in the preBötC restores respiratory rhythms and produces respiratory entrainment in absence of ongoing respiration

A, long trace recordings of $\int DIA_{EMG}$, and derived respiratory frequency (breaths min^{-1}, BPM) during photostimulation at either high frequency stimulation (20 ms pulse at 20 Hz, HFP) and continuous photostimulation (10 s, CP). Note the ability of the rat to reach high level of respiratory rate upon HFP and CP. Arrows indicate the time at which rat was connected (left) and disconnected (right) with a respiratory ventilator (RV) to reach the apnoeic threshold and reinstate spontaneous breathing. *B*, details of respiratory traces during photostimulation entrainment at 1 Hz (left), 2

Hz (centre) and 3 Hz (right) in absence of spontaneous breathing. Boxes in *B* indicate the time in which laser is turned on. Note the immediate recruitment of DIA_{EMG} upon laser onset.

Pulse duration (ms)	Avg angle (deg)	Radius/vector length (max value = 1)
125	13.0	0.90
250	22.5	0.83
500	32.6	0.68
1000	44.0	0.63

Table 2.1 Group average values for induced phase for different photostimulation pulse durations showing best reset for the shortest pulse durations used and increasing phase values for increasing pulse duration

CHAPTER III*

Cholinergic Modulation of the paraFacial Respiratory Group

---

* In press in the Journal of Physiology.

Rozlyn C.T. Boutin*, Zaki Alsahafi*, Silvia Pagliardini

My contribution to this work was for sections 3.3.4, and 3.3.6 of, for all aspects including performing the experiments, analyzing the data, and writing the manuscript. Rozlyn C.T. Boutin was responsible for sections 3.3.2 and 3.3.3 for all aspects including performing the experiments, analyzing the data, and writing the manuscript. Silvia Pagliardini was the supervisory author responsible for the experimental design, experimental execution and data analysis of sections 3.3.1 and 3.3.5 and manuscript preparation.

3.1 Introduction

Breathing is an essential behavior for mammalian life controlled by neuronal networks located in the brainstem (Feldman *et al*., 2013). The region of the preBötzinger complex (preBötC) in the ventral medulla contains rhythmogenic neurons responsible for inspiratory rhythm generation (Smith *et al*., 1991; Feldman *et al*., 2013) while rostral to the preBötC, the region of the paraFacial Respiratory Group (pFRG) has been proposed to be critical for expiratory rhythm generation (Janczewski *et al*., 2002; Janczewski & Feldman, 2006; Pagliardini *et al*., 2011; Huckstepp *et al*., 2015; Huckstepp *et al*., 2016). In adult rodents, the pFRG acts as a conditional expiratory oscillator, being silent in resting conditions but rhythmically active during the expiratory phase in response to release of inhibition or direct stimulation (Pagliardini *et al*., 2011; Huckstepp *et al*., 2016). Through projections to premotoneurons in the caudal ventral respiratory group (or nucleus retroambiguus), the pFRG sends rhythmic excitatory drive to the main expiratory motoneurons and muscles, the abdominals (ABD), which then force air out of the lungs beyond their resting level (i.e., active expiration) to thereby facilitate the subsequent inspiratory phase and promote ventilation (Janczewski & Feldman, 2006; Pagliardini *et al*., 2011). Compelling evidence has shown that this pathway exists in mammals and that is able to generate an excitatory rhythmic drive to low thoracic and lumbar

motoneurons and eventually excite abdominal muscles (Boers *et al*., 2006; Janczewski & Feldman, 2006; Giraudin *et al*., 2008).

Partially overlapping with the adjacent and more ventro-medial chemosensitive region of the Retrotrapezoid Nucleus (RTN) (Guyenet & Bayliss, 2015), recent evidence suggests that the pFRG, which lies mostly lateral to the facial nucleus, is likely distinct from RTN neurons since respiratory responses to selective activation and inactivation of the two areas are different (Abbott *et al*., 2009; Abbott *et al*., 2011; Pagliardini *et al*., 2011; Huckstepp *et al*., 2015). Recent evidence also demonstrates that activity of RTN neurons is state-dependent, with a contribution to tidal volume unaffected by sleep states, and little contribution to respiratory frequency and active expiration observed in rapid eye movement (REM) sleep compared to more potent respiratory effects observed in wakefulness and nonREM sleep (Burke *et al*., 2015).

We recently reported that recruitment of expiratory ABD muscle activity in adult rats frequently occurs during periods of REM in natural sleep and in REM-like states under urethane anesthesia (Pagliardini *et al*., 2012; Pagliardini *et al*., 2013; Andrews & Pagliardini, 2015). Moreover, this recruitment leads to increased respiratory stability and increased tidal volume and minute ventilation (Andrews & Pagliardini, 2015). Currently, the source of rhythmic excitatory drive to ABD muscles in REM sleep is unknown. Given the proposed role of pFRG neurons in

promoting expiratory activity in ABD muscles, in generating active expiration (Janczewski & Feldman, 2\\006; Pagliardini *et al*., 2011), and in interacting with preBötC to pace respiratory rhythms (Mellen *et al*., 2003; Janczewski & Feldman, 2006; Pagliardini *et al*., 2011; Huckstepp *et al*., 2016), one possibility is that pFRG neurons become rhythmically active during REM sleep (either through release of inhibition (Pagliardini *et al*., 2011) or through an incoming excitatory inputs) to provide an excitatory rhythmic drive to ABD muscles.

In this study, we tested the hypothesis that cholinergic transmission, which is potentiated in periods of REM sleep in the reticular formation from its ascending and descending sources in the brainstem (Kodama *et al*., 1992), is involved in the modulation of pFRG neurons and generation of active expiratory activity in urethane anesthetized rats.

Immunohistological results suggest that the pFRG region contains cholinergic fibers and terminals. In addition, local application of the acetylcholinesterase enzyme inhibitor physostigmine promoted recruitment of ABD_{EMG} activity as well as an increase in tidal volume and minute ventilation. Similarly, local application of the cholinomimetic agent carbachol (CCh) into the pFRG induced potent recruitment of ABD_{EMG} activity, expiratory flow, and an increase in both tidal volume and minute ventilation. The effects induced by CCh were completely inhibited by pre-

application of the muscarinic antagonist scopolamine (SCOP) and strongly inhibited by more selective M3 muscarinic antagonists 4DAMP and J104129.

Within the same region of the ventral surface of the medulla, chemosensitive neurons of the RTN have been identified and characterized (Guyenet & Bayliss, 2015). Currently, it is still debated if expiratory rhythmogenic pFRG neurons represent a separate neuronal group from the more chemosensitive neurons in RTN. In order to further distinguish between respiratory response elicited by the medial and lateral region surrounding the facial nucleus (i.e., lateral pFRG vs medial RTN) we tested respiratory effects induced by local application of CCh in the two areas. While both regions produced active recruitment of ABD muscles, we observed a difference in the resulting respiratory frequency response between the two sites, further supporting the hypothesis for a distinct respiratory function between the medial and lateral parafacial regions.

In summary, these results demonstrate that cholinergic muscarinic transmission contributes to excitation of pFRG neurons and promotes active recruitment of ABD_{EMG} activity and active expiratory flow, therefore acting as a potential mechanism by which state-dependent control during REM could take place.

3.2 Methods

Animal handling and experimental protocols were approved by the Health Science Animal Policy and Welfare Committee of the University of Alberta according to the guidelines established by the Canadian Council on Animal Care, and they are in compliance with the guidelines of Journal of Physiology (Drummond, 2009).

3.2.1 Immunohistochemistry

Immunohistochemistry was performed according to previously published protocols (Pagliardini *et al.*, 2003; Pagliardini *et al.*, 2011). Four adult male rats were anesthetized with urethane (i.p., 2g/kg) and transcardially perfused with 4% paraformaldehyde dissolved in phosphate buffer (PB). The brains were collected, post-fixed, and 50µm brainstem transverse sections were cut with a VT1000 Vibratome (Leica, Wetzlar, Germany). Free-floating sections were rinsed in phosphate-buffered saline (PBS) and incubated with 10 % normal donkey antiserum (NDS) and 0.3 % Triton X-100 for 60 min to reduce non-specific staining and increase antibody penetration. Sections were then incubated overnight with primary antibodies diluted in PBS containing 1 % NDS and 0.3 % Triton X-100. The following day, sections were washed in PBS, incubated with the specific secondary antibodies conjugated to the fluorescent probes (Cy3 - conjugated anti-goat; Cy2-conjugated anti-mouse; Jackson Immuno Research, West Grove, PA, USA) diluted

in 1 % NDS and PBS for 2 h. Sections were further washed in PBS, mounted, and coverslipped with Fluorsave mounting medium (Calbiochem, Billerica, MA, USA). The primary antibodies used for this study detected the following proteins: neuronal nuclear marker (NeuN; raised in mouse; Millipore, 1:500), vesicular acetylcholine transporter (VChaT; raised in in goat; Millipore, 1:1000), choline acetyl transferase (ChAT; raised in goat; Millipore, 1:500). Slides were then observed under a LSM512 Zeiss confocal microscope. Images of the pFRG area and the adjacent facial nucleus were acquired, exported as TIFF files and arranged to prepare final figures.

3.2.2 Acute Experimental procedures

A total of 61 adult male Sprague-Dawley rats (280-350g) were used for acute experiments. Rats were initially anesthetized in isofluorane (2 % in air) while the femoral vein was cannulated and urethane (1.5 g/Kg body weight) was gradually delivered to induce permanent and irreversible anesthesia. Additional doses of anesthesia were delivered as necessary to maintain a surgical plane of anesthesia. The trachea was cannulated and respiratory flow was detected with a flow head connected to a transducer (GM Instruments, Kilwinning, UK). Coupled EMG wire electrodes (CoonerWire, Chatsworth, CA) were inserted into the genioglossal (GG), oblique abdominal (ABD) and diaphragm (DIA) muscles. Wires were connected to amplifiers (AM Systems, Carlsborg, WA) and activity was sampled at 2 kHz (Powerlab 16/30; AD Instruments, Colorado Springs, CO). Rats were vagotomized

by resecting a portion of the vagus nerve (2 mm) at the mid-cervical level and body temperature was kept constant at 37 ± 1°C with a servo-controlled heating pad (Harvard Apparatus, Holliston, MA). In order to reduce tracheal secretion, scopolamine 3-methylbromide (0.1ml/100g) was injected subcutaneously at the beginning of the experiment.

Anesthetized and instrumented rats were then positioned on the stereotaxic frame with bregma 5mm below lambda. Physostigmine (PHYSO, 5 mM, 200 nl) Carbachol (CCh, 1 - 10 mM, 50 – 100 nl), scopolamine (SCOP; 10 mM, 200 nl), Pirenzepine (PZ; 1 – 10 mM, 100 nl), 4-diphenylacetoxy-N-methylpiperidine methiodide (4-DAMP;1 mM, 100 nl), J104129 (1 – 10 mM, 100 nl) and AF-DX-116 (1 mM, 100 nl) diluted in HEPES buffer (Gourine *et al.*, 2010) were pressure injected through a sharp glass electrode (30 mm tip diameter) into the pFRG. Fluorescent beads (200 nm diameter, 0.1-1 %, Invitrogen, Carlsbad, CA) were added to the injected solution to locate the injection site. Stereotaxic coordinates for injections into the pFRG were (in mm) 1.8 rostral, 2.5 lateral and 3.4-3.5 ventral to the obex. Stereotaxic coordinates for injections into the RTN were (in mm) 1.8 - 2.1 rostral, 1.8 lateral and 3.5 - 3.6 ventral to the obex. Control experiments were performed by injecting HEPES buffer (vehicle; 50 – 200 nl) solution in the same locations.

3.2.3 Unit recordings

In 8 experiments we recorded multi-unit activity within the pFRG after local application of CCh. Anesthetized rats positioned on the stereotaxic frame received a bilateral microinjection of CCh (10 mM, 200 nl); once active recruitment of expiratory ABD muscle activity was observed, a 12 mΩ tungsten electrode (AM-Systems) was connected with a One Axis IVM Scientifica micromanipulator and units were recorded at stereotaxic coordinates (in mm) 1.8 rostral, 2.4 - 2.5 lateral and 3.4 - 3.5 ventral to the obex. Localization of the electrode was confirmed by histological examination of post-fixed tissue.

3.2.4 Histology

At the end of each experiment, rats were transcardially perfused with 4% paraformaldehyde dissolved in PB. The brains were collected, post-fixed, and 50µm thick serial transverse sections were either directly mounted on slides and coverslipped for detection of fluorescent beads (i.e., injection site) or counterstained with thionine for identification of brainstem cytoarchitecture. Slides were coverslipped and observed under a Leica DM5500B fluorescent microscope to locate injection sites. Images were acquired with Metamorph (Molecular Devices) program, exported as TIFF files and arranged to identify rostrocaudal and

mediolateral coordinates of injection sites, electrode placement (referenced to the Paxinos rat brain atlas), and to prepare final figures.

3.2.5 Data analysis

Signals from EMG electrodes were amplified at x10 k, filtered between 300Hz and 1 kHz, and sampled at 2 kHz with a PowerLab 16/35 acquisition system. Field Unit activity was amplified at x10 k, filtered between 100 Hz and 10 kHz, and sampled at 10 kHz. Data was then analyzed using LabChart7 Pro (AD Instruments), Excel 2013 and Origin9 (Origin-Lab) softwares. The absolute value of EMG signals was digitally rectified and integrated with a time constant of 0.08 s to calculate peak amplitude. Baseline activity was averaged over 5 minutes before drug injection and normalized. Respiratory changes upon PHYSO and CCh application are indicated as percentage of change compared to baseline values. The respiratory airflow signal was used to calculate respiratory rate, tidal volume and minute ventilation. Tidal volume was obtained by integration of airflow amplitude and converted to ml of air by comparison with a 5 - point calibration curve (0.5 - 5 ml range). Statistical significance of respiratory changes before and during drug injection was tested with a paired t-test, with threshold for significance set at 0.05. Effects of muscarinic antagonists on ABD_{EMG} recruitment were evaluated by comparing peak amplitude activity following CCh injection and subsequent CCh+ muscarinic antagonist injection. For experiments that compared medial and lateral injections, changes in

physiological parameters were compared to pre-injection values and data are reported as percentage of change in both conditions. Data are reported as mean ± standard error.

3.3 Results

3.3.1 Cholinergic innervation is present in, and localized to, the pFRG region

In order to investigate the presence of endogenous cholinergic innervation in the region of the pFRG, coronal brainstem sections were immunolabelled for choline acetyl transferase and vesicular acetylcholine transporter, two markers that respectively identify cholinergic fibers and terminals in the region surrounding the facial nucleus (Fig. 3.1). Labelling of fibers and cholinergic terminals was observed lateral to the caudal edge of the facial nucleus, at the level of the injection sites depicted in figures 3.5 and 3.8. Fig. 3.1 displays expression of VChat positive presynaptic terminals, cholinergic fibers, and cell bodies in the pFRG and in the adjacent facial nucleus (for comparison). Within the pFRG, we observed intense staining for ChaT positive fibers and several VChat positive puncta in close contact with neurons located lateral to the caudal tip of the facial nucleus (Fig. 3.1), the site of injection of CCh and putative location of the pFRG (Pagliardini *et al.*, 2011; Huckstepp *et al.*, 2015). More rostrally (> 400 mm from the caudal tip of the facial nucleus), staining for ChAT and VChat was limited. These results support the hypothesis that cholinergic innervation is present in this area and may influence pFRG activity.

3.3.2 Inhibition of endogenous acetylcholinesterases in the pFRG increases abdominal expiratory activity

We then tested the hypothesis that endogenous acetylcholine (ACh) affects rhythmic activity of pFRG neurons and consequently promotes expiratory modulated activity of ABD muscles. We locally applied an inhibitor of the acetylcholinesterase enzyme (PHYSO, 5 mM, 200 nl) that blocks degradation of ACh and therefore progressively increases endogenous ACh levels within the pFRG. Bilateral local PHYSO application into the pFRG gradually increased tonic ABD_{EMG} activity until it maximally developed within 2.0 ± 0.6 min and lasted for 13.2 ± 0.5 min (n = 8; Fig. 3.2). In addition to potentiating expiratory ABD_{EMG} activity (202 ± 58 % increase in expiration compared to ABD_{EMG} activity during the preceding inspiration, $p = 6.3 \times 10^{-4}$; n = 8; 285 ± 115 % increase in expiration compared to pre-injection values, p = 0.019; n = 8), peak inspiratory $\int DIA_{EMG}$ activity increased of 26.0 ± 17.2 % ($p = 6.8 \times 10^{-4}$; n = 8), peak ∫GG activity increased of 64.8 ± 46.2 % (p = 0.021; n = 5), and tidal volume increased of 22.8 ± 5.5% ($p = 5.5 \times 10^{-4}$; n = 8) compared to pre-injection values. In 4 experiments potentiation of inspiratory EMG activity shortly preceded recruitment of ABD activity, while in the remaining experiments, potentiation in the investigated muscles occurred at the same time. Respiratory frequency decreased from 51.2 ± 3.3 to 44.4 ± 2.3 breaths per minute (BPM, $p = 1.7 \times 10^{-3}$; n = 8) compared to control. As a consequence, minute

ventilation was only marginally increased (+9.2 ± 5.1 %; p = 0.043; n = 8). In 6 out of 8 experiments, PHYSO-induced ABD_{EMG} recruitment was sufficient to generated active expiration (i.e., negative deflection in airflow in late expiration; FIGURE 3.2).

In order to verify that ABD activation was not dependent on a potential brain activation state, we recorded hippocampal/cortical EEG activity in a subset of animals (n = 6; Fig. 3.3). Infusions of PHYSO did not alter ongoing spontaneous brain alternations, but onset of ABD recruitment occurred most frequently with onset of the activated state. Furthermore, the occurrence of ABD recruitment outlasted the ongoing alternations into activated (theta) states by an average of 2.0 ± 0.8 minutes (n = 6). These results indicate that the effects on ABD activity were dependent on local inhibition of degradation of ACh within the pFRG occurring at the onset or during an activated state and not on the induction of a generalized activated brain state.

3.3.3 Activation of cholinergic receptors in pFRG recruits abdominal expiratory activity and active expiration

We tested the hypothesis that cholinergic neurotransmission is involved in the recruitment of rhythmic activation of the expiratory oscillator in the pFRG. Local bilateral application of carbachol (CCh, 10 mM, 100 nl) into the pFRG generated strong recruitment of active expiration (n = 11; Fig. 3.4). The cholinergic agonist CCh induced an initial activation of tonic expiratory activity in the ABD muscles

(46.3 ± 12.6 s delay from the first CCh injection), promptly followed by recruitment of potent phasic expiratory activity upon bilateral injection that lasted for 14.92 ± 1.93 min (n = 11). During this time, respiratory frequency decreased from 49.3 ± 1.5 to 41.6 ± 2.1 bpm ($p = 3 \times 10^{-5}$; n = 11), peak inspiratory $\int DIA_{EMG}$ activity increased of 46.8 ± 20.3 % (p = 0.01; n = 11) and peak ∫GG activity increased of 109.7 ± 35.7 % ($p = 7.9 \times 10^{-4}$; n = 11). Integrated ABD_{EMG} activity before CCh injection displayed either a tonic activity through the respiratory cycle (n = 8) or a weak expiratory modulated activity (n = 3). In both cases, ABD_{EMG} activity increased during inspiration of 21.2 ± 8.9 % compared to pre-injection values (p = 0.02; n = 11) and activity during expiration displayed a peak in late expiration that was 176 ± 33 % larger compared to pre-injection values ($p = 1.2 \times 10^{-5}$) and a 123 ± 16 % increase compared to ABD_{EMG} activity during the preceding inspiration ($p = 1.3 \times 10^{-7}$; Fig. 3.4). Activation of ABD muscles occurred either in synchrony with potentiation of DIA and GG_{EMG} activity (6/11) or followed shortly after their activation (5/11). As a consequence of pFRG activation by CCh, tidal volume increased of 29.4± 6.7 % ($p = 1.3 \times 10^{-4}$; n = 9) and minute ventilation increased of 9.9 ± 3.0 % ($p = 9 \times 10^{-3}$; n = 9). A strong recruitment of ABD_{EMG} activity and active expiration was consistently observed when injection was positioned around the lateral caudal tip of the facial nucleus. Injection sites are indicated in diagrams presented in Fig. 3.5.

Furthermore, similar to PHYSO experiments, infusions of CCh into the pFRG did not significantly alter ongoing spontaneous brain alternations (n=6) and occurrence of ABD recruitment was not associated with brain state alternations.

3.3.4 Activation of late expiratory activity neurons within pFRG during carbachol stimulation

In 8 experiments we recorded multi-unit activity from the region of pFRG upon local microinjection of CCh and recruitment of active expiration. In this region we were able to identify expiratory modulated neurons (n = 8 in 8 rats), inspiratory neurons (n = 5), and tonic neurons (n = 10). In addition, we identified units with a clear discharge during late expiration (n = 11 in 8 rats; Fig. 3.6); these units were in phase with peak of ABD_{EMG} activity and became silent upon waning of the CCh-induced expiratory effect. These results suggest that neurons with a late expiratory phenotype are localized within the pFRG region and are likely activated by local CCh application (Fig. 3.6).

3.3.5 Activation of pFRG is antagonized by scopolamine and M3 receptor antagonists

We further tested the hypothesis that the cholinergic effect on pFRG neurons is mediated by muscarinic receptors by determining if application of muscarinic antagonists blocks CCh-induced recruitment of ABD_{EMG} activity and active expiration. In 7 experiments, after confirmation that CCh injections (10 mM, 100 nl)

into the pFRG successfully induced active expiration and a complete washout of the CCh effect (~60 mins), we bilaterally injected scopolamine (SCOP, 10 mM 200 nl) shortly followed by a second CCh injection (~5 min; fig. 3.7 A). SCOP, a wide spectrum muscarinic receptor antagonist completely blocked CCh-induced recruitment of ABD_{EMG} activity ($p = 0.3$), changes in DIA_{EMG} ($p = 0.99$), and GG_{EMG} activity ($p = 0.91$), changes in tidal volume ($p = 0.3$) and respiratory frequency ($p = 0.3$; $n = 7$; fig. 3.7 B). Interestingly, prior to SCOP injection, three out of seven rats displayed weak expiratory related activity (fig. 3.7A) that was eliminated by injection of SCOP in the pFRG. Application of CCh within 5 minutes from SCOP application did not induce expiratory ABD_{EMG} activity or active expiration or cause any significant respiratory change.

Recovery from SCOP injection (i.e., CCh -induced ABD_{EMG} activation) was tested at 1 and 2 hrs after injection and active expiration was successfully observed only after 2 hr from SCOP injection ($n = 3/3$; fig. 3.7A). Verification of injection sites was performed by identification of fluorescent beads added to the drug and vehicle solutions (534-red beads for CCh injections and 488-green beads for SCOP injection) as displayed in fig. 3.7C.

To further identify the muscarinic receptor subtype involved in the CCh-induced generation of active expiration, we co-applied CCh with selective antagonists

towards M1>M3 (Pirenzepine, PZ), M2 (AF-DX116) and M3>M1 (4-diphenylacetoxy-N-methylpiperidine methiodide, 4-DAMP; J104129) receptors and compared with the responses obtained after a first application of CCH (10 mM, 100 nl) and with the results following a second (repeated) CCH application (fig. 3.7D). Repeated applications of CCH into pFRG evoked an ABD_{EMG} response that was 86.0 ± 4.0% of its initial response ($n = 6$; $p = 9.0 \times 10^{-3}$). The M2 selective antagonist AF-DX116 displayed a small but significant reduction in blocking ABD recruitment compared to the initial maximal response (75.7 ± 3.8 %; $p = 4 \times 10^{-3}$; $n = 4$) but no significant change compared to repeated CCH application ($p = 0.11$). Further, 4-DAMP, an antagonist that is more selective for M3 and M1 but has very low affinity for M2 receptors was able to reduce ABD recruitment to 35.6 ± 11.5 % ($p = 0.006$; $n = 4$) of the initial maximal response, and to 41.2 ± 7.2 % of the response to a repeated application of CCH ($p = 9.5 \times 10^{-5}$). The results suggest that M1/M3 subtypes are likely involved in the CCh-induced ABD recruitment.

Application of a more selective M3 antagonist, J104129, at equimolar concentrations was able to reduce ABD recruitment to 36.2 ± 5.3 % ($p = 0.001$; $n = 4$) of the initial maximal response and to 42.0 ± 7.4 % of the repeated application of CCH ($p = 1.1 \times 10^{-4}$). Injection of the more selective M1 antagonist PZ reduced ABD recruitment only to 70.5 ± 11.9 % ($p = 0.045$; $n = 4$) of the initial maximal response but showed no significant change compared to a repeated CCH application

($p = 0.18$). When 10-folds higher concentration of PZ was tested (10 mM), ABD recruitment was reduced to 32.3 ± 12.2 % ($p = 5.7 \times 10^{-3}$; $n = 4$) of the initial maximal response. Given the similar Ki of J104129 and PZ for human M1 receptors (Ki = 19 nM and 16 nM, respectively) and the reduced selectivity of PZ for M1 versus M3 compared to J104129, we attribute the high-dose effect of PZ to inhibition of M3 receptors.

Notwithstanding the limitation of these experiments due to lack of highly specific muscarinic agonists and antagonists currently available, we conclude that M3 receptors are the most likely receptor subtype responsible for CCh-induced generation of active expiration.

To exclude possible contributions of nicotinic receptors to CCH within the pFRG we also applied a wide spectrum nicotinic receptor antagonist, hexametonium bromide (HEX), into the pFRG. Both co-application of 1 mM HEX or 10 mM HEX did not affect ABD recruitment compared to the initial maximal response ($p = 0.3$ and $p = 0.25$, respectively; $n = 4$). These results suggest that nicotinic receptors have likely no effect on pFRG activation and ABD recruitment.

3.3.6 CCh response in the medial and lateral regions surrounding the facial nucleus

Previous work has shown that the chemosensitive area medial and ventral to the facial nucleus, corresponding to the RTN, display excitatory response to local application of cholinergic agonists (Dev & Loeschcke, 1979; Nattie & Li, 1990). An ongoing issue in respiratory neurophysiology is related to the identity of pFRG neurons and the possibility of being a distinct class of respiratory neurons from the adjacent RTN neurons.

In order to further test the hypothesis that regions medial and lateral to the ventral surface of the facial nucleus correspond to functionally different structures involved in respiratory control, namely RTN (medially) and pFRG (laterally), we injected a smaller volume and a lower concentration of CCh (50 nl, 1 mM) at 1.8 and 2.5 mm from the midline, with the objective of identifying local differences in the physiological response to CCh between the two areas (Fig. 3.8). CCh injection in the lateral pFRG caused respiratory rate depression compared to pre-injection values (-27.1 ± 3.1 %; $p = 7.7 \times 10^{-6}$; n = 11; pre-injection values were compared to the max respiratory frequency response following injection). On the other hand, CCh injections medial to the facial nucleus increased the respiratory rate of 21.0 ± 5.2 % compared to pre-injection values ($p = 7.2 \times 10^{-4}$; n = 11). The change in respiratory rate response between medial and lateral injections was significant ($p = 3.9 \times 10^{-6}$).

CCh injections increased peak inspiratory $\int DIA_{EMG}$ activity in both lateral (+ 41.6 ± 12.1 %; p = 0.002) and medial (+19.2 ± 5.6 %; p = 0.003) injection sites. In addition, upon CCh injection VT was increased in both lateral (+ 28.3 ± 4.9 %; $p = 3.9 \times 10^{-4}$) and medial (+ 12.8 ± 2.7 %; $p = 3.0 \times 10^{-4}$) injections sites as well as minute ventilation (+ 11.0 ± 4. 8 %, p = 0.01 in lateral injections; +20.6 ± 5.0 %, p = 0.001 in medial injections). Again, comparison between lateral and medial injections indicated significant differences in the ratio of change for VT ($p = 5.9 \times 10^{-3}$) and minute ventilation (p = 0.03) but no significant difference in change of $\int DIA_{EMG}$ peak amplitude (p = 0.06) between the two sites (Fig. 3.8).

In seven out of eleven experiments local bilateral application of 1 mM CCh into the lateral pFRG generated strong recruitment of abdominal muscles. In the remaining four experiments, although we observed respiratory rate depression and changes in tidal volume, excitation was not sufficient to induce ABD_{EMG} recruitment and active expiration. Overall, ABD_{EMG} activity increased of 22.0 ± 11.5 % (p = 0.04; n = 11) during inspiration and of 113.6 ± 42.9 % during expiration compared to pre-injection values (p = 0.01; n = 11).

In four out of the eleven experiments, medial injections increased $\int ABD_{EMG}$ activity, while in the remaining seven experiments ABD_{EMG} did not display significant recruitment. Overall, ABD_{EMG} activity was not significantly increased during inspiration (+ 6.0 ± 5.1 %; p = 0.13; n = 11) or during expiration (+ 46.1 ±

30.9 %; p = 0.08; n = 11) compared to pre-injection values. Fig. 3.8 indicates the core location of the injection sites for these experiments and summarises the comparison between medial and lateral injections. The spread of the fluorescent beads injected with the drug solution was ~250 mm in diameter, at 2.5 mm from the midline, with the rostrocaudal extent of the injection ranging from 50 ± 9.53 mm caudal of the caudal tip of the facial nucleus to 227.28 ± 26.42 mm rostral of the caudal tip of the FN. No overlap between the two injection sites was observed.

3.4 Discussion

This study investigated the effect of cholinergic receptor activation on pFRG activity and consequent generation of expiratory ABD_{EMG} activity and active expiration. We demonstrated that cholinergic fibers and terminals are present in the area surrounding the facial nucleus and that stimulation of cholinergic receptors (either by CCh or PHYSO local application) activated late expiratory pFRG neurons, potentiated respiration, and promoted generation of long lasting active expiration. This effect was not associated with a generalized brain state activation. In addition, we demonstrated that this effect could be blocked by local application of the muscarinic antagonist SCOP and was strongly depressed by M3 muscarinic receptor antagonists. Further, we demonstrated a distinct respiratory response between CCh injection in the region medial to the facial nucleus (corresponding to the previously identified RTN chemosensitive neurons) and the region lateral to the facial nucleus (corresponding to the key expiratory rhythm generating area of the pFRG), further supporting the hypothesis that two specific regions are responsible for distinct respiratory function.

Acetylcholine has been implicated in several aspects of the neural control of respiration, such as respiratory frequency and motor output (Burton *et al.*, 1994; Shao & Feldman, 2009), state dependent modulation of breathing (Kubin & Fenik,

2004), and central and peripheral chemosensitivity, being an important neurotransmitter in the carotid bodies (Nurse, 2010) and having a stimulatory effect on central chemoreceptors (Dev & Loeschcke, 1979; Fukuda & Loeschcke, 1979; Loeschcke, 1982; Gillis *et al.*, 1988; Nattie & Li, 1990; Sobrinho *et al.*, 2015). Anatomical evidence also suggests that cholinergic innervation is present in the brainstem reticular formation with the majority of cholinergic inputs deriving from the pontine structures of the pedunculopontine tegmental nucleus and the laterodorsal tegmental nucleus (Woolf & Butcher, 1989; Jones, 1990; Woolf, 1991; Yeomans, 2012). An additional source of cholinergic innervation derives from local cholinergic neurons present in the reticular formation (Jones, 1990; Woolf, 1991). Stimulation of mesopontine structures elicits multiple and diverse respiratory responses with occurrence of apneas, tachypnea, EMG depression or activation depending on the site of stimulation within these structures (Topchiy *et al.*, 2010). In addition activation of some of the descending projections to the oral pontine nucleus and subceruleus reproduce theta rhythms and muscles atonia observed during REM sleep with diverse respiratory and cortical effects depending on the site of stimulation (Kubin & Fenik, 2004), thus suggesting a complex role of mesopontine structures on respiratory modulation across brain states.

Consistent with this idea, we could identify labelling of cholinergic fibers in the pFRG region and the presence of several cholinergic terminals in neurons located

lateral and caudal to the facial nucleus (the target area of our pFRG microinjections), as demonstrated by our immunohistochemical data. We conclude that cholinergic fibers run and send synaptic contact to neurons located in the pFRG area. The source of this cholinergic innervation is currently unknown.

Recent evidence from our laboratory shows that spontaneous recruitment of ABD_{EMG} activity often occurs during REM sleep and REM-like states under urethane anesthesia (Pagliardini *et al.*, 2012; Andrews & Pagliardini, 2015). During REM epochs, expiratory ABD_{EMG} recruitment is associated with reduced respiratory variability and an increased tidal volume and minute ventilation compared to respiratory events preceding ABD_{EMG} recruitment. We therefore hypothesized that cholinergic neurotransmission, which is particularly active during REM sleep (McCarley, 2007; Boucetta *et al.*, 2014) and REM-like sleep states under urethane anesthesia (Boucetta & Jones, 2009), may be involved in the recruitment of expiratory ABD muscles through release of acetylcholine in the pFRG region, a key site for providing rhythmic excitatory drive to expiratory muscles. Consistent with this idea, local application of CCh into the pFRG induced strong and long lasting recruitment of active expiration associated with a decrease in breathing rate, activation of ABD_{EMG} muscles, and consequent increase in tidal volume and minute ventilation. Blocking of acetylcholinesterase activity by means of PHYSO promoted

gradual recruitment of ABD muscle activity until active expiration was fully developed, suggesting that an increase in endogenous ACh concentration in the pFRG is sufficient to generate active expiration. In conjunction with recruitment of active expiration, we also observed potentiation of DIA and GG inspiratory activity, which may be promoted by a stimulatory effect of pFRG neurons on preBötC or inspiratory premotoneurons (Pagliardini *et al.*, 2011), even before full active expiration is developed.

We further tested the hypothesis that muscarinic receptors are involved in this pathway and were able to block CCh-mediated respiratory response by local pre-application of the muscarinic receptor antagonist SCOP. Scopolamine application did not affect ongoing ventilatory properties, similar to the observed effects of local inhibition of pFRG neurons in resting condition (Huckstepp *et al.*, 2015). Interestingly, when expiratory related ABD_{EMG} activity was present prior to SCOP injection, this activity was reduced by SCOP injection, demonstrating that endogenous release of acetylcholine possibly influences expiratory modulated activity in pFRG of urethane anesthetized rats. Scopolamine successfully blocked response to CCh until the drug washed out and the CCh-mediated response was consequently recovered. Even though we can't exclude a contribution of nicotinic neurotransmission to pFRG modulation, our results with scopolamine strongly support a muscarinic mechanism for CCh-mediated pFRG activation. To further test

for specific subtype of muscarinic receptors involved in the CCh-mediated pFRG activation, we used more selective antagonists for blocking M1, M2 and M3 receptor subtypes since they have been reported to be present in the respiratory networks in the medulla (Nattie & Li, 1990; Mallios *et al.*, 1995; Muere *et al.*, 2015): our results suggest that activation of pFRG by CCh is most likely mediated by M3 muscarinic receptors.

It is interesting to observe that the excitatory cholinergic effect on expiratory ABD motoneurons is distinct from what observed in genioglossus and postural muscles when either cholinergic neurotransmission is locally modulated (Grace *et al.*, 2013) or PPT area is locally stimulated with CCh in an animal model of sleep (Kubin & Fenik, 2004). While both phenomena also occur in natural sleep (i.e., genioglossus and postural muscle activity are depressed, reviewed in (Chase & Morales, 1990), ABD muscles are activated (Andrews & Pagliardini, 2015)), the mechanisms through which they occur may be different. It is well known that majority of postural muscles are depressed during REM sleep. This may be due to active inhibition promoted by either GABA or glycine (Peever, 2011) or by active inhibitory mechanisms that may use acetylcholine as major neurotransmitter (Grace *et al.*, 2013). Despite this general inhibition, other muscles either maintain their activity (diaphragm) or are activated during periods of REM sleep. We propose that ABD muscles, at least in rodents, are recruited during periods of REM sleep and this

activation may be mediated by cholinergic transmission at the level of the expiratory oscillator, the pFRG. Activation of the oscillator, located in the pFRG, likely activated premotoneurons in the caudal ventral respiratory group (or nucleus retroambiguus) that eventually send a rhythmic excitatory drive to the abdominal motoneurons located in low thoracic, high lumbar levels of the spinal cord (Janczewski *et al.*, 2002; Boers *et al.*, 2006; Janczewski & Feldman, 2006; Giraudin *et al.*, 2008; Huckstepp *et al.*, 2016).

Recent data support the hypothesis that pFRG neurons located lateral to the facial nucleus in the ventral medulla are important for expiratory rhythm generation and are functionally distinct from the more medially located chemosensitive RTN neurons (Abbott *et al.*, 2011; Pagliardini *et al.*, 2011; Huckstepp *et al.*, 2015). Local optogenetic stimulation or release of inhibition within this region activates pFRG neurons with a late expiratory activity and promote recruitment of ABD_{EMG} activity and active expiration (Pagliardini *et al.*, 2011). Further, optogenetic stimulation of pFRG neurons affects breathing rhythms by resetting ongoing inspiratory activity (Pagliardini *et al.*, 2011). Distinct respiratory effects were obtained when the more medial Phox2b-expressing chemosensitive RTN neurons were stimulated (Abbott *et al.*, 2011).

Furthermore, acute silencing of either the lateral pFRG region or the medial RTN region in both resting condition and under an increased respiratory drive (hypoxia or hypercapnia) induced distinct respiratory responses (Huckstepp *et al.*, 2015). The different respiratory responses to neuronal inhibition support the hypothesis that the medial (i.e., RTN) and lateral (i.e., pFRG) parafacial region have a distinct role in respiratory control. Our current results provide further evidence for this hypothesis by demonstrating that cholinergic stimulation of the two sites (medial and lateral) elicits distinct responses in respiratory frequency, tidal volume and ABD recruitment. In this set of experiments we used smaller volumes and lower CCh concentration, in order to avoid spread of drug into the site of comparison and to better evaluate the site of injection. It is therefore not surprising that not all of the experiments provided an intense response in terms of ABD_{EMG} recruitment, as the excitation was potentially not sufficient to drive the activity of the expiratory oscillatory network. In this regard, we observed some ABD_{EMG} recruitment upon medial injections; this may be due to i) unwanted spread of the drug lateral to the facial nucleus, ii) the presence of some expiratory oscillator neurons in the medial region, or iii) more likely, indirect activation of pFRG neurons via RTN activation. We believe that the latter hypothesis is most likely since previous work has demonstrated the important role of Phox2b-expressing chemosensitive RTN neurons in providing a tonic drive to both inspiratory and expiratory activity (Abbott *et al.*,

2009; Marina *et al.*, 2010; Abbott *et al.*, 2011). Nonetheless, changes in respiratory frequency upon CCh injections are indicative of a differential response to CCh for the two sites. The depression in breathing occurring upon lateral (pFRG) injection is consistent with the reported effects occurring upon release of inhibition with GABAergic and glycinergic antagonists and consequent activation of pFRG neurons (Pagliardini *et al.*, 2011; Huckstepp *et al.*, 2015). The cellular and network mechanisms associated with a reduced respiratory rate during ongoing pFRG activation are yet not clear. One possibility is that pFRG neurons interact with preBötC neurons to reduce respiratory rate. On the other hand, the small but significant increase in respiratory rate upon CCh injection is likely driven by the preBötC through excitation provided by RTN neurons (Abbott *et al.*, 2009; Abbott *et al.*, 2011).

3.5 Conclusions

We conclude that cholinergic innervation is present in the pFRG area, and likely acts through muscarininc receptors that depolarize and activate rhythmic pFRG neurons. The source of cholinergic innervation is currently unknown. Pedunculopontine tegmental and laterodorsal tegmental nuclei are the most likely candidates since they contain cholinergic neurons, are active in REM epochs and have been shown to project to the reticular formation (Woolf & Butcher, 1989; Jones, 1990). Pre or post-synaptic muscarinic receptors may be involved in the process as cholinergic fibers and terminals are present in the area of pFRG. Further studies will be necessary to investigate the presence of direct cholinergic projections to pFRG neurons in order to determine the correlation between REM active structures, rhythmic activation of pFRG neurons, and expression of active recruitment of expiratory ABD muscles.

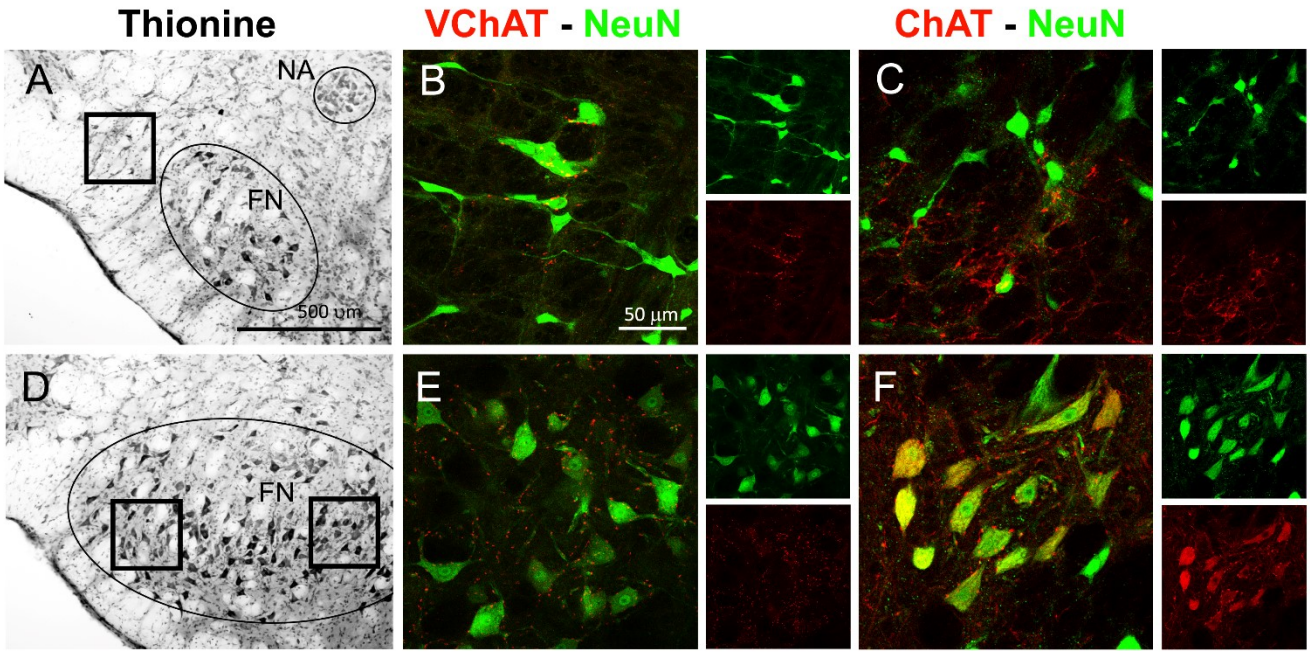

Figure 3.1 Distribution of cholinergic terminals in both pFRG and the motoneurons in the facial nucleus. A-B) Thionine counterstaining of the ventral medulla at the level of the caudal tip of the facial nucleus (A) and,more rostrally, in the core of the FN. **C,D**) Vesicular acetylcholine transporter (VChaT; red) and Neun (green) immunoreactivity for cholinergic presynaptic terminals in the pFRG (C) and in the facial nucleus (**D**). Small panels on right illustrate single staining for each marker. The immunopositive puncta surrounding pFRG neurons indicate the presence of cholinergic terminals in the region caudal and lateral to the facial nucleus. **E,F)** Choline acetyl transferase (Chat, red) and Neun (green) immunoreactivity for cholinergic fibers and cell bodies in the pFRG (**E**) and in the facial nucleus (**F**). Black square in A indicates the location where images in C and

E were taken. Black squares in D indicates the location where images in E (right) and F (left) were taken. Calibration bars: A,B = 500 µm, C – F = 50 µm.

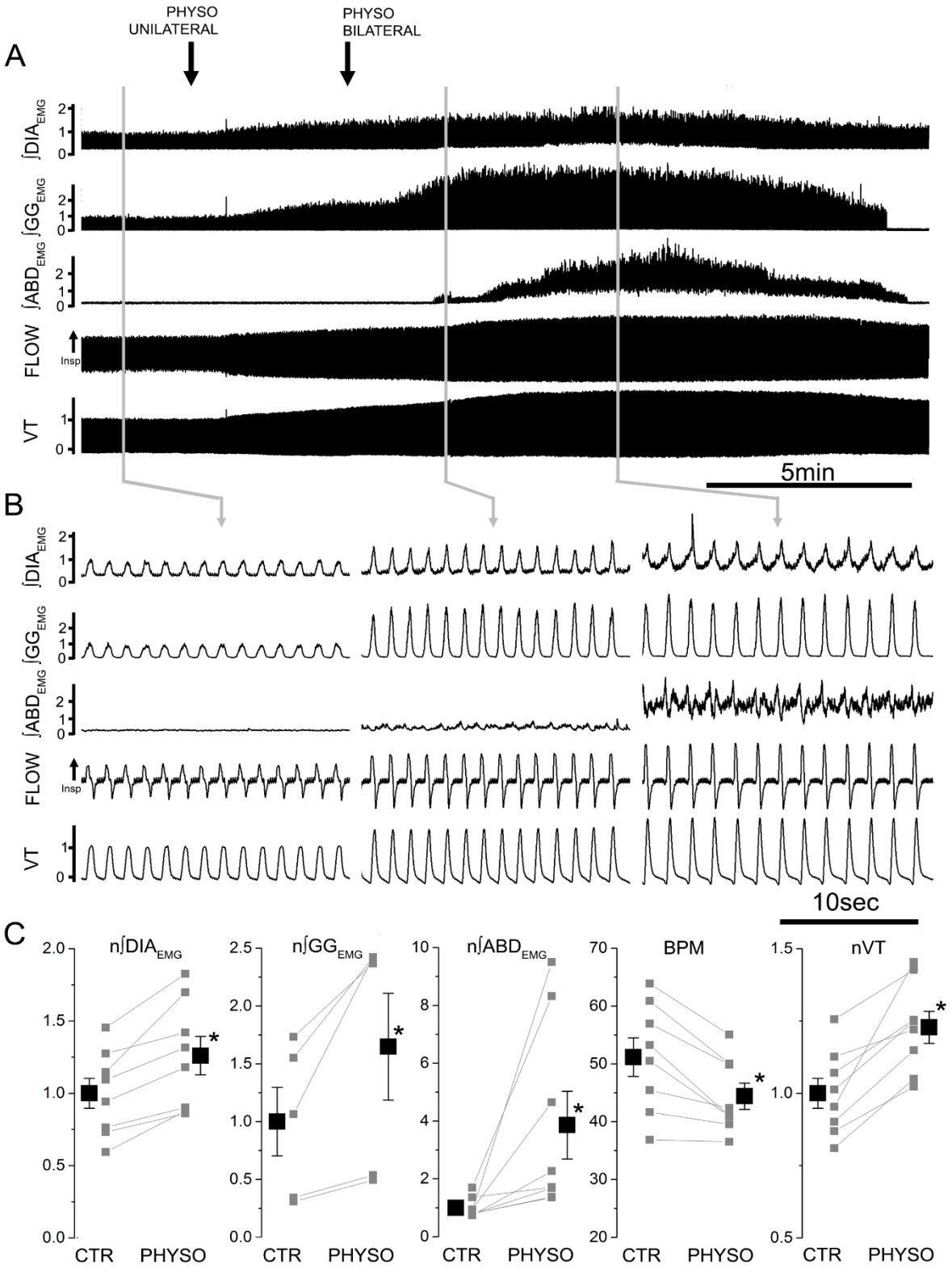

Figure 3.2 Local application of physostigmine (PHYSO, 5 mM, 200 nl) in pFRG

induces long lasting ABD recruitment and active expiration. A) Long trace recordings of $\int DIA_{EMG}$, $\int GG_{EMG}$ and $\int ABD_{EMG}$, respiratory airflow and tidal volume (VT) during local bilateral application of PHYSO (black arrows indicate time of injections on the two sides of the ventrolateral medulla). **B)** Details of respiratory traces before (left), and after PHYSO application (centre and right). Note progressive activation of expiratory modulated ABD_{EMG} activity. **C)** Single experiment data (gray) and averaged data (black) on the effect of bilateral application of PHYSO on $\int DIA_{EMG}$, $\int GG_{EMG}$ and $\int ABD_{EMG}$, breath per minute (BPM) and tidal volume (VT). EMG and tidal volume data are normalized to control values and asterisks indicate statistical significance ($p < 0.05$) relative to pre-injection control values.

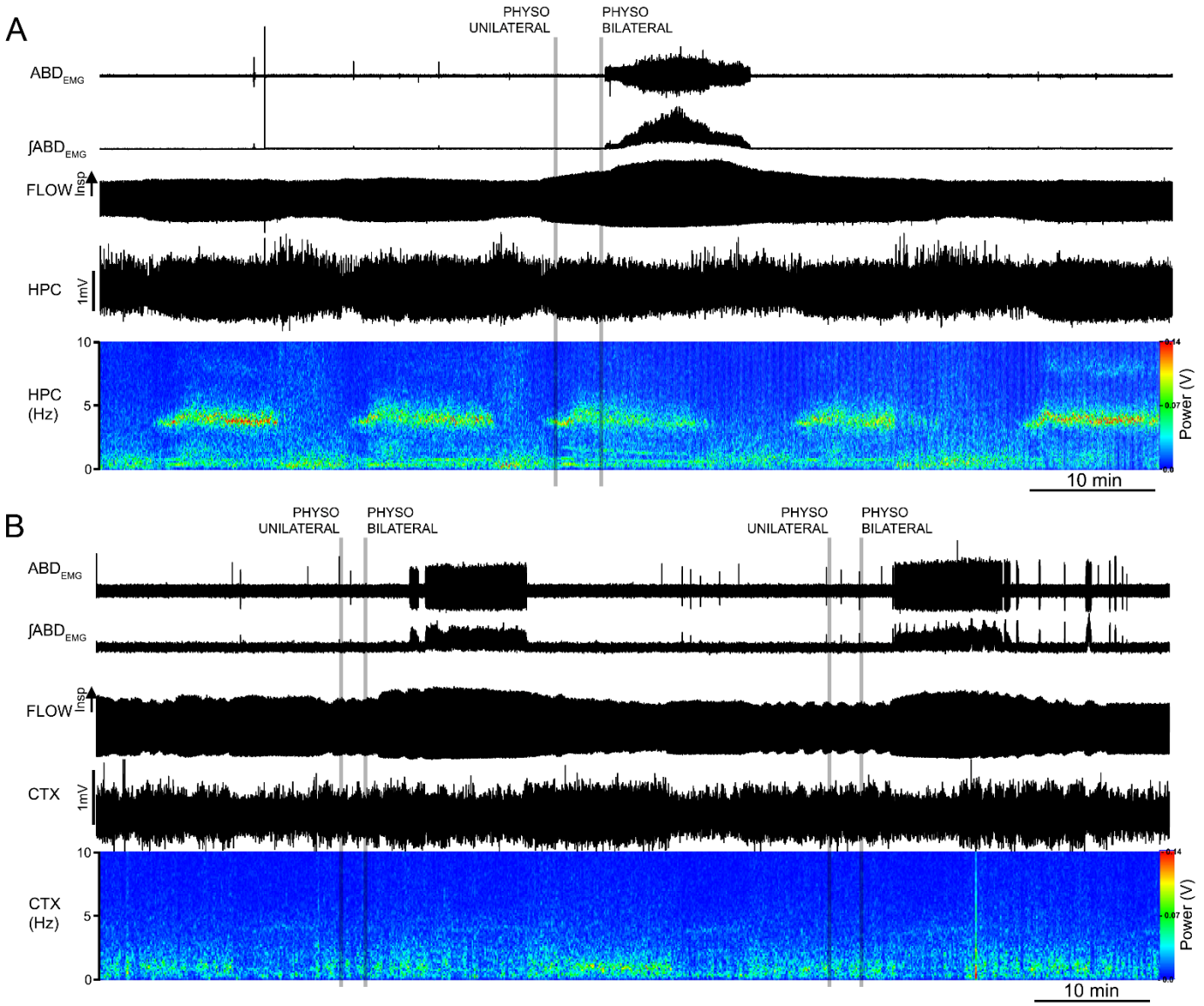

Figure 3.3 Local application of physostigmine (PHYSO, 5 mM, 200 nl) in pFRG does not affect spontaneous brain state alternations. A) Long trace recordings of ABD_{EMG}, $\int ABD_{EMG}$, respiratory airflow, hippocampal activity and its power spectrogram during local bilateral application of PHYSO (grey lines indicate time of injections on the two sides of the ventrolateral medulla) during activated state (high power at 4Hz frequency). Note lack of effect in spontaneous brain state

alternation and the persistence of expiratory activity with brain state changes. **B)** Long trace recordings of $ABD_{EMG,}$ $\int ABD_{EMG}$, respiratory airflow, cortical activity and its power spectrogram during local bilateral application of PHYSO during deactivated state (high power at 1Hz frequency). Note lack of effect in spontaneous brain state alternation and the onset of expiratory activity occurring with activated states.

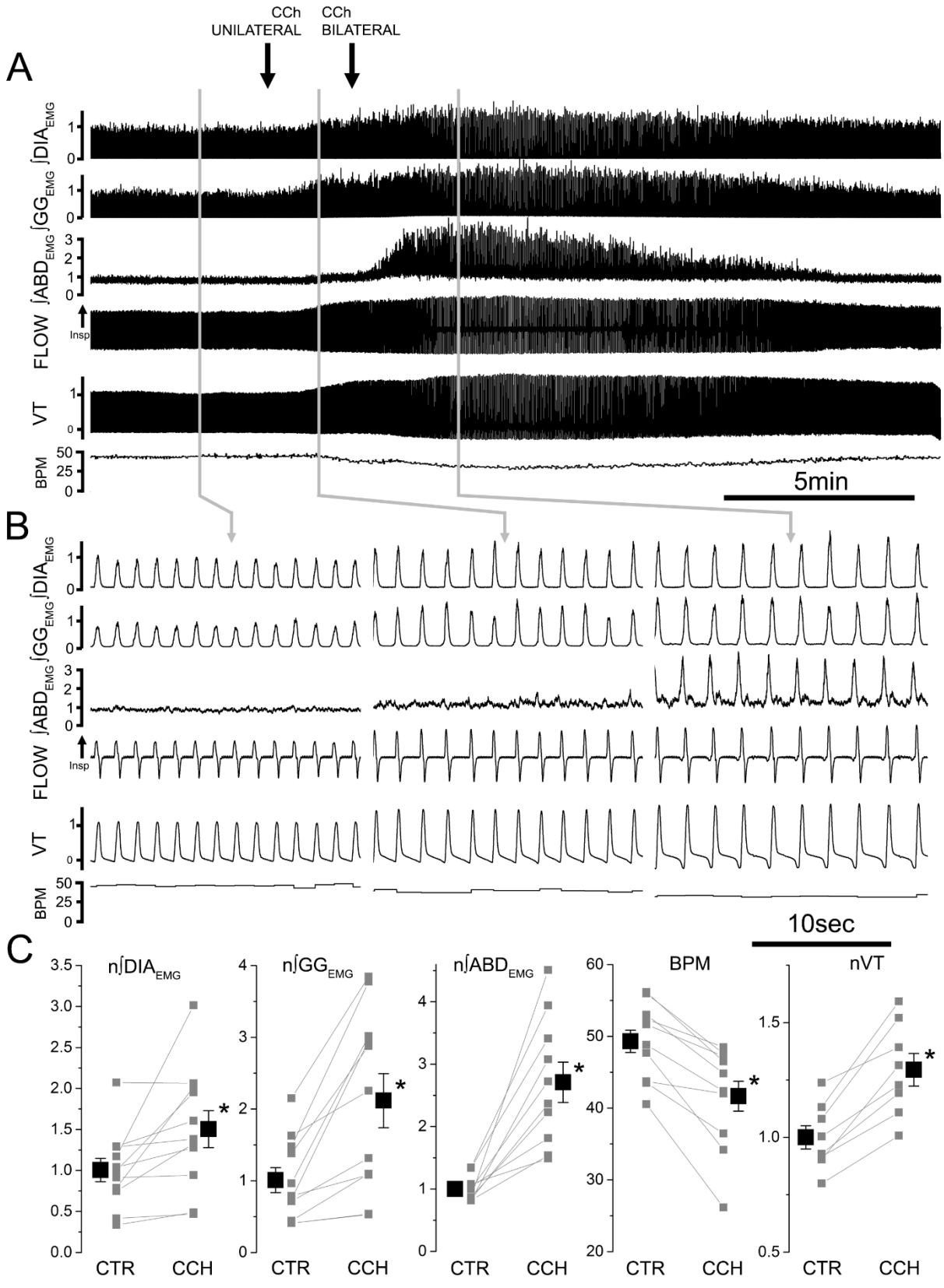

Figure 3.4 Local application of carbachol (CCh, 10 mM, 100 nl) in pFRG

induces long lasting ABD recruitment and active expiration. Effect of bilateral application of CCh on $\int DIA_{EMG}$, $\int GG_{EMG}$ and $\int ABD_{EMG}$, respiratory airflow, tidal volume (VT), and respiratory rate (BPM). Black arrows indicate time of injections. **B)** Details of respiratory traces before (left), after the first (unilateral, centre) and second (bilateral, right) CCh injections into the pFRG of urethane anesthetized rats. Note progressive activation of expiratory modulated ABD_{EMG} activity following CCh injection. **C)** Single experiment (grey) and averaged data results (black) on the effect of bilateral application of CCh on $\int DIA_{EMG}$, $\int GG_{EMG}$ and $\int ABD_{EMG}$, breath per minute (BPM) and tidal volume (VT). Respiratory muscle EMGs and tidal volume data are normalized to control and asterisks indicate statistical significance ($p < 0.05$) relative to pre-injection control values.

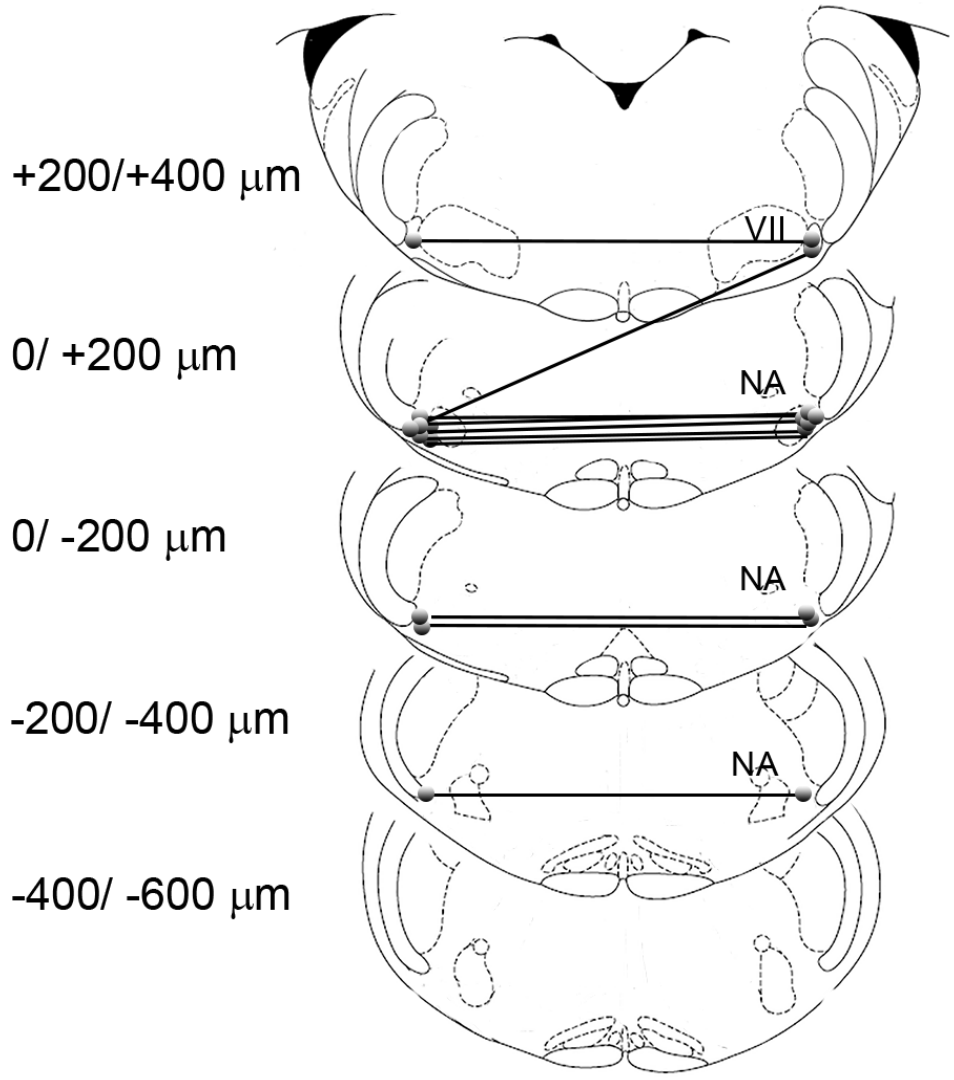

Figure 3.5 Representative sections of adult rat brainstem indicating CCh injection sites in the pFRG of urethane anesthetized rats that promoted recruitment of ABD activity and active expiration (modified from (Paxinos and Watson, 1998); 0 μm corresponds to the caudal tip of facial nucleus (VII). Each symbol represents an

injection site and lines connect the two injection sites performed in each experiment (n = 10). NA: nucleus ambiguus.

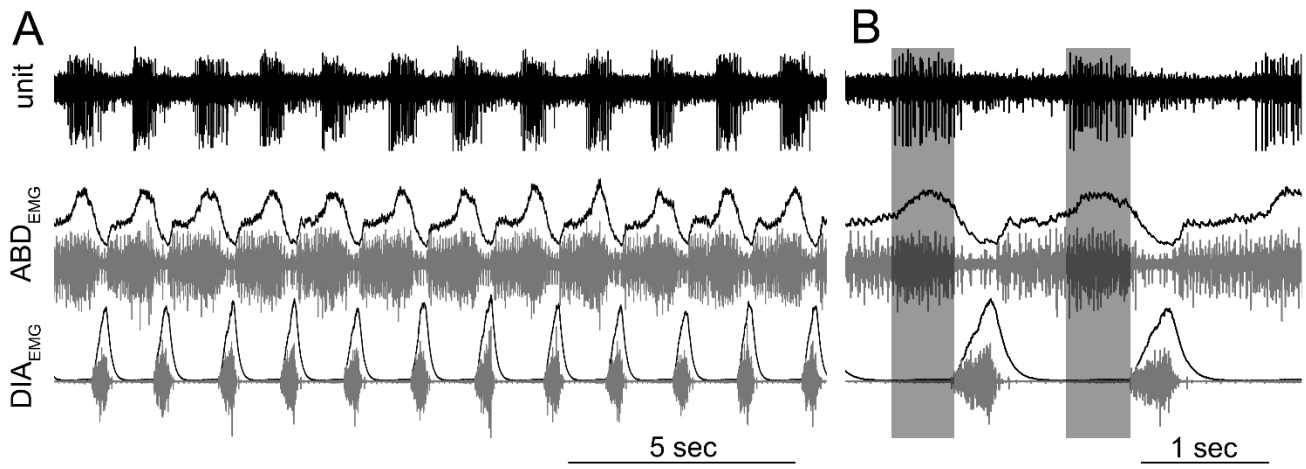

Figure 3.6 Late expiratory neurons are located at the site of CCh injection during recruitment of active expiration. Multiunit activity recorded at injection site, integrated and raw DIA and ABD_{EMG} activity recorded during expression of active expiration induced by local microinjection of CCh into the pFRG. **A**) long trace recording, **B**) detail of multiunit activity across two respiratory events.

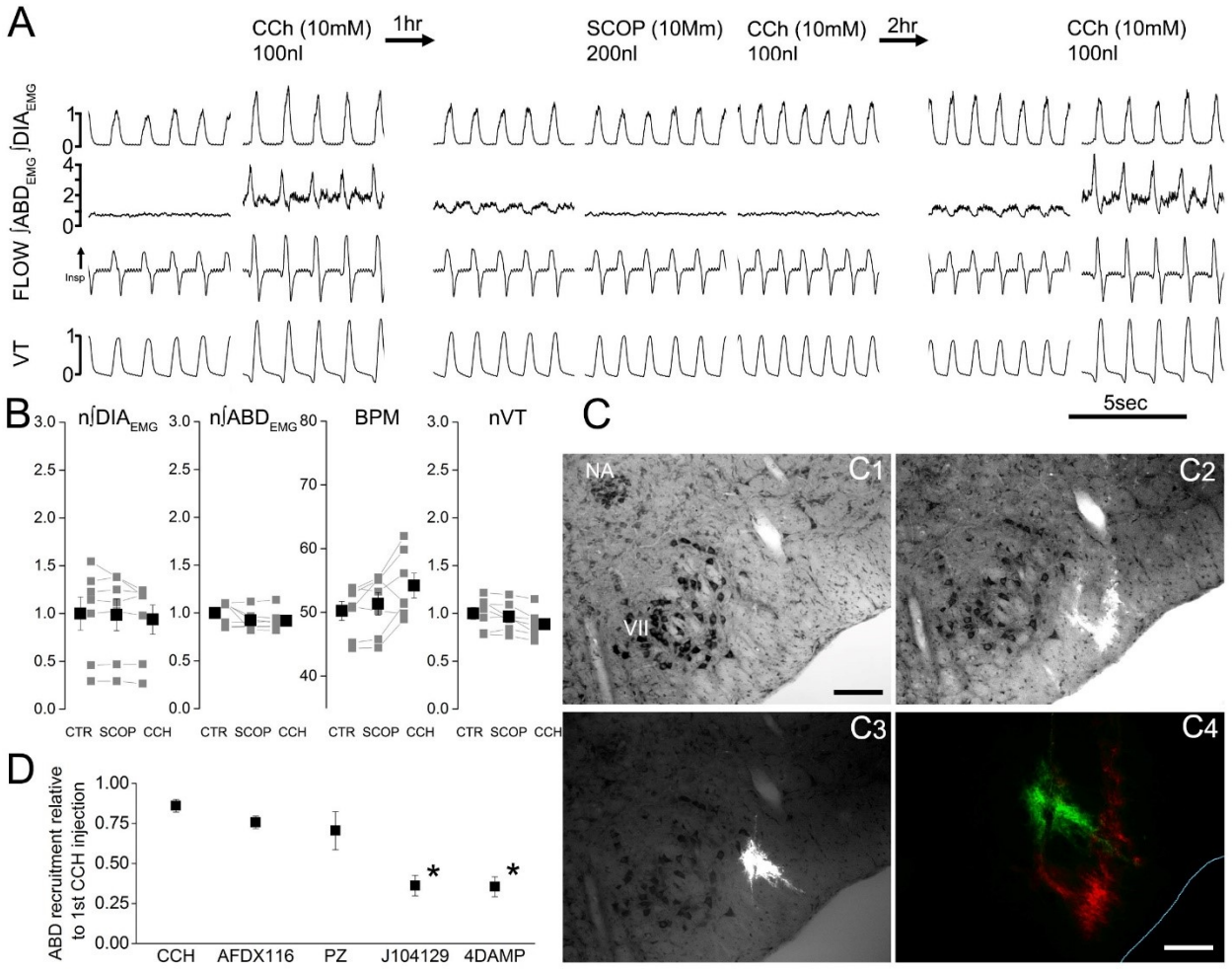

Figure 3.7 Scopolamine blocks CCh induced recruitment of ABD_{EMG} and active expiration. A) Details of traces from $\int DIA_{EMG}$, $\int ABD_{EMG}$, respiratory flow and tidal volume (VT) before and after first CCh injection (left), before and after SCOP and CCh (centre), and CCh injection after the recovery period (right). **B)** Effect of bilateral application of SCOP followed by CCh injection on normalized $\int DIA_{EMG}$ and $\int ABD_{EMG}$, BPM and normalized tidal volume (VT). Note lack of significant changes on respiratory parameters ($p > 0.05$) after SCOP and CCh injection relative

to pre-injection control values (grey, individual experiments; black, averaged data). **C)** Images taken from a transverse section at the caudal tip of the facial nucleus counterstained with thionine (C1) and illustrating injection site for SCOP (C2) and multiple injection sites for CCh (C3). C4 illustrate proximity of injections of the two drugs (SCOP, green; CCh, red). **D**) Effects of the muscarinic antagonists AF-DX116, PZ, J104129 and 4-DAMP on CCh-induced ABD_{EMG} activity. Data are reported as relative to initial (first injection) CCh-induced contraction of ABD muscles calculated in the first 5 minutes post injection. Significant changes relative to second CCh injection are indicated with an asterisk. Calibration bar C1 - C3, 200 µm; C4 100 µm. NA: nucleus ambiguus, VII: facial nucleus.

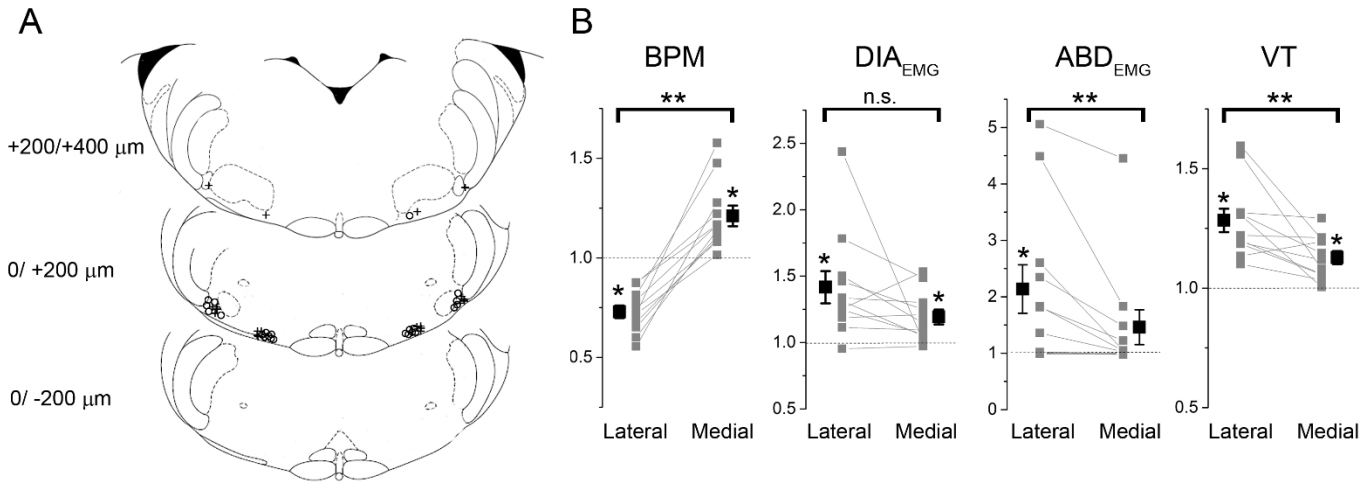

Figure 3.8 Local application of carbachol (CCh, 1 mM, 50 - 100 nl) in the region lateral or medial to the facial nucleus induces different respiratory responses. **A**) Representative sections of adult rat brainstem [modified from Paxinos and Watson (1998)] indicating location of medial and lateral injection sites along the rostro-caudal axis. 0 corresponds to the caudal tip of facial nucleus (VII). Each symbol represents an injection site. Open circles identify injections sites where strong abdominal muscle recruitment was observed. Cross symbols indicate injection sites that did not elicit ABD recruitment. **B)** Summary plots indicating

changes in respiratory rate (BPM), peak $\int DIA_{EMG}$ and $\int ABD_{EMG}$ activity, and tidal volume (V_T) (relative to pre-injection values (grey, individual experiments; black, averaged data). Connecting lines indicate differential responses across sites in the same rat. * indicates significant change upon CCh injection compared to pre-injection values;** indicates significant changes between lateral or medial injections ($P < 0.05$). n.s., not significant.

CHAPTER IV

General discussion

4.1 Overview

Studying how respiratory oscillators respond to various forms of stimulations is an important and essential experimental approach to enhance our understanding of respiratory rhythmogenesis and, more generally, in the field of respiratory neurophysiology. The hypothesis of a dual respiratory oscillators, where the preBötC drives inspiration and the pFRG drives active expiration, has been proposed and supported by various pieces of evidence throughout different experimental approaches (Mellen *et al*., 2003; Janczewski and Feldman, 2006; Feldman and Del Negro, 2006; Pagliardini *et al*., 2011; Feldman *et al*., 2013 Huckstepp *et al*., 2015, 2016). In the experiments reported in this research thesis I studied each respiratory oscillator independently and reported how the two oscillators respond to different forms of stimulation. Understanding the preBötC and the pFRG functions in respiratory control is important given their proposed roles as respiratory oscillators. Previous work has shown the essential role that the preBötC and the pFRG play in respiratory control, as illustrated in Chapter 1 (Smith *et al*., 1991; Gray *et al*., 2001; Onimaru and Homma, 2003; Abbott *et al*., 2011; Pagliardini *et al*., 2011). The projects presented in this thesis investigate the effects of manipulating the activity of respiratory oscillators (preBötC and pFRG) by examining various respiratory parameters.

4.2 Optogenetic excitation of preBötzinger complex neurons potently drives inspiratory activity in vivo

The second chapter of this thesis focused on the preBötC responses evoked by different patterns of optogenetic stimulation. The advantage of such a highly temporally controlled stimulation enhances the reliability of our results and mimics the endogenous excitatory inputs to the preBötC. Other neural excitation or inhibition techniques have been previously used to interrupt the respiratory oscillators activity (Mellen *et al*., 2003; Mulkey *et al*., 2004; Janczenski and Feldman, 2006), however the high temporal precision achieved here with optogenetics improved our ability to control the stimulation onset, duration, and the site of stimulation, thus the evoked results were reliable. Respiratory rhythm entrainment or resetting was achieved by manipulating other brain regions, such as carotid sinus nerve (Paydarfar *et al*., 1998), chemoreceptors stimulation (Eldridge, 1972), and neurons of the para facial region (Abbott *et al*., 2011) or by using other techniques such as mechanical ventilator (Baconnier *et al*., 1993) and phasic lung inflation (Mellen and Feldman, 2000). However, the respiratory responses achieved here by stimulating the preBötC, the core of the inspiratory rhythm generation, are more powerful in terms of changes in respiratory frequency, entrainment of respiratory activity, and the induced respiratory reset.

Our results demonstrate that laser stimulation of the preBötC neurons expressing ChR2 driven by synapsin promoter increases the respiratory frequency up to four fold of the pre-stimulation frequency, entrain respiration to frequencies much higher than the baseline levels, and reset the respiratory rhythm with the occurrence of a refractory period. Moreover, either short or long laser pulses applied to the preBötC neurons in presence of a reduced respiratory drive resulted in rhythmic diaphragmatic contractions which increased the respiratory frequency to levels comparable to the baseline levels.

Therefore, the ability of laser stimulation to reliably affect the preBötC behaviour provides additional evidence for both the preBötC role as the main respiratory oscillator and the importance of excitatory mechanisms within the preBötC network. The combination of both accurate injection sites based on preBötC stereotaxic coordinates, post-mortem histological examinations, and accurate laser prop positioning during light stimulation allowed us to ensure that the evoked results are due to preBötC excitation. The light power is reduced when the light travels through the tissue. Given that the cell bodies of preBötC neurons are located 300-500 μm from the ventral surface of the medulla we expect that the dendrites extending ventrally are the site affected by light pulses. Moreover, by applying pharmacological agents we exclude the involvement of other non-respiratory neurons in the reported respiratory responses.

The preBötC network is the kernel for inspiratory rhythmogenesis and it is composed of a heterogeneous neural population, these neural populations differ either in their rhythmogenic role, their excitatory or inhibitory phenotype, their genetic origin, or their anatomical markers (Smith *et al.*, 1991; Feldman *et al.*, 2003; Bouvier *et al.*, 2010; Gray *et al.*, 2010; Sherman *et al.*, 2015).

One of the limitations of the work presented here is the fact that the results obtained with ChR2 driven by a synapsin promoter illustrate the effects of a generalized excitation of the preBötC network, independent from the phenotype of preBötC neurons. Lack of specificity within this context was not of a major concern, as our experimental goal was to examine the preBötC network response to a fine excitatory drive since this approach was currently unexplored.

More recent work has been done to examine the independent roles of different neuronal populations within the preBötC microcircuit. Laser pulses were applied bilaterally to either SST or Dbx1 neurons expressing ChR2 within the preBötC region. Photostimulation of preBötC Dbx1 neurons generates ectopic inspiratory bursts, interestingly no ectopic burst was generated when laser pulses were delivered during early expiration or post-inspiration period (Cui *et al.*, 2016), which further supports our results that demonstrate the presence of a refractory period during which preBötC excitation is incapable of generating additional inspiratory busts. Another interesting finding from this study is the differential responses achieved by

either preBötC Dbx1 or SST photostimulation during an inflation-induced apnea. PreBötC Dbx1 neurons laser stimulation during an inflation-induced apnea generated inspiratory bursts whereas preBötC SST neurons stimulation failed to break the induced apnea (Cui *et al*., 2016), which suggests that the preBötC ability to generate inspiratory bursts and overcome the strong inhibitory inputs is mediated by preBötC Dbx1 neurons. However, selective photostimulation of the preBötC Dbx1 neurons was less effective in driving the inspiratory activity in comparison to the results achieved here by a generalized non-selective stimulation of the preBötC neurons. This reduced response may be due to a lower level of ChR2 channels in the preBötC neurons in transgenic animals versus viral injections or alternatively may be informative of further unknown rhythmogenic processes in the preBötC. For example, a preBötC neuronal subpopulation other than the Dbx1 one might contribute to the inspiratory rhythm generation process or Dbx1 neurons may become more active when other neighboring preBötC neuronal subpopulations were activated. An alternate possibility is associated with the activation of an inhibitory ring in the preBötC area that reduces respiratory period (Smith *et al*., 2007).

Consistent with the concept of dissecting the preBötC microcircuit more work has been done to investigate the role of inhibition within preBötC. Janczewski and colleagues (2013) proposed that inhibition is not a necessary element for respiratory rhythm generation, however it plays a role in shaping the respiratory motor output.

Optogenetic perturbations of the inhibitory preBötC neurons modulate respiratory patterns but rhythm generation persists even when the inhibitory preBötC neurons were suppressed (Sherman *et al*., 2015). Moreover, recent results demonstrate that breathing persists after blocking post synaptic inhibition (Cui *et al*., 2016). However, other results demonstrated that blocking inhibition within the preBötC region perturb the respiratory rhythm. Marchenko and colleagues (2016) reported that perturbing the preBötC synaptic inhibition affects both the respiratory rhythm and pattern indicating that inhibition is an essential element required for normal eupneic breathing. Therefore, the exact role of inhibition in the process of respiratory rhythm generation is yet to be clarified.

The findings presented in the second chapter therefore support the proposed role of the preBötC as the inspiratory oscillator and excitation as an essential element of the rhythmogenic process within the preBötC microcircuits. The next step in the respiratory research field would be to further investigate the preBötC internal rhythmogenic mechanisms by dissecting preBötC network into its components then manipulate each neuronal subpopulation individually within the preBötC network.

The approach of independently manipulating neuronal subpopulations within the same network or any other approach with similar concepts would be an important tool to further investigate the components of the preBötC network.

Additionally, specific transcription factors give rise to several neuronal subpopulations within the preBötC network, therefore using specific genetic markers along with combining both optogenetic stimulation and pharmacological manipulation is a useful method to dissect the preBötC network and to examine the properties of each neural population within the network (Cui *et al*., 2016). However, neurons derived from the same genetic precursor could be involved in different functions within the preBötC network (Pre-inspiratory-Inspiratory-Post inspiratory) for example preBötC Dbx1 neurons could be either pre inspiratory, inspiratory, or premotoneurons, so it will be helpful to develop an experimental approach to examine the effects of dissecting and manipulating different functions of neural subpopulations derived from the same genetic precursor one function at a time.

4.3 Cholinergic Modulation of the paraFacial Respiratory Group

In the third chapter of this thesis I studied the neuromodulatory properties of the proposed expiratory oscillator RTN/pFRG. Previous work from our laboratory showed that the RTN/pFRG activation induced by laser stimulation evokes active expiration in adult urethane anesthetized rats (Pagliardini *et al*., 2011). Recent work from our laboratory demonstrated that in urethane anesthetized adult rats a recruitment of abdominal muscles occurred during REM sleep particularly when other respiratory parameters, such as: respiratory rate or period, tend to be more variable along with frequent occurrence of apnea, and shallow breathing (Andrews

and Pagliardini, 2015). Here, we aimed to investigate the effect of acetylcholine, a neurotransmitter released during REM sleep, on pFRG activity, abdominal muscles recruitment and active expiration. We identified puncta and fibers immunoreactive for both Chat and VChat around the lateral edge of the pFRG region which provides an evidence for the presence of cholinergic innervation within the pFRG region. Excitation of the pFRG cholinergic receptors by local application of either cholinergic agonists or acetylcholinesterase inhibitors induced active expiration and abdominal muscles recruitment. In order to further investigate the generation of active expiration, I performed unit activity recordings from neurons in the pFRG region to demonstrate the presence of late expiratory modulated neurons within the injection site. Late expiratory modulated neurons within the pFRG were coincident with expiratory abdominal recruitment. These effects were blocked by local application of the muscarinic antagonist scopolamine, and strongly suppressed by specific M3 muscarinic antagonist. However, these results do not constitute a conclusive evidence for the role of acetylcholine in abdominal muscles recruitment. Our results support the hypothesis that cholinergic innervation may play a role in pFRG level of excitation and the subsequent abdominal muscles recruitment. In this context, it was important to prove that abdominal activation was not evoked by an induction of a generalized brain state activation. Therefore, we recorded EEG activity during spontaneous brain state alternation under urethane anesthesia and we

showed that the cholinomimetics caused respiratory changes but had no effect on the ongoing spontaneous brain state alternations, which suggests that the reported results are evoked by manipulating the pFRG acetylcholine levels not on an induced generalized brain activation.

In addition, my work contributed to further description of pharmacological properties of the parafacial region. Currently, in this area, two or more neuronal populations with different functions have been identified, the medial region (RTN) acts as the chemosensitive area whereas the lateral pFRG acts as a conditional expiratory oscillator (Abbott *et al*., 2009,2011; Pagliardini *et al*., 2011; Li *et al*., 2016; Huckstepp *et al*., 2015,2016). The RTN has been postulated as the site of homoeostatic regulation that adjusts respiration to maintain constant levels of CSF $PC0_2$/pH (Feldman *et al*., 2003; Mulkey *et al*., 2004; Guyenet *et al*., 2008). The lateral parafacial neurons shows a pre inspiratory pattern of discharge which developmentally changed to be more expiratory modulated (Onimaru *et al*., 1988, 1997, Guyenet *et al*., 2010; Molkov *et al*., 2010; Pagliardini *et al*., 2011; Smith *et al*., 2013). The location of the RTN in close proximity to the pre inspiratory and the expiratory modulated parafacial neurons required further investigation in order to identify these neuronal population and to find out whether they are identical, overlap, or distinct. Hence, in our study we investigate the RTN and pFRG responses to cholinergic perturbations in order to distinguish between their respiratory functions.

Our results showed that cholinergic agonist injections into RTN region have different effects than those into lateral pFRG region. A comparison between the two sites of injection suggests that lateral pFRG and RTN could be involved in different roles in the respiratory control network as their activation evoke different responses and support the current hypothesis that medial and lateral pFRG have distinct respiratory functions (Huckstepp *et al*., 2015).

Our results demonstrated that lateral pFRG injections caused active expiration. However, in few experiments also medial pFRG injections evoked active expiration. In these cases when medial pFRG injections evoked active expiration the resulted active expiration was less reliable and that might be resulted from either lateral pFRG indirect activation through a transmitted signal via a connection between medial and lateral pFRG regions, or injection unwanted spread to lateral pFRG region.

The differential effects on the respiratory frequency were consistent throughout all experiments, lateral injection resulted in a respiratory depression, whereas medial injection increased the respiratory frequency.

The results of RTN stimulation are consistent with the effects on respiratory frequency obtained in previous studies (Abbott *et al*., 2009).

Several studies have investigated the role of acetylcholine in different aspects of the ventilatory control and sleep states modulation. Acetylcholine levels during REM sleep in the dorsal tegmentum field two times higher than during nREM or wakefulness (Kodama *et al*., 1990). Local acetylcholine agonists or antagonists microinjection into chemosensitive areas in the surface layer of ventral medulla increased or suppressed the ventilatory parameters, respectively (Dev & Loeschcke, 1979). Here, we further investigate the proposed role of the cholinergic inputs in ventilatory control along with the proposed role of the pFRG as an expiratory oscillator. Physostigmine, carbachol, scopolamine, and M3 specific antagonists injections were targeted to the pFRG based on it is anatomical coordinates, therefore our stimulation affected a heterogeneous neuronal population within the pFRG. In order to control the transfected area, we delivered low volumes of drugs following the previously published pFRG stereotaxic coordinates (Pagliardini *et al*., 2011). In addition, when performing experimental comparison between the effects on pFRG vs RTN we further reduced the injection volume and concentration (50 nl, 1 mM) in order to dissect the two adjacent para facial groups, and to prevent cross injections spread between the two parafacial areas. Therefore, post-mortem histological examinations were important to reveal the injection sites and to confirm that the injected solution was localized within the region of interest.

In conclusion, the results presented in the third chapter provide evidence for the cholinergic modulation on pFRG neurons and the subsequent abdominal activation and active expiration. First, histological examinations revealed the presence of cholinergic fibers and terminals within the pFRG region. Second, manipulating the pFRG cholinergic receptors with either agonists or antagonists local injections has great influence on the ventilatory parameters, which suggests a cholinergic innervation influence on the pFRG behaviour. REM sleep characteristics which include increased levels of acetylcholine and active expiration with recruitment of abdominal muscles could be due to pFRG excitation induced by cholinergic inputs. Therefore, our results here provide a hypothesis for a working model to explain the expiratory activity observed during REM sleep. Our results further support the recent work of Huckstepp and colleagues (2015), which suggests a presence of two distinct neuronal populations within the pFRG region with different respiratory functions.

The next step in this study will be to investigate the source of the cholinergic inputs to the pFRG neurons, and to examine the differential cholinergic sensitivity between medial and lateral parafacial regions. Retrograde tracing of the pFRG neurons will be a useful tool in order to identify the source of the cholinergic innervation to the pFRG neurons. With the use of retrogradely transported viruses that express Cre recombinase and the use of Cre dependent optogenetic and

chemogenetic viruses it will be possible to identify these projections and probe their physiological role in expiratory rhythm generation across sleep/wake cycles. Further, it will be important to understand how the two parafacial neuronal populations interact with each other during wakefulness, sleep, and increased metabolic demand. Moreover, the overlapping between medial and lateral parafacial regions is yet to be described, however recent work physiologically defined the medial and lateral pFRG based on their location around the facial nucleus (Huckstepp *et al*., 2015). Neurons within medial and lateral parafacial regions have been shown to express Phox2b genes , glutamate treansporter-2 (VGlut) , and neurokinin -1 receptor (NK1) (Mulkey *et al*.,2004, Thoby-Brisson et al., 2009, Huckstepp et al.,2016). Previous work has examined either medial or lateral parafacial regions responses to various forms of stimulation. Lateral pFRG photostimulation induces active expiration and active abdominal muscles contraction (Pagliardini *et al*., 2011) whereas photostimulation of the RTN-Phox2b neurons caused active expiration only in conscious awake rats (Abbott *et al*., 2011). Pharmacological destruction of the RTN Phox2b neurons increased the apneic threshold and reduced the central chemo reflexes (Takakura *et al*., 2008), however genetic mutationsthat eliminate the embryonic precursor of pFRG (e-pF) resulted in slow breathing at birth with poor survival in newborn rats (Thoby-Brisson *et al*., 2009). Moreover, local application of a mixture of GABA and glycine antagonists

disinhibit lateral pFRG neurons which evoked active expiration (Pagliardini *et al*., 2011; Huckstepp *et al*., 2015), however hyperpolarizing the lateral pFRG neurons didn't alter the respiratory parameters (Huckstepp *et al*., 2015) whereas hyperpolarizing medial pFRG neurons under similar conditions caused hypoventilation (Li *et al*., 2006). In summary, distinct ventilatory responses achieved by stimulating or inhibiting either lateral or medial pFRG further support the hypothesis that they may have different contributions in the respiratory control process.

4.4 Conclusions

The results presented in this thesis have generated data that 1) support the role of the preBötC complex as the inspiratory oscillator; and 2) provide the first evidence for cholinergic modulation of pFRG neurons.

Previous data showed the preBötC essential role in the inspiratory rhythm generation process. We examined the respiratory responses elicited by a highly controlled fine excitatory drive to the preBötC neurons for the first time *in vivo*. Future research also needed to breakdown the respiratory oscillators into smaller functionally different neural populations to examine how the respiratory oscillators components interact with each other within the same microcircuit.

Our results further suggest that cholinergic muscarinic transmission contributes to the pFRG excitation and active expiration under anesthesia. Future work in this area of research will aim to investigate the source of the pFRG cholinergic innervation, the mechanisms involved in respiratory control during REM sleep, and the distinct roles of the parafacial regions.

References

Abbott SB, Coates MB, Stornetta RL & Guyenet PG (2013). Optogenetic stimulation of c1 and retrotrapezoid nucleus neurons causes sleep state-dependent cardiorespiratory stimulation and arousal in rats. *Hypertension* 61, 835–841.

Abbott SB, DePuy SD, Nguyen T, Coates MB, Stornetta RL & Guyenet PG (2013b). Selective optogenetic activation of rostral ventrolateral medullary catecholaminergic neurons produces cardiorespiratory stimulation in conscious mice. *J Neurosci.* 33, 3164–3177.

Abbott SB, Kanbar R, Bochorishvili G, Coates MB, Stornetta RL & Guyenet PG (2012). C1 neurons excite locus coeruleus and A5 noradrenergic neurons along with sympathetic outflow in rats. *J Physiol* 590, 2897–2915.

Abbott SB, Stornetta RL, Coates MB & Guyenet PG. (2011). Phox2b-expressing neurons of the parafacial region regulate breathing rate, inspiration, and expiration in conscious rats. *J Neurosci* **31,** 16410-16422.

Abbott SB, Stornetta RL, Fortuna MG, Depuy SD, West GH, Harris TE & Guyenet PG. (2009). Photostimulation of retrotrapezoid nucleus phox2b-expressing neurons in vivo produces long-lasting activation of breathing in rats. *J Neurosci* **29,** 5806-5819.

Abbott, S. B. G., Stornetta, R. L., Coates, M. B., & Guyenet, P. G. (2011). Phox2b-expressing Neurons of the Parafacial region regulate breathing rate, inspiration, and expiration in conscious rats. *Journal of Neuroscience*, *31*(45), 16410–16422.

Abbott, S. B. G., Stornetta, R. L., Fortuna, M. G., Depuy, S. D., West, G. H., Harris, T. E., & Guyenet, P. G. (2009). Photostimulation of retrotrapezoid nucleus phox2b-expressing neurons in vivo produces long-lasting activation of breathing in rats. *Journal of Neuroscience*, *29*(18), 5806–5819.

Alheid, G. F., Jiao, W., & McCrimmon, D. R. (2011). Caudal nuclei of the rat nucleus of the solitary tract differentially innervate respiratory compartments within the ventrolateral medulla. *Neuroscience*, *190*, 207-227.

Andrews, C. G., & Pagliardini, S. (2015). Expiratory activation of abdominal muscle is associated with improved respiratory stability and an increase in minute ventilation in REM epochs of adult rats. *Journal of Applied Physiology*, *119*(9), 968-974.

Aravanis AM, Wang LP, Zhang F, Meltzer LA, Mogri MZ, Schneider MB & Deisseroth K (2007). An optical neural interface: in vivo control of rodent motor cortex with integrated fiberoptic and optogenetic technology. *J Neural Eng* 4, S143–156.

Baconnier, P. F., Benchetrit, G., Pachot, P., & Demongeot, J. (1993). Entrainment of the respiratory rhythm: a new approach. *Journal of theoretical biology*, *164*(2), 149-162.

Ballanyi, K., Onimaru, H., & Homma, I. (1999). Respiratory network function in the isolated brainstem-spinal cord of newborn rats. *Progress in Neurobiology*, 59(6), 583-634.

Boers J, Kirkwood PA, de Weerd H & Holstege G. (2006). Ultrastructural evidence for direct excitatory retroambiguus projections to cutaneous trunci and abdominal external oblique muscle motoneurons in the cat. *Brain research bulletin* **68,** 249-256.

Bonis JM, Neumueller SE, Krause KL, Pan LG, Hodges MR & Forster HV (2013). Contributions of the Kolliker-Fuse nucleus to coordination of breathing and swallowing. *Resp Physiol Neurobiol* 189, 10–21.

Boucetta S & Jones BE. (2009). Activity profiles of cholinergic and intermingled GABAergic and putative glutamatergic neurons in the pontomesencephalic tegmentum of urethane-anesthetized rats. *J Neurosci* **29,** 4664-4674.

Boucetta S, Cisse Y, Mainville L, Morales M & Jones BE. (2014). Discharge profiles across the sleep-waking cycle of identified cholinergic, GABAergic, and glutamatergic neurons in the pontomesencephalic tegmentum of the rat. *J Neurosci* **34,** 4708-4727.

Bouvier, J., Thoby-Brisson, M., Renier, N., Dubreuil, V., Ericson, J., Champagnat, J., ... & Fortin, G. (2010). Hindbrain interneurons and axon guidance signaling critical for breathing. *Nature neuroscience*, *13*(9), 1066-1074.

Buchschacher, G. L. (2003). *Lentiviral vector systems for gene transfer*. Eurekah. com; Landes Bioscience; Kluwer Academic/Plenum Pub..

Burke PG, Kanbar R, Basting TM, Hodges WM, Viar KE, Stornetta RL & Guyenet PG. (2015). State-dependent control of breathing by the retrotrapezoid nucleus. *The Journal of physiology* **593,** 2909-2926.

Burton MD, Nouri K, Baichoo S, Samuels-Toyloy N & Kazemi H. (1994). Ventilatory output and acetylcholine: perturbations in release and muscarinic receptor activation. *Journal of applied physiology* **77,** 2275-2284.

Butler, J. (2012). Optogenetics: shining a light on the brain. *Bioscience Horizons*, *5*, hzr020.

Chase MH & Morales FR. (1990). The atonia and myoclonia of active (REM) sleep. *Annual review of psychology* **41,** 557-584.

Clement EA, Richard A, Thwaites M, Ailon J, Peters S & Dickson CT (2008). Cyclic and sleep-like spontaneous alternations of brain state under urethane anaesthesia. *PLoS ONE* 3, e2004.

Cohen, M. (1979). Neurogenesis of respiratory rhythm in mammals. *Physiological Reviews*, 59, 1105-1173.

Connelly, C. A., Ellenberger, H. H., & Feldman, J. L. (1990). Respiratory activity in retrotrapezoid nucleus in cat. *American Journal of Physiology-Lung Cellular and Molecular Physiology*, *258*(2), L33-L44.

Coordination of wingbeat and respiration in the Canada goose. I. Passive wing flapping. *J Appl Physiol* 73, 1014–1024.

Cui, Y., Kam, K., Sherman, D., Janczewski, W. A., Zheng, Y., & Feldman, J. L. (2016). Defining preBötzinger Complex Rhythm-and Pattern-Generating Neural Microcircuits In Vivo. *Neuron*, *91*(3), 602-614.

Del Negro, C. A., Koshiya, N., Butera, R. J., & Smith, J. C. (2002). Persistent sodium current, membrane properties and bursting behavior of pre-Bötzinger complex inspiratory neurons in vitro. *Journal of Neurophysiology*, *88*(5), 2242-2250.

Del Negro, C. A., Morgado-Valle, C., Hayes, J. A., Mackay, D. D., Pace, R. W., Crowder, E. A., & Feldman, J. L. (2005). Sodium and calcium current-mediated pacemaker neurons and respiratory rhythm generation. *The Journal of Neuroscience*, *25*(2), 446-453.

Dev NB & Loeschcke HH. (1979). A cholinergic mechanism involved in the respiratory chemosensitivity of the medulla oblongata in the cat. *Pflugers Arch* **379,** 29-36.

Dick TE, Oku Y, Romaniuk JR & Cherniack NS (1993). Interaction between central pattern generators for breathing and swallowing in the cat. *J Physiol.* 465, 715–730.

Dobbins EG & Feldman JL (1995). Differential innervation of protruder and retractor muscles of the tongue in rat. *J Comp Neurol* 357, 376–394.

Dobbins, E. G., & Feldman, J. L. (1994). Brainstem network controlling descending drive to phrenic motoneurons in rat. *Journal of Comparative Neurology*, *347*(1), 64-86.

Doi A & Ramirez JM (2008). Neuromodulation and the orchestration of the respiratory rhythm. *Resp Physiol Neurobiol* 164, 96–104.

Drummond GB. (2009). Reporting ethical matters in the Journal of Physiology: standards and advice. *The Journal of physiology* **587,** 713-719.

Eldridge FL (1972a). The effect of intermittent carotid sinus nerve and carotid body stimulation on respiratory output. *Chest 61 (Suppl.),* 44S.

Eldridge FL (1972b). The importance of timing on the respiratory effects of intermittent carotid sinus nerve stimulation. J Physiol222, 297–318.

Eldridge FL, Paydarfar D, Wagner PG & Dowell RT (1989). Phase resetting of respiratory rhythm: effect of changing respiratory "drive". *Am J Physiol Regul Integr Comp Physiol* 257, R271–R277.

Eldridge, F. L. (1972). The importance of timing on the respiratory effects of intermittent carotid sinus nerve stimulation. *The Journal of physiology*,*222*(2), 297.

Ellenberger, H. H., & Feldman, J. L. (1990). Brainstem connections of the rostral ventral respiratory group of the rat. *Brain research*, *513*(1), 35-42.

Ezure, K., & Tanaka, I. (2006). Distribution and medullary projection of respiratory neurons in the dorsolateral pons of the rat. *Neuroscience*, *141*(2), 1011-1023.

Ezure, K., Tanaka, I., & Kondo, M. (2003). Glycine is used as a transmitter by decrementing expiratory neurons of the ventrolateral medulla in the rat. *The Journal of neuroscience*, *23*(26), 8941-8948.

Feldman JL, Del Negro CA & Gray PA. (2013). Understanding the rhythm of breathing: so near, yet so far. *Annual review of physiology* **75,** 423-452.

Feldman, J. L., & Del Negro, C. A. (2006). Looking for inspiration: new perspectives on respiratory rhythm. *Nature Reviews Neuroscience*, *7*(3), 232-241.

Feldman, J. L., Del Negro, C. A., & Gray, P. A. (2013). Understanding the rhythm of breathing: so near yet so far. *Annual review of physiology*, *75*, 423.

Feldman, J. L., Mitchell, G. S., & Nattie, E. E. (2003). Breathing: rhythmicity, plasticity, chemosensitivity. *Annual review of neuroscience*, *26*, 239.

Fenno, L., Yizhar, O., & Deisseroth, K. (2011). The development and application of optogenetics. *Neuroscience*, *34*(1), 389.

Fortuna, M. G., West, G. H., Stornetta, R. L., & Guyenet, P. G. (2008). Bötzinger expiratory-augmenting neurons and the parafacial respiratory group. *The Journal of Neuroscience*, *28*(10), 2506-2515.

Fritschy JM, Frondoza CG & Grzanna R (1991). Differential effects of reserpine on brainstem catecholaminergic neurons revealed by Fos protein immunohistochemistry. *Brain Res* 562, 48–56. Funk GD, Milsom WK & Steeves JD (1992).

Fukuda Y & Loeschcke HH. (1979). A cholinergic mechanism involved in the neuronal excitation by H+ in the respiratory chemosensitive structures of the ventral medulla oblongata of rats in vitro. *Pflugers Arch* **379,** 125-135.

Funk, G. D., Smith, J. C., & Feldman, J. L. (1993). Generation and transmission of respiratory oscillations in medullary slices: role of excitatory amino acids. *Journal of neurophysiology*, *70*(4), 1497-1515.

Gargaglioni LH, Bicegoa KC & Branco LG (2008). Brain monoaminergic neurons and ventilatory control in vertebrates. *Resp Physiol Neurobiol* 164, 112–122.

Gariepy JF, Missaghi K, Chevallier S, Chartre S, Robert M, Auclair F, Lund JP & Dubuc R (2012). Specific neural substrate linking respiration to locomotion. *Proc Natl Acad Sci U S A* 109, E84-92.

Gillis RA, Walton DP, Quest JA, Namath IJ, Hamosh P & Dretchen KL. (1988). Cardiorespiratory effects produced by activation of cholinergic muscarinic receptors on the ventral surface of the medulla. *The Journal of pharmacology and experimental therapeutics* **247,** 765-773.

Giraudin A, Cabirol-Pol MJ, Simmers J & Morin D. (2008). Intercostal and abdominal respiratory motoneurons in the neonatal rat spinal cord: spatiotemporal organization and responses to limb afferent stimulation. *Journal of neurophysiology* **99,** 2626-2640.

Giraudin A, LeBon-Jego M, Cabirol MJ, Simmers J & Morin D (2012). Spinal and pontine relay pathways mediating respiratory rhythm entrainment by limb proprioceptive inputs in the neonatal rat. *J Neurosci* 32, 11841–11853.

Gourine AV, Kasymov V, Marina N, Tang F, Figueiredo MF, Lane S, Teschemacher AG, Spyer KM, Deisseroth K & Kasparov S. (2010). Astrocytes control breathing through pH-dependent release of ATP. *Science (New York, NY* **329,** 571-575.

Grace KP, Hughes SW & Horner RL. (2013). Identification of the mechanism mediating genioglossus muscle suppression in REM sleep. *American journal of respiratory and critical care medicine* **187,** 311-319.

Granata AR, Numao Y, Kumada M & Reis DJ (1986). A1 noradrenergic neurons tonically inhibit sympathoexcitatory neurons of C1 area in rat brainstem. *Brain Res* 377, 127–146.

Gray PA, Janczewski WA, Mellen N, McCrimmon DR & Feldman JL (2001). Normal breathing requires preBotzinger complex neurokinin-1 receptor-expressing neurons. *Nat Neurosci* 4, 927–930.

Gray, P. A., Hayes, J. A., Ling, G. Y., Llona, I., Tupal, S., Picardo, M. C. D., ... & Del Negro, C. A. (2010). Developmental origin of preBötzinger complex respiratory neurons. *The Journal of Neuroscience*, *30*(44), 14883-14895.

Gray, P. A., Hayes, J. A., Ling, G. Y., Llona, I., Tupal, S., Picardo, M. C. D., ... & Del Negro, C. A. (2010). Developmental origin of preBötzinger complex respiratory neurons. *The Journal of Neuroscience*, *30*(44), 14883-14895.

Gray, P. A., Janczewski, W. A., Mellen, N., McCrimmon, D. R., & Feldman, J. L. (2001). Normal breathing requires preBötzinger complex neurokinin-1 receptor-expressing neurons. *Nature neuroscience*, *4*(9), 927-930.

Gray, P. A., Rekling, J. C., Bocchiaro, C. M., & Feldman, J. L. (1999). Modulation of respiratory frequency by peptidergic input to rhythmogenic neurons in the preBötzinger complex. *Science*, *286*(5444), 1566-1568.

Guyenet PG & Bayliss DA. (2015). Neural Control of Breathing and CO2 Homeostasis. *Neuron* **87,** 946-961.

Guyenet PG, Stornetta RL & Bayliss DA (2008). Retrotrapezoid nucleus and central chemoreception. *J Physiol* 586, 2043–2048.

Guyenet, P. G., & Wang, H. (2001). Pre-Bötzinger neurons with preinspiratory discharges "in vivo" express NK1 receptors in the rat. *Journal of neurophysiology*, *86*(1), 438-446.

Guyenet, P. G., Bayliss, D. A., Stornetta, R. L., Fortuna, M. G., Abbott, S. B., & DePuy, S. D. (2009). Retrotrapezoid nucleus, respiratory chemosensitivity and breathing automaticity. *Respiratory physiology & neurobiology*, *168*(1), 59-68.

Guyenet, P. G., Mulkey, D. K., Stornetta, R. L., & Bayliss, D. A. (2005). Regulation of ventral surface chemoreceptors by the central respiratory pattern generator. *The Journal of neuroscience*, *25*(39), 8938-8947.

Guyenet, P. G., Sevigny, C. P., Weston, M. C., & Stornetta, R. L. (2002). Neurokinin-1 receptor-expressing cells of the ventral respiratory group are functionally heterogeneous and predominantly glutamatergic. *The Journal of neuroscience*, *22*(9), 3806-3816.

Guyenet, P. G., Stornetta, R. L., & Bayliss, D. A. (2008). Retrotrapezoid nucleus and central chemoreception. *The Journal of physiology*, *586*(8), 2043-2048.

Guyenet, P. G., Stornetta, R. L., & Bayliss, D. A. (2010). Central respiratory chemoreception. *Journal of Comparative Neurology*, *518*(19), 3883-3906.

Hayes JA, Wang X & Del Negro CA (2012). Cumulative lesioning of respiratory interneurons disrupts and precludes motor rhythms in vitro. *Proc Natl Acad Sci U S A* 109, 8286–8291.

Henry JP, Botton D, Sagne C, Isambert MF, Desnos C, Blanchard V, Raisman-Vozari R, Krejci E, Massoulie J & Gasnier B (1994). Biochemistryand molecularbiologyof the vesicular monoamine transporter from chromaffin granules. *J Exp Biol* 196, 251–262.

Hodges MR & Richerson GB (2008). Contributions of 5-HT neurons to respiratory control: neuromodulatory and trophic effects. *Resp Physiol Neurobiol* 164, 222–232.

Howard, P., Bromberger-Barnea, B., Fitzgerald, R. S., & Bane, H. N. (1969). Ventilatory responses to peripheral nerve stimulation at different times in the respiratory cycle. *Respiration physiology*, *7*(3), 389-398.

Huckstepp RT, Cardoza KP, Henderson LE & Feldman JL. (2015). Role of parafacial nuclei in control of breathing in adult rats. *J Neurosci* **35,** 1052-1067.

Huckstepp RT, Henderson LE, Cardoza KP & Feldman JL. (2016). Interactions between respiratory oscillators in adult rats. *eLife* **5**.

Huckstepp, R. T., Cardoza, K. P., Henderson, L. E., & Feldman, J. L. (2015). Role of parafacial nuclei in control of breathing in adult rats. *The Journal of Neuroscience*, *35*(3), 1052-1067.

Huckstepp, R. T., Henderson, L. E., Cardoza, K. P., & Feldman, J. L. (2016). Interactions between respiratory oscillators in adult rats. *eLife*, *5*, e14203.

Janczewski WA & Feldman JL. (2006). Distinct rhythm generators for inspiration and expiration in the juvenile rat. *The Journal of physiology* **570,** 407-420.

Janczewski WA, Onimaru H, Homma I & Feldman JL. (2002). Opioid-resistant respiratory pathway from the preinspiratory neurones to abdominal muscles: in vivo and in vitro study in the newborn rat. *The Journal of physiology* **545,** 1017-1026.

Janczewski WA, Tashima A, Hsu P, Cui Y & Feldman JL (2013). Role of inhibition in respiratory pattern generation. *J Neurosci* 33, 5454–5465.

Janczewski, W. A., & Feldman, J. L. (2006). Distinct rhythm generators for inspiration and expiration in the juvenile rat. *The Journal of physiology*,*570*(2), 407-420.

Janczewski, W. A., Onimaru, H., Homma, I., & Feldman, J. L. (2002). Opioid-resistant respiratory pathway from the preinspiratory neurones to abdominal muscles: in vivo and in vitro study in the newborn rat. *The Journal of physiology*, *545*(3), 1017-1026.

Janczewski, W. A., Tashima, A., Hsu, P., Cui, Y., & Feldman, J. L. (2013). Role of inhibition in respiratory pattern generation. *The Journal of Neuroscience*, *33*(13), 5454-5465.

Jiang, C., & Lipski, J. (1990). Extensive monosynaptic inhibition of ventral respiratory group neurons by augmenting neurons in the Bötzinger complex in the cat. *Experimental brain research*, *81*(3), 639-648.

Jones BE. (1990). Immunohistochemical study of choline acetyltransferase-immunoreactive processes and cells innervating the pontomedullary reticular formation in the rat. *The Journal of comparative neurology* **295,** 485-514.

Kam K, Worrell JW, Janczewski WA, Cui Y & Feldman JL (2013a). Distinct inspiratory rhythm and pattern generating mechanisms in the preBotzinger complex. *J Neurosci* 33, 9235–9245.

Kam K, Worrell JW, Ventalon C, Emiliani V & Feldman JL (2013b). Emergence of population bursts from simultaneous activation of small subsets of preBotzinger complex inspiratory neurons. *J Neurosci* 33, 3332–3338.

Kobayashi, K., Lemke, R. P., & Greer, J. J. (2001). Ultrasound measurements of fetal breathing movements in the rat. *Journal of Applied Physiology*, *91*(1), 316-320.

Kodama T, Lai YY & Siegel JM. (1992). Enhancement of acetylcholine release during REM sleep in the caudomedial medulla as measured by in vivo microdialysis. *Brain research* **580,** 348-350.

Kodama, T., Takahashi, Y., & Honda, Y. (1990). Enhancement of acetylcholine release during paradoxical sleep in the dorsal tegmental field of the cat brain stem. *Neuroscience letters*, *114*(3), 277-282.

Koizumi H, Koshiya N, Chia JX, Cao F, Nugent J, Zhang R & Smith JC (2013). Structural-functional properties of identified excitatory and inhibitory interneurons within pre-Botzinger complex respiratory microcircuits. *J Neurosci* 33, 2994–3009.

Koshiya N, Oku Y, Yokota S, Oyamada Y, Yasui Y & Okada Y (2014). Anatomical and functional pathways of rhythmogenic inspiratory premotor information flow originating in the pre-Botzinger complex in the rat medulla. *Neuroscience* 268C, 194–211.

Kubin L & Fenik V. (2004). Pontine cholinergic mechanisms and their impact on respiratory regulation. *Respiratory physiology & neurobiology* **143,** 235-249.

Kuwana S, Tsunekawa N, Yanagawa Y, Okada Y, Kuribayashi J & Obata K (2006). Electrophysiological and morphological characteristics of GABAergic respiratory neurons in the mouse pre-Botzinger complex. *Eur J Neurosci* 23, 667–674.

Lalley PM (2008). Opioidergic and dopaminergic modulation of respiration. Resp Physiol *Neurobiol* 164, 160–167.

Lambas-Senas L, Chamba G, Fety R & Renaud B (1986). Comparative responses of the central adrenaline- and noradrenaline-containing neurons after reserpine injections. *Biochem Pharmacol* 35, 2207–2211.

Li Y-Q, Takada M & Mizuno N (1993). Identification of premotor interneurons which project bilaterally to the trigeminal motor, facial or hypoglossal nuclei: a fluorescent retrograde double-labeling study in the rat. *Brain Res* 611, 160–164.

Li, A., Zhou, S., & Nattie, E. (2006). Simultaneous inhibition of caudal medullary raphe and retrotrapezoid nucleus decreases breathing and the CO2 response in conscious rats. *The Journal of physiology*, *577*(1), 307-318.

Li, P., Janczewski, W. A., Yackle, K., Kam, K., Pagliardini, S., Krasnow, M. A., & Feldman, J. L. (2016). The peptidergic control circuit for sighing. *Nature*.

Liu, Y. Y., Ju, G., & Wong-Riley, M. T. (2001). Distribution and colocalization of neurotransmitters and receptors in the pre-Bötzinger complex of rats. *Journal of Applied Physiology*, *91*(3), 1387-1395.

Loeschcke HH. (1982). Central chemosensitivity and the reaction theory. *The Journal of physiology* **332,** 1-24.

Mallios VJ, Lydic R & Baghdoyan HA. (1995). Muscarinic receptor subtypes are differentially distributed across brain stem respiratory nuclei. *The American journal of physiology* **268,** L941-949.

Marchenko, V., Koizumi, H., Mosher, B., Koshiya, N., Tariq, M. F., Bezdudnaya, T. G., ... & Smith, J. C. (2016). Perturbations of Respiratory Rhythm and Pattern by Disrupting Synaptic Inhibition within Pre-Bötzinger and Bötzinger Complexes. *eneuro*, *3*(2), ENEURO-0011.

Marina N, Abdala AP, Trapp S, Li A, Nattie EE, Hewinson J, Smith JC, Paton JF & Gourine AV. (2010). Essential role of Phox2b-expressing ventrolateral brainstem neurons in the chemosensory control of inspiration and expiration. *J Neurosci* **30,** 12466-12473.

McCarley RW. (2007). Neurobiology of REM and NREM sleep. *Sleep medicine* **8,** 302-330.

McCrimmon DR, Feldman JL & Speck DF (1986). Respiratory motoneuronal activity is altered by injections of picomoles of glutamate into cat brain stem. *J Neurosci* 6, 2384–2392.

McKay, L. C., Janczewski, W. A., & Feldman, J. L. (2005). Sleep-disordered breathing after targeted ablation of preBötzinger complex neurons. *Nature neuroscience*, *8*(9), 1142.

Mellen NM, Janczewski WA, Bocchiaro CM & Feldman JL. (2003). Opioid-induced quantal slowing reveals dual networks for respiratory rhythm generation. *Neuron* **37,** 821-826.

Mellen, N. M., & Feldman, J. L. (2000). Phasic lung inflation shortens inspiration and respiratory period in the lung-attached neonate rat brain stem spinal cord. *Journal of neurophysiology*, *83*(5), 3165-3168.

Mellen, N. M., Janczewski, W. A., Bocchiaro, C. M., & Feldman, J. L. (2003). Opioid-induced quantal slowing reveals dual networks for respiratory rhythm generation. *Neuron*, *37*(5), 821-826.

Molkov, Y. I., Abdala, A. P., Bacak, B. J., Smith, J. C., Paton, J. F., & Rybak, I. A. (2010). Late-expiratory activity: emergence and interactions with the respiratory CPG. *Journal of neurophysiology*, *104*(5), 2713-2729.

Moore JD, Deschenes M, Furuta T, Huber D, Smear MC, Demers M & Kleinfeld D (2013). Hierarchy of orofacial rhythms revealed through whisking and breathing. *Nature* 497, 205–210.

Moore JD, Kleinfeld D & Wang F (2014). How the brainstem controls orofacial behaviors comprised of rhythmic actions. *Trends Neurosci* 37, 370–380.

Morgado-Valle C, Baca SM & Feldman JL (2010). Glycinergic pacemaker neurons in PreBotzinger complex of neonatal mouse. *J Neurosci* 30, 3634–3639.

Muere C, Neumueller S, Miller J, Olesiak S, Hodges MR, Pan L & Forster HV. (2015). Evidence for respiratory neuromodulator interdependence after cholinergic disruption in the ventral respiratory column. *Respiratory physiology & neurobiology* **205,** 7-15.

Mulkey, D. K., Stornetta, R. L., Weston, M. C., Simmons, J. R., Parker, A., Bayliss, D. A., & Guyenet, P. G. (2004). Respiratory control by ventral surface chemoreceptor neurons in rats. *Nature neuroscience*, *7*(12), 1360-1369.

Nagel, G., Szellas, T., Huhn, W., Kateriya, S., Adeishvili, N., Berthold, P., ... & Bamberg, E. (2003). Channelrhodopsin-2, a directly light-gated cation-selective membrane channel. *Proceedings of the National Academy of Sciences*, *100*(24), 13940-13945.

Nattie EE & Li AH. (1990). Ventral medulla sites of muscarinic receptor subtypes involved in cardiorespiratory control. *Journal of applied physiology* **69,** 33-41.

Nattie, E. E., & Li, A. (2002). Substance P-saporin lesion of neurons with NK1 receptors in one chemoreceptor site in rats decreases ventilation and chemosensitivity. *The Journal of physiology*, *544*(2), 603-616.

Nurse CA. (2010). Neurotransmitter and neuromodulatory mechanisms at peripheral arterial chemoreceptors. *Experimental physiology* **95,** 657-667.

Okazaki, M., Takeda, R., Yamazaki, H., & Haji, A. (2002). Synaptic mechanisms of inspiratory off-switching evoked by pontine pneumotaxic stimulation in cats. *Neuroscience research*, *44*(1), 101-110.

Oku Y & Dick TE (1992). Phase resetting of the respiratory cycle before and after unilateral pontine lesion in cat. *J Appl Physiol* 72, 721–730.

Oku, Y., Masumiya, H., & Okada, Y. (2007). Postnatal developmental changes in activation profiles of the respiratory neuronal network in the rat ventral medulla. *The Journal of physiology*, *585*(1), 175-186..

Olszewski, J., & Baxter, D. (1954). Cytoarchitecture of the human brain stem. *Cytoarchitecture of the human brain stem*.

Onimaru, H., & Homma, I. (2003). A novel functional neuron group for respiratory rhythm generation in the ventral medulla. *The Journal of Neuroscience*, *23*(4), 1478-1486.

Onimaru, H., Arata, A., & Homma, I. (1988). Primary respiratory rhythm generator in the medulla of brainstem-spinal cord preparation from newborn rat. *Brain research*, *445*(2), 314-324.

Onimaru, H., Arata, A., & Homma, I. (1997). Neuronal mechanisms of respiratory rhythm generation: an approach using in vitro preparation. *The Japanese journal of physiology*, *47*(5), 385-403.

Onimaru, H., Kumagawa, Y., & Homma, I. (2006). Respiration-related rhythmic activity in the rostral medulla of newborn rats. *Journal of Neurophysiology*, *96*(1), 55-61.

Orem, J., & Kubin, L. (2000). Respiratory physiology: central neural control.*Principles and practice of sleep medicine*, *4*, 213-223.

Pagliardini S, Gosgnach S & Dickson CT. (2013). Spontaneous sleep-like brain state alternations and breathing characteristics in urethane anesthetized mice. *PLoS ONE* **8,** e70411.

Pagliardini S, Greer JJ, Funk GD & Dickson CT. (2012). State-dependent modulation of breathing in urethane-anesthetized rats. *J Neurosci* **32,** 11259-11270.

Pagliardini S, Janczewski WA, Tan W, Dickson CT, Deisseroth K & Feldman JL. (2011). Active expiration induced by excitation of ventral medulla in adult anesthetized rats. *J Neurosci* **31,** 2895-2905.

Pagliardini S, Janczewski WA, Tan W, Dickson CT, Deisseroth K & Feldman JL (2011). Active expiration induced by excitation of ventral medulla in adult anesthetized rats. *J Neurosci* 31, 2895–2905.

Pagliardini S, Ren J & Greer JJ (2003). Ontogeny of the pre-Botzinger complex in perinatal rats. *J Neurosci* 23, 9575–9584.

Pagliardini, S., Greer, J. J., Funk, G. D., & Dickson, C. T. (2012). State-dependent modulation of breathing in urethane-anesthetized rats. *The Journal of Neuroscience*, *32*(33), 11259-11270.

Pagliardini, S., Janczewski, W. A., Tan, W., Dickson, C. T., Deisseroth, K., & Feldman, J. L. (2011). Active expiration induced by excitation of ventral medulla in adult anesthetized rats. *The Journal of Neuroscience*, *31*(8), 2895-2905.

Pagliardini, S., Ren, J., & Greer, J. J. (2003). Ontogeny of the pre-Bötzinger complex in perinatal rats. *The Journal of neuroscience*, *23*(29), 9575-9584.

Paydarfar D & Eldridge FL (1987). Phase resetting and dysrhythmic responses of the respiratory oscillator. *Am J PhysiolRegul Integr Comp Physiol* 252, R55–R62.

Paydarfar D, Eldridge FL & Kiley JP (1986). Resetting of mammalian respiratory rhythm: existence of a phase singularity. *Am J PhysiolRegul Integr Comp Physiol* 250, R721–R727.

Paydarfar D, Eldridge FL & Paydarfar JA (1998). Phase resetting of the respiratory oscillator by carotid sinus nerve stimulation in cats. *J Physiol* 506, 515–528.

Peever J. (2011). Control of motoneuron function and muscle tone during REM sleep, REM sleep behavior disorder and cataplexy/narcolepsy. *Archives italiennes de biologie* **149,** 454-466.

Potts JT, Rybak IA & Paton JF (2005). Respiratory rhythm entrainment by somatic afferent stimulation. *J Neurosci* 25, 1965–1978.

Ramirez, J. M., Schwarzacher, S. W., Pierrefiche, O., Olivera, B. M., & Richter, D. W. (1998). Selective lesioning of the cat pre-Bötzinger complex in vivo eliminates breathing but not gasping. *The Journal of Physiology*, *507*(3), 895-907.

Rekling, J. C., & Feldman, J. L. (1998). PreBötzinger complex and pacemaker neurons: hypothesized site and kernel for respiratory rhythm generation. *Annual review of physiology*, *60*(1), 385-405.

Schuldiner S (1994). A molecular glimpse of vesicular monoamine transporters. *J Neurochem* 62, 2067–2078.

Schwarzacher SW, Rub U & Deller T (2011). Neuroanatomical characteristics of the human pre-Botzinger complex and its involvement in neurodegenerative brainstem diseases. *Brain* 134, 24–35.

Shao XM & Feldman JL. (2009). Central cholinergic regulation of respiration: nicotinic receptors. *Acta Pharmacol Sin* **30,** 761-770.

Shen, L., & Duffin, J. (2002). Caudal expiratory neurones in the rat. *Pflügers Archiv*, *444*(3), 405-410.

Sherman D, Worrell JW, Cui Y & Feldman JL (2015). Optogenetic perturbation of preBotzinger complex inhibitory neurons modulates respiratory pattern. *Nat Neurosci* 18, 408–414.

Smith JC, Ellenberger HH, Ballanyi K, Richter DW & Feldman JL. (1991). Pre-Botzinger complex: a brainstem region that may generate respiratory rhythm in mammals. *Science (New York, NY* **254,** 726-729.

Smith, J. C., Abdala, A. P. L., Koizumi, H., Rybak, I. A., & Paton, J. F. (2007). Spatial and functional architecture of the mammalian brain stem respiratory network: a hierarchy of three oscillatory mechanisms. *Journal of neurophysiology*, *98*(6), 3370-3387.

Smith, J. C., Abdala, A. P., Borgmann, A., Rybak, I. A., & Paton, J. F. (2013). Brainstem respiratory networks: building blocks and microcircuits. *Trends in neurosciences*, *36*(3), 152-162.

Smith, J. C., Ellenberger, H. H., Ballanyi, K., Richter, D. W., & Feldman, J. L. (1991). Pre-Bötzinger complex: a brainstem region that may generate respiratory rhythm in mammals. *Science (New York, NY)*, *254*(5032), 726.

Sobrinho CR, Kuo F-S, Barna BF, Moreira TS & Mulkey DK. (2015). Cholinergic control of ventral surface chemoreceptors involves Gq/IP3-mediated inhibition of KCNQ channels. *The Journal of physiology*, n/a-n/a.

Solomon IC, Edelman NH & Neubauer JA (1999). Patterns of phrenic motor output evoked by chemical stimulation of neurons located in the pre-Botzinger complex in vivo. *J Neurophysiol* 81, 1150–1161.

Speck DF & Feldman JL (1982). The effects of microstimulation and microlesions in the ventral and dorsal respiratory groups in medulla of cat. *J Neurosci* 2, 744–757.

Stornetta RL, Rosin DL, Wang H, Sevigny CP, Weston MC & Guyenet PG (2003). A group of glutamatergic interneurons expressing high levels of both neurokinin-1 receptors and somatostatin identifies the region of the pre-Botzinger complex. *J Comp Neuro* l455, 499–512.

Stornetta, R. L., Moreira, T. S., Takakura, A. C., Kang, B. J., Chang, D. A., West, G. H., ... & Guyenet, P. G. (2006). Expression of Phox2b by brainstem neurons involved in chemosensory integration in the adult rat. *The Journal of Neuroscience*, *26*(40), 10305-10314.

Stuber, G. D., & Mason, A. O. (2013). Integrating optogenetic and pharmacological approaches to study neural circuit function: current applications and future directions. *Pharmacological reviews*, *65*(1), 156-170.

Takakura, A. C., Moreira, T. S., Stornetta, R. L., West, G. H., Gwilt, J. M., & Guyenet, P. G. (2008). Selective lesion of retrotrapezoid Phox2b-expressing neurons raises the apnoeic threshold in rats. *The Journal of physiology*,*586*(12), 2975-2991.

Takeda, S., Eriksson, L. I., Yamamoto, Y., Joensen, H., Onimaru, H., & Lindahl, S. G. (2001). Opioid action on respiratory neuron activity of the isolated respiratory network in newborn rats. *The Journal of the American Society of Anesthesiologists*, *95*(3), 740-749.

Tan W, Janczewski WA, Yang P, Shao XM, Callaway EM & Feldman JL (2008). Silencing preBotzinger complex somatostatin-expressing neurons induces persistent apnea in awake rat. *Nat Neurosci* 11, 538–540.

Tan W, Pagliardini S, Yang P, Janczewski WA & Feldman JL (2010). Projections of preBotzinger complex neurons in adult rats. *J Comp Neurol* 518, 1862–1878.

Tan, W., Pagliardini, S., Yang, P., Janczewski, W. A., & Feldman, J. L. (2010). Projections of preBötzinger complex neurons in adult rats. *Journal of Comparative Neurology*, *518*(10), 1862-1878.

Tan, W., Sherman, D., Turesson, J., Shao, X. M., Janczewski, W. A., & Feldman, J. L. (2012). Reelin demarcates a subset of pre-Bötzinger complex neurons in adult rat. *Journal of Comparative Neurology*, *520*(3), 606-619.

Thoby-Brisson M, Trinh JB, Champagnat J & Fortin G (2005). Emergence of the pre-Botzinger respiratory rhythm generator in the mouse embryo. *J Neurosci* 25, 4307–4318.

Thoby-Brisson, M., Karlén, M., Wu, N., Charnay, P., Champagnat, J., & Fortin, G. (2009). Genetic identification of an embryonic parafacial oscillator coupling to the preBötzinger complex. *Nature neuroscience*, *12*(8), 1028-1035.

Thoby-Brisson, M., Trinh, J. B., Champagnat, J., & Fortin, G. (2005). Emergence of the pre-Bötzinger respiratory rhythm generator in the mouse embryo. *The Journal of neuroscience*, *25*(17), 4307-4318.

Tian, G. F., Peever, J. H., & Duffin, J. (1998). Bötzinger-complex expiratory neurons monosynaptically inhibit phrenic motoneurons in the decerebrate rat.*Experimental brain research*, *122*(2), 149-156.

Topchiy I, Waxman J, Radulovacki M & Carley DW. (2010). Functional topography of respiratory, cardiovascular and pontine-wave responses to glutamate microstimulation of the pedunculopontine tegmentum of the rat. *Respiratory physiology & neurobiology* **173,** 64-70.

Wallén-Mackenzie, Å., Gezelius, H., Thoby-Brisson, M., Nygård, A., Enjin, A., Fujiyama, F., ... & Kullander, K. (2006). Vesicular glutamate transporter 2 is required for central respiratory rhythm generation but not for locomotor central pattern generation. *The Journal of Neuroscience*, *26*(47), 12294-12307.

Wang H, Germanson TP & Guyenet PG (2002). Depressor andtachypneic responses to chemical stimulation of the ventral respiratory group are reduced by ablation of neurokinin-1 receptor-expressing neurons. *J Neurosci* 22, 3755–3764.

Wang X, Hayes JA, Revill AL, Song H, Kottick A, Vann NC, LaMar MD, Picardo MC, Akins VT, Funk GD & Del Negro CA (2014). Laser ablation of Dbx1 neurons in the pre-Botzinger complex stops inspiratory rhythm and impairs output in neonatal mice. *eLife* 3, e03427.

Wang, H., Stornetta, R. L., Rosin, D. L., & Guyenet, P. G. (2001). Neurokinin-1 receptor-immunoreactive neurons of the ventral respiratory group in the rat. *Journal of Comparative Neurology*, *434*(2), 128-146.

Wenninger JM, Pan LG, Klum L, Leekley T, Bastastic J, Hodges MR, Feroah TR, Davis S & Forster HV (2004). Large lesions in the pre-Botzinger complex area eliminate eupneic respiratory rhythm in awake goats. *J Appl Physiol* 97, 1629–1636.

Winfree AT (2001). *The Geometry of Biological Time*. Springer, New York.

Winter SM, Fresemann J, Schnell C, Oku Y, Hirrlinger J & Hulsmann S (2009). Glycinergic interneurons are functionally integrated into the inspiratory network of mouse medullary slices. *Pflugers Arch* 458, 459–469.

Winter SM, Fresemann J, Schnell C, Oku Y, Hirrlinger J & Hulsmann S (2010). Glycinergic interneurons in the respiratory network of the rhythmic slice preparation. *Adva Exp Med Biol* 669, 97–100.

Woch G, Ogawa H, Davies RO & Kubin L (2000). Behavior of hypoglossal inspiratory premotor neurons during the carbachol-induced, REM sleep-like suppression of upper airway motoneurons. *Exp Brain Res* 130, 508–520.

Woolf NJ & Butcher LL. (1989). Cholinergic systems in the rat brain: IV. Descending projections of the pontomesencephalic tegmentum. *Brain research bulletin* **23,** 519-540.

Woolf NJ. (1991). Cholinergic systems in mammalian brain and spinal cord. *Progress in neurobiology* **37,** 475-524.

Yeomans JS. (2012). Muscarinic receptors in brain stem and mesopontine cholinergic arousal functions. *Handb Exp Pharmacol***,** 243-259.

Zar JH (1996). *Biostatistical Analysis*. Prentice Hall, Upper Saddle River, NJ , USA.

Zhang, F., Wang, L. P., Boyden, E. S., & Deisseroth, K. (2006). Channelrhodopsin-2 and optical control of excitable cells. *Nature methods*,*3*(10), 785-792.